5-1-2020

Mechanical and thermal behavior of multiscale bi-nano-composites using experiments and machine learning predictions

Vahid Daghigh

Mechanical and thermal behavior of multiscale bi-nano-composites using experiments and machine learning predictions

By

Vahid Daghigh

A Dissertation
Submitted to the Faculty of
Mississippi State University
in Partial Fulfillment of the Requirements
for the Degree of Doctor of Philosophy
in Aerospace Engineering
in the Department of Aerospace Engineering

Mississippi State, Mississippi

May 2020

Mechanical and thermal behavior of multiscale bi-nano-composites using experiments and machine learning predictions

By

Vahid Daghigh

Approved:

_____
David S. Thompson
(Major Professor/Graduate Coordinator)

_____
Thomas E. Lacy Jr.
(Co-Major Professor)

_____
Mark F. Horstemeyer
(Committee Member)

_____
James C. Newman Jr.
(Committee Member)

_____
Sasan Nouranian
(Committee Member)

_____
Keith Koenig
(Committee Member)

_____
Jason M. Keith
Dean
Bagley College of Engineering

Name: Vahid Daghigh

Date of Degree: May 1, 2020

Institution: Mississippi State University

Major Field: Aerospace Engineering

Major Professor: David S. Thompson, Effective Advisor: Thomas E. Lacy Jr.

Title of Study: Mechanical and thermal behavior of multiscale bi-nano-composites using experiments and machine learning predictions

Pages in Study 122

Candidate for Degree of Doctor of Philosophy

The mechanical and thermal properties of natural short latania fiber (SLF)-reinforced poly(propylene)/ethylene-propylene-diene-monomer (SLF/PP/EPDM) bio-composites reinforced with nano-clays (NCs), pistachio shell powders (PSPs), and/or date seed particles (DSPs) were studied using experiments and machine learning (ML) predictions. This dissertation embraces three related investigations: (1) an assessment of maleated polypropylene (MAPP) coupling agent on mechanical and thermal behavior of SLF/PP/EPDM composites, (2) heat deflection temperature (HDT) of bio-nano-composites using experiments and ML predictions, and (3) fracture toughness ML predictions of short fiber, nano- and micro-particle reinforced composites. The *first* project (Chapter 2) investigates the influence of MAPP on tensile, bending, Charpy impact and HDT of SLF/PP/EPDM composites containing various SLF contents. The *second* project (Chapter 3) introduces two new bio-powder-additives (DSP and PSP) and characterizes the HDT of PP/EPDM composites using experiments and K-Nearest Neighbor Regressor (KNNR) ML predictions. The composites contain various contents of SLF (0, 5, 10, 20, and 30wt%), NCs (0, 1, 3, 5wt%), micro-sized PSPs (0, 1, 3, 5wt%) and micro-sized DSPs (0, 1, 3, 5wt%). The *third* project (Chapter 4) characterizes the fracture toughness of the same composite series used in the second project, by

applying Charpy impact tests, finite element analysis, and a ML approach using the Decision Tree Regressor (DTR) and Adaptive Boosting Regressor (ABR). 2wt% MAPP addition enhanced the composite tensile/flexural moduli and strength up to 9% compared with the composites with zero MAPP. In addition, energy impact absorption was profoundly increased (up to78%) and HDT (up to 4 C^o) was improved upon MAPP addition to the composites. SLF, NC, DSP and PSP could separately and conjointly increase HDT and fracture toughness values. The KNNR ML approach could accurately predict the composite's HDT values and, Decision Tree Regressor (DTR) and Adaptive Boosting Regressor ML algorithms worked well with fracture toughness predictions. Pictures taken through a transmission electron microscope, scanning electron microscope and X-Ray proved the NC dispersion and exfoliation as one of the factors in HDT and fracture toughness improvements.

DEDICATION

To My Lovely parents

Shaheen and Reza

ACKNOWLEDGEMENTS

First and foremost, I wish to express my profound appreciation and respect to Dr. Thomas E. Lacy Jr. for his great mentorship, support and guidance through this research which enhanced my knowledge. I learned a great deal from him, more importantly from the manner with which he helped me even before I join his research team from 2013 to 2016. I feel I am indebted to him forever. Additionally, I acknowledge Dr. Charles U. Pittman Jr.'s contribution to provide interesting discussions, exciting challenges and a multi-aspect scientific views which led to my deeper understanding of the research.

I also thank my committee members for their valuable advice and comments on this work. I am thankful to Dr. Mark F. Horstemeyer and Dr. Sasan Nouranian for their guidance and useful comments. I am grateful to Dr. James C. Newman Jr., Dr. Keith Koenig, and Dr. David S. Thompson for their support and encouragement to pave this challenging research road.

Special thanks to Mr. Stephan J. Horstemeyer and Dr. Rooban Venkatesh K G Thirumalai for their valuable support at CAVS, Mississippi State University. I would also like to thank my past colleagues: Dr. Trenton M. Ricks, and Dr. Kalyan Raj Kota for their friendship, support and helpful comments.

Last but not the least, I would like to thank my parents, Shaheen and Reza, and my dear brothers, Behrun and Hamid, for their endless passionate support during my education and research at Mississippi State University.

TABLE OF CONTENTS

APPENDIX

LIST OF TABLES

LIST OF FIGURES

CHAPTER I

INTRODUCTION

1.1 Motivation

Traditional composite materials containing stiff and strong fibers such as glass, carbon, and aramid, with polymeric matrices, are commonly used in such industries as aerospace, automotive, sporting and construction [1-3]. However, they have had drawbacks such as health risk for inhalation, non-renewability, non-recyclability, and non-biodegradability. Thus, the idea of bio-composites has come into play in the past two decades [4]. Fiber reinforced polymer (FRP) green composites are increasingly used in many applications due to their high specific modulus and strength, as well as eco-friendly characteristics [5]. Natural fibers such as coir [6], sisal [7], bamboo [8], banana [9], rice husk [10], jute [11], kenaf [12], basalt [2, 13-15], flax [16], coconut [17] *etc.* have been used to successfully reinforce cost-effective FRP green composites. Nevertheless, latania natural fiber-reinforced composites have been rarely investigated. Latania fibers are provided from the stem of latania plants from the palm tree family [5, 18].

Mechanical properties of various natural fibers are tabulated in Table 1.1. A typical hollow structure of sisal fiber interior section was depicted by Silva *et al*. [19] (Fig. 1.2). These holes in the fiber might reduce the composite's strength. Fig. 1.3. shows a cross section view of a latania fiber [18]. Comparing Figures 1.1 and 1.2 indicates that the porosity of a latania fiber is less than that of the sisal fiber.

Table 1.1 Mechanical properties of various natural fibers for composite applications [4].

Natural fibers	Tensile strength (MPa)	Elongation at break (%)	Young modulus (GPa)
Flax	300–1500	1.3–10	24–80
Jute	200–800	1.16–8	10–55
Sisal	80–840	2–25	9–38
Kenaf	295–1191	3.5	2.86
Pineapple	170–1627	2.4	60-82
Banana	529–914	3	27–32
Coir	106–175	14.21–49	4–6
Oil palm (empty fruit)	130–248	9.7–14	3.58
Oil palm (fruit)	80	17	
Ramie	348–938	1.2–8	44–128
Hemp	310–900	1.6–6	30–70
Wool	120–174	25–35	2.3–3.4
Spider silk	875–972	17–18	11–13
Cotton	264–800	3–8	5–12.6

One of the prevalent matrices used in natural composites is polypropylene (PP). Widespread use of PP in packaging, automotive, textile, and non-structural applications are based on the ease of PP's processing [20]. PP though has a relatively low impact strength leading to its limited use in structural designs, most importantly at lower temperatures. Addition of various elastomers as modifiers contribute to an increase in PP's toughness and strength. The impact strength of modified thermoplastics can be four times higher than the unmodified ones [5, 21]. One type of modifier is the ethylene–propylene–diene monomer (EPDM) [5, 18, 22] which can significantly improve the modified PP's impact strength.

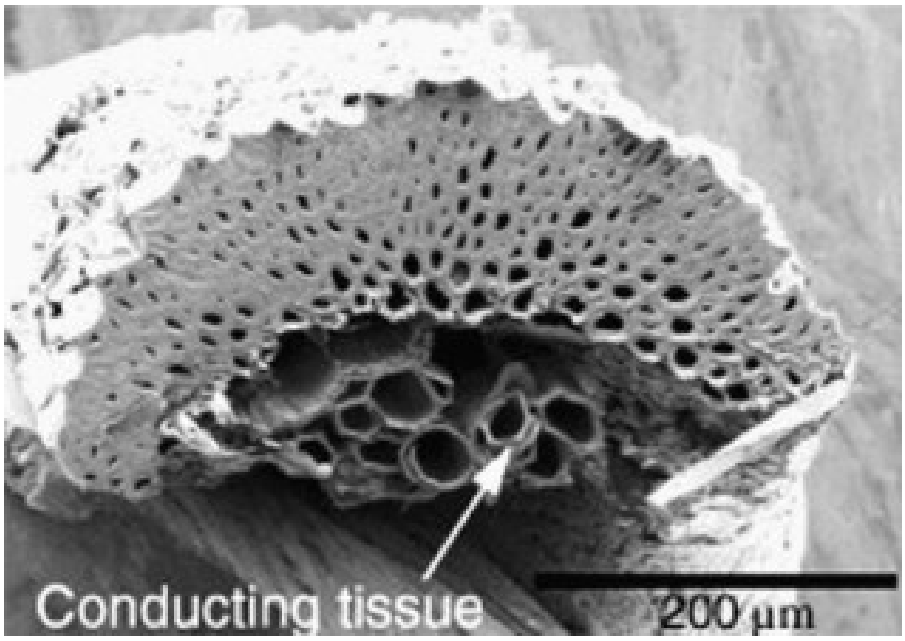

Figure 1.1 Cross section of a sisal fiber [19].

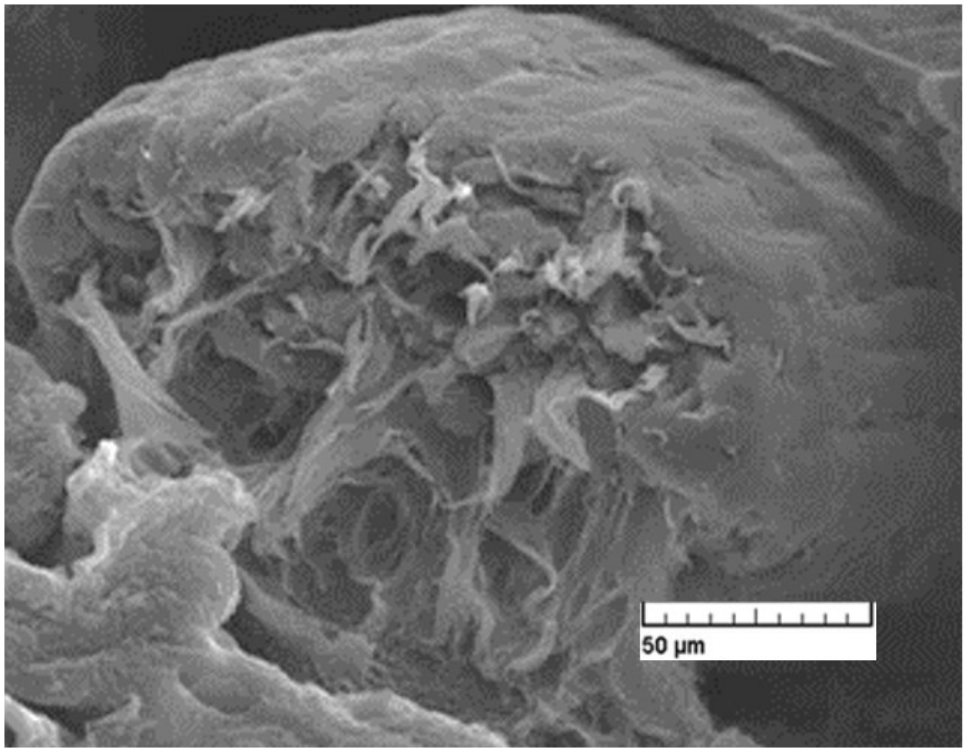

Figure 1.2 Cross section of a latania fiber [18]

Increasing demands to enhance the mechanical and thermal performance of green structural composite materials has led to investigations of new natural reinforcing fillers. Natural powder fillers have not received much attention in literature as opposed to some synthesized fillers such as silica and calcium carbonate [13, 23-24]. Since pistachio shells and date seeds are waste bio-materials, their successful use as reinforcement materials can further contribute towards environmentally friendly engineering solutions. Pistachio shells and date seeds are ligno-cellulosic agricultural residues. Since they have no current important industrial usages and are normally incinerated or dumped. Burning agricultural residues may cause environmental air pollution, soil erosion and decrease in soil biological activities [25-26].

1.2 Machine Learning Approach

As a subset of artificial intelligence (AI), machine learning (ML) aims to understand and analyze the data structure fitting them into models which are capable of prediction and, if possible, optimization. ML algorithms let computers get training on input data, and use statistical methods to predict the outputs [27]. There are many similarities between ML and statistics, however, the relation between ML and statistics is analogous to that of pharmacology and chemistry.

Nowadays, ML has benefited many technology users. Facial recognition technology, social media, self-driving cars, and optical character recognition (OCR) technology that converts text images into movable type are just some of the ML applications [27]. ML is growing fast and has a bright future in expanding the boundaries of simulation, modeling, prediction and optimization of mechanical and thermal behaviors of structural materials. K-Nearest Neighbor Regressor (KNNR) ML approach is used to predict heat deflection temperatures (Chapter 3), and the Decision Tree Regressor (DTR) and Adaptive Boosting Regressor (ABR) are employed to predict fracture toughness (Chapter 4) of multiscale bio-nano-composites.

1.3 References

[1] S. Behnia, V. Daghigh, K. Nikbin, A.B. Fereidoon, J. Ghorbani, "Influence of stacking sequence and notch angle on the Charpy impact behavior of hybrid composites," *Mechanics of Composite Materials,* vol. 52, no. 4, pp. 489-496, 2016.

[2] V. Daghigh, S.M.R. Khalili, R.E. Farsani, "Creep behavior of basalt fiber metal laminate composites," *Composites Part B: Engineering,* vol. 91, pp. 275-282, 2016.

[3] M. Lamea, V. Daghigh, M. Soroush, K. Nikbin, "The buckling behavior of vacuum-infused open-hole unidirectional basalt fiber composites-Experimental and numarical investigations," *Mechanics of Composite Materials ,* vol. 55, no. 6, pp. 1-12, 2019.

[4] H. Cheung, M. Ho, K. Lau, F. Cardon, D. Hui , "Natural fibre-reinforced composites for bioengineering and environmental engineering applications," *Composites Part B: Engineering,* vol. 40, pp. 655-663, 2009.

[5] M. Nasihatgozar, V. Daghigh, T. E. Lacy Jr., H. Daghigha, K. Nikbin, A. Simoneau, "Mechanical characterization of novel latania natural fiber reinforced PP/EPDM composites," *Polymer Testing,* vol. 56, pp. 321-328, 2016.

[6] D. V. O. de Moraes, R. Magnabosco, G. H. B. Donato, S. H. P. Bettini, M. C. Antunes, "Influence of loading frequency on the fatigue behaviour of coir fibre reinforced PP composite," *Polymer Testing,* vol. 41, pp. 184-190, 2015.

[7] P. Wambua, J. Ivens, I. Verpoest, "Natural fibres: can they replace glass in fibre reinforced plastics?," *Composite Science and Technology,* vol. 63, no. 9, pp. 1259-1264, 2013.

[8] Verma, C.S. and Chariar, V.M., "Development of layered laminate bamboo composite and their mechanical properties," *Composites Part B: Engineering,* vol. 43, no. 3, pp. 1063-1069., 2013.

[9] Srinivasan, V.S., Boopathy, S.R., Sangeetha, D. and Ramnath, B.V., 2014. Evaluation of mechanical and thermal properties of banana–flax based natural fibre composite. Materials & Design, 60, pp.620-627., "Evaluation of mechanical and thermal properties of banana–flax based natural fibre composite," *Materials & Design,* vol. 60, pp. 620-627., 2014.

[10] Dias, A.B., Müller, C.M., Larotonda, F.D. and Laurindo, J.B., "Mechanical and barrier properties of composite films based on rice flour and cellulose fibers," *LWT-Food Science and Technology,* vol. 44, no. 2, pp. 535-542, 2011.

[11] Gon, D., Das, K., Paul, P. and Maity, S., "Jute composites as wood substitute," *International Journal of Textile Science,* vol. 1, no. 6, pp. 84-93, 2012.

[12] FM. Salleh, A. Hassan, R. Yahya, A.D. Azzahari, "Effects of extrusion temperature on the rheological, dynamic mechanical and tensile properties of kenaf fiber/HDPE composites," *Composite Part B: Engineering,* vol. 58, pp. 259-266,, 2014.

[13] R. Eslami Farsani, SMR Khalili, V. Daghigh, R. Fazaeli, "Creep Behavior of Basalt and Glass Fiber Reinforced Epoxy Composites," *Journal of Mechanical Research and Application ,* vol. 3, no. 1, pp. 29-36, 2011.

[14] SMR Khalili, RE Farsani, V Daghigh, "Aging Influence on Charpy Impact Behavior of Basalt Fiber Reinforced Epoxy Composites," *International Journal of Advanced Design and Manufacturing Technology ,* vol. 6, no. 2, pp. 81-85, 2013.

[15] S.M.R. Khalili, V. Daghigh, R.E. Farsani, "Mechanical behavior of basalt fiber-reinforced and basalt fiber metal laminate composites under tensile and bending loads," *Journal of Reinforced Plastcis and Composites,* vol. 30, no. 8, pp. 647-659, 2011.

[16] A. El-Sabbagh, L. Steuernagel, G. Ziegmann, "Processing and modeling of the mechanical behavior of natural fiber thermoplastic composite: flax/polypropylene," *Polymer Composites,* vol. 30, no. 4, pp. 510-519, 2009.

[17] C. Merlini, G. M.O. Barra, D. P. Schmitz, S. D.A.S. Ramôa, A. Silveira, T. Medeiros Araujo, A. Pegoretti, "Polyaniline-coated coconut fibers: structure, properties and their use as conductive additives in matrix of polyurethane derived from castor oil," *Polymer Testing,* vol. 38, pp. 18-25, 2014.

[18] V. Daghigh, T. E. Lacy Jr., C. U. Pittman Jr., H. Daghigh, "Influence of maleated polypropylene coupling agent on mechanical and thermal behavior of latania fiber-reinforced PP/EPDM composites," *Polymer Composites,* vol. 39, no. S3, pp. E1751-E1759, 2018.

[19] F.A. Silva, N. Chawla, R.D.T. Filho, "Tensile behaviour of high performance natural (sisal) fibers," *Composite Science and Technology,* vol. 68, pp. 3438-3443, 2008.

[20] H.M. da, V.D. Costa, M. Ramos, C.G. Rocha, "Analysis of thermal properties and impact strength of PP/SRT, PP/EPDM and PP/SRT/EPDM mixtures in single screw extruder," *Polymer Testing,* vol. 25, pp. 498-503, 2006.

[21] A. Lúcia, N.A. Silva, F.M.B. Coutinho, "Some properties of polymer blends based on EPDM/PP," *Polymer Testing,* vol. 15, pp. 45-52, 1996.

[22] B.Z. Jang, D.R. Uhlmann, J.B. Vander Sande, "Crystalline morphology of polypropylene and rubber-modified polypropylene," *J. App. Poly Sci.,* vol. 29, pp. 4377-4393, 1984.

[23] R.E. Farsani, S.M.R. Khalili, V. Daghigh, "Charpy impact response of basalt fiber reinforced epoxy and basalt fiber metal laminate composites: experimental study," *International Journal of Damage Mechanics,* vol. 23, no. 6, pp. 729-744, 2014.

[24] T. Ghabeer, R. Dweiri, S. Al-Khateeb, "Thermal and mechanical characterization of polypropylene/eggshell biocomposites," *Journal of Reinforced Plastics and Composites ,* vol. 32, no. 6, p. 402–409, 2013.

[25] G. Tepić, T. Pejakov, B. Lalić, V. Vukadinović, S. Milisavljević, "The application of recycled aluminum and plastics in environmental protection," *Metalurgija,* vol. 52, no. 3, pp. 395-398, 2013.

[26] A. Nourbakhsh, A. Ashori, A. Tabrizi, "Characterization and biodegradability of polypropylene composites using agricultural residues and waste fish," *Composites Part B: Engineering,* vol. 56, pp. 279-283, 2014.

[27] L. Tagliaferri, "An Introduction to Machine Learning," https://www.digitalocean.com/community/tutorials/an-introduction-to-machine-learning, 2017.

[28] S. Mohanty, S.K. Verma, S.K. Nayak, "Dynamic mechanical and thermal properties of MAPE treated jute/HDPE composites," *Composite Science and Technology ,* vol. 66, pp. 538-547, 2006.

[29] H. Anuar, A. Zuraida, "Improvement in mechanical properties of reinforced thermoplastic elastomer composite with kenaf bast fibre," *Composites Part B Engineering,* vol. 42, no. 3, pp. 462-465, 2011.

[30] H.M. da Costa, V.D. Ramos, W.S. da Silva, A.S. Sirqueira, "Analysis and optimization of polypropylene (PP)/ethylene–propylene– diene monomer (EPDM)/scrap rubber tire (SRT) mixtures using RSM methodology," *Polymer Testing,* vol. 29, no. 5, pp. 572-578, 2010.

[31] K.A. Dubey, S.K. Sinha, Y.K. Bhardwaj, L. Panicker, L. Varshney, "Carbon black-filled PE/PP/EPDM blends: phase selective localization of carbon black and EPDM-induced phase stabilization," *Polymer-Plastics Technology and Engineering,* vol. 53, pp. 442-450, 2014.

CHAPTER II

INFLUENCE OF MALEATED POLYPROPYLENE COUPLING AGENT ON MECHANICAL AND THERMAL BEHAVIOR OF LATANIA FIBER-REINFROCED PP/EPDM COMPOSITES

2.1 Abstract

The influence of maleated polypropylene (MAPP) on the mechanical/thermal properties of short latania fiber-reinforced poly(propylene)/ethylene-propylene-diene-monomer (SLF/PP/EPDM) composites was investigated. Two different MAPP weight percentages (0 and 2wt%) and five different fiber weight contents (0, 5, 10, 20, and 30wt%) were considered, where the density of MAPP at the fiber surfaces progressively decreased. For a given fiber loading, addition of 2wt% MAPP led to roughly a 3–9% increase in tensile/flexural moduli and strengths over SLF/PP/EPDM composites with no MAPP. Moreover, composites containing MAPP displayed a profound improvement (37–78%) in impact energy absorption. In addition, composite heat deflection temperatures notably increased by 3–4°C with MAPP addition. Microscopic imaging suggested that matrix crazing, fiber pull-out, and fiber fractures were key failure mechanisms. Hence, SLF/PP/EPDM composites modified with 2%wt MAPP may serve as a low-cost alternative to other natural fiber thermoplastic composites.

2.2 Introduction

Composite materials play a major role in most industries including aerospace, automotive, home appliance, construction, marine, and sporting goods [1]. Use of synthetic

materials raises environmental concerns, so there is an increasing investment in developing natural composite materials. “Green” composites composed of natural materials and fibers may consume less energy over their lifecycles, improve specific stiffness and toughness versus glass fibers [2-5], exhibit biodegradability, and enhance biocompatibility [6-8] for medical applications [9]. Moreover, European Parliament rules seek CO_2 emission targets for new cars to be lower than 120, 95 and 70 g/km by 2015, 2020, and 2025, respectively [10]. The use of automotive biodegradable materials can help achieve this. These goals encourage research on natural materials and green composites [11-15].

Often natural fibers surfaces are chemically treated to facilitate fiber-matrix compatibility and bonding [14]. In addition, the use of coupling agents in natural fiber composites can improve fiber/matrix adhesion [12-13, 16-19]. Many researchers, therefore, have investigated the effect of adding coupling agents or using fiber surface treatments [20]. For example, maleated polypropylene (MAPP) coupling agents and maleic anhydride (MAH) grafted poly(ethylene octane) compatibilizers increased the tensile, bending, and impact strengths of hemp fiber/polypropylene (PP) composites [13]. Moreover, the maximum decomposition temperatures were raised by hemp fiber addition. The mechanical and thermal properties of jute fabric-reinforced poly(butylene succinate) (PBS) biodegradable composites were influenced by fiber surface treatments [16]. Use of alkali-silane-treated jute fabric/PBS increased the tensile modulus (10.8%), tensile strength (16.4%), flexural modulus (21.9%) and flexural strength (24.2%) compared to composites with untreated jute surfaces.

Maleated polyethylene (maleic anhydride-grafted to polyethylene, MAPE) and MAPP are widely used coupling agents. In natural fiber composites, chemically bond to hydroxyl groups on cellulosic fiber surfaces by rectification reactions that open the maleic anhydride rings; both

MAPE and MAPP lower fiber surface polarity and entangle with nonpolar polymer matrices like polyethylene, PP, ethylene-propylene-diene-monomer (EPDM), etc. [13, 17, 21-24].

Yang *et al*. [17] improved the tensile and impact properties of polyethylene (PE) reinforced with wood or rice husk flours by adding MAPE or MAPP. MAPE gave better tensile properties than using MAPP, but MAPP led to greater improvements in impact properties than for MAPE. Scanning electron microscope (SEM) micrographs of MAPE/PE composite impact specimens displayed numerous filler particles and no filler particle pull-outs. In contrast, MAPP/PE composites showed traces of filler particle pull-out, and fractured filler particles. The tensile and flexural strengths of wood fiber/PP composites with blended m-isopropenyl-α, α-dimethylbenzyl-isocyanate (m-TMI) into isotactic PP (m-TMI-g-PP) increased 45% and 85%, respectively [18]. Also, the optimum composite tensile and impact properties corresponded to 4wt% MAPP addition to 30 and 40wt% oil-palm fiber reinforced HDPE [19]. Use of MAPE and raising the amount of hemp fiber increased both the compressive moduli and yield stresses relative to neat HDPE [21]. Also, addition of MAPE and hemp fiber increased the impact energy absorption when the fiber loading rose to 15wt%. Flax, hemp or sisal fiber/PP composites stiffness, strength, and impact properties were optimized by varying MAPP/fiber weight ratios, in the range 0.10-0.13 [22]. As an aside, the flax, hemp and sisal fibers considered in Ref. [22] were initially surface treated via alkalinization; a combination of fiber surface chemical treatment and use of coupling agents can improve composite properties.

To the best of the authors' knowledge, Daghigh *et al*. [25] were the first to investigate the mechanical (tensile) properties of untreated natural latania fiber-reinforced PP/EPDM composites. This work was extended to characterize the tensile, impact and fracture mechanics properties of untreated latania versus untreated jute fiber-reinforced PP/EPDM [26]. The tensile

and impact properties of seldom studied latania fiber-reinforced PP/EPDM were superior to those with widely used jute fiber reinforcement [25-26]. No reports have described optimizing the ratio of a coupling agent to latania fiber composites. Latania is one of the palm tree families originating in the islands of the western Indian Ocean. Fibers are obtained from the phloem or the bast surrounding the stem of the plant. [24]. Herein, we report how MAPP addition to latania fiber/PP/EPDM composites affects mechanical (tensile, bending, impact) and thermal properties. Untreated latania fiber loadings of 0, 5, 10, 20 and 30wt% and MAPP weight percents of 0 and 2wt% were investigated. The optimized MAPP to latania fiber ratio was found.

2.3 Experimental Procedure

2.3.1 Materials

PP and MAPP were supplied by Masoom Co., Iran and Sigma Aldrich Chemical Co., USA, respectively [25-26]. Latania fibers were provided from the Agricultural Department, Tehran, Iran. Figs. 2.1 (a) and (b) show latania fibers before and after being chopped [26].

(a)

(b)

Figure 2.1 Latania fibers before being chopped (a), Latania fibers after being chopped (b). Ref. [26].

2.3.2 Specimen Preparations

A guillotine machine (Wiser A-8992 Altaussee, Germany) was used to cut the latania fibers into roughly 10 mm lengths. The fibers were then shortened to a maximum length of 2 mm

during blending with PP/EPDM. Short latania fiber (SLF)-reinforced PP/EPDM batches containing 0, 5, 10, 20 and 30wt% of fiber were each prepared by single extrusions of granulated PP/EPDM and chopped latania fibers at 180°C and through a 60 RPM dual (twin) screw extruder (Collins Extrusions Ltd, Birmingham, UK). The extruder strands were pulled through a cool water bath to avoid thermal decomposition or possible fiber burning. These blends were cooled to room temperature and then pelletized. The pellets were then desiccated at 80°C for 24 h. Finally, tensile, bending, Charpy impact and heat deflection temperature (HDT) test specimens were produced using an injection moulding machine (EM 80, Aslanian Co.) at 165-180°C using the exact procedures described in [11, 25-26].

2.4 Mechanical and Thermal Testing Procedures and Equipment

ASTM D-638 tensile tests and ASTM D-790 three-point bending tests were conducted using a SANTAM Universal Testing Machine-STM-20 (Santam Co., Tehran, Iran) with a 2 kN-load cell, at the cross-head speed of 5 mm/min consistent with [26]. ASTM D-256 Charpy impact tests were performed using a Santam Instrumented Impact Tester (Model: ZBC1251, Santam Co.) [26]. ASTM D-648 HDT tests were carried out using a HDT-Tester HV-2000A, (GoTech Co., Taiwan) for a prescribed stress, maximum deflection and rate of temperature increase of 1.82 MPa, 0.25 mm and 2ºC/min, respectively. A total of three repeat experiments were performed for each specimen geometry and material combination. After testing, the failure surfaces of tensile, bending and impact specimens were studied by SEM (Oxford Instruments, Model 7718, England), in order to examine the fracture morphology and the fiber/matrix interfaces. Gold coating was employed to increase the SEM clarity.

2.5 Results and Discussion

2.5.1 The Influence of MAPP on the Tensile Behavior of SLF/PP/EPDM Composites

ASTM standard D-638 tensile tests were conducted on SLF/PP/EPDM composites containing varying amounts of fibers to determine the effect of MAPP on tensile properties. The properties of neat SLF/PP/EPDM specimens with no MAPP are compared with the corresponding composites with 2wt% MAPP. The tensile moduli (Fig.2.2) and tensile strengths (Fig.2.3) of the neat composite (no MAPP) both steadily increased with increasing fiber content.

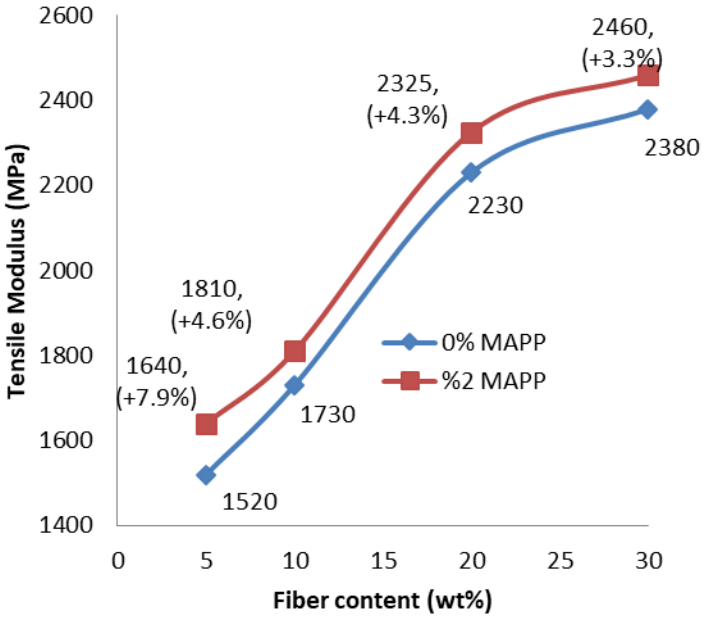

Figure 2.2 Tensile modulus versus fiber content for SLF/PP/EPDM composites without and with 2wt% MAPP [26].

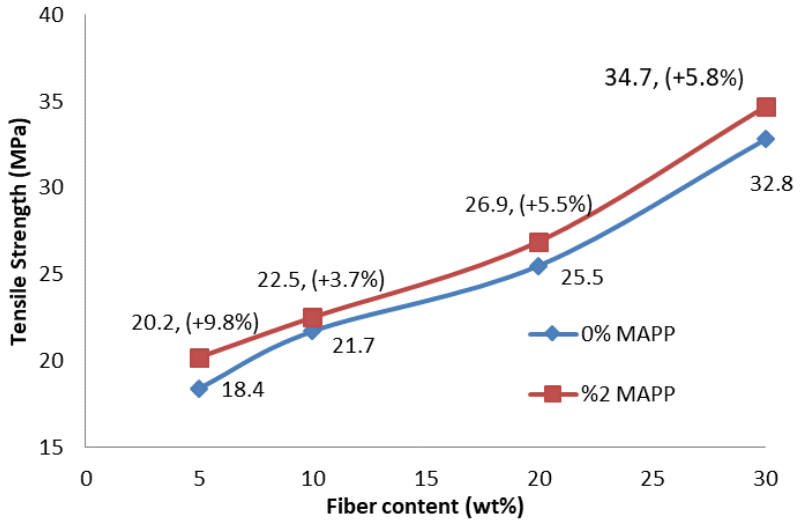

Figure 2.3 Tensile strength versus fiber content for SLF/PP/EPDM composites without and with 2wt% MAPP [26].

Increasing the fiber loading from 5wt% to 30wt% resulted in an improvement in modulus and strength of over 50% and 70%, respectively. Addition of 2wt% MAPP to the composites led to a further enhancement in tensile moduli and strengths of roughly 3-7% and 3-9%, respectively (Figs. 2.2-2.3). In general, the relative amount of tensile property improvement decreased as the fiber content was increased from 5 to 30wt%, because the ratio of MAPP to SLFs decreases. This makes sense since a fixed amount of MAPP (2%wt) must be transported to the fiber surfaces during extrusion and then distributed over a much larger total fiber surface area as the fiber loading is increased. For example, the tensile moduli increased by 7.9%, 4.6%, 4.3%, and 3.3% for MAPP/SLF weight ratios of 0.4, 0.2, 0.1, and 0.067, respectively (Fig. 2.2). The tensile strength increased by 9.8%, 3.7%, 5.5% and 5.8% for MAPP/SLF weight ratios of 0.4, 0.2, 0.1, and 0.067, respectively (Fig. 2.3). Over this range of SLF loadings (5-30wt%), use of MAPP leads to improved coupling between the SLF and PP/EPDM. The tensile strength enhancement (9.8%) due

to MAPP for SLF/PP/EPDM composites with 5wt% fibers (MAPP/SLF ratio, 0.4) is slightly better than that reported by Arrakhiz [27] for pine cone fiber-reinforced PP and FG1901X compatibilizer, which gave a 6% tensile strength enhancement over that of neat PP. Also, the improvement in SLF/PP/EPDM composite tensile properties with increasing SLF content for specimens with no coupling agent is caused by physical anchoring of SLF in the polymer [27]. Better fiber-to-matrix adhesion between the fiber and matrix accounts for the positive role of MAPP on tensile properties improvement [28-29]. The tensile properties for SLF/PP/EPDM with 2wt% MAPP are the same as mentioned in [26].

2.5.2 Influence of MAPP on Flexural Behavior of SLF/PP/EPDM Composites

ASTM standard D-760 three-point flexural tests were performed on SLF/PP/EPDM composites containing varying fiber amounts to assess the effect of MAPP on flexural properties. Composite flexural moduli and strengths are shown in Figs. 2.4 and 2.5, respectively, for the neat SLF/PP/EPDM specimens with no MAPP versus the corresponding composites with 2wt% MAPP. Similar to the cases for tensile specimens, the flexural moduli for the neat composites steadily increased with increasing SLF loadings (Fig. 2.4). Increasing the fiber content from 5wt% to 30wt% resulted in roughly an 8% improvement in modulus. Addition of 2wt% MAPP further increased the composite moduli by roughly 4-9%, depending on the fiber loading. Adding 2wt% MAPP resulted in bending modulus increases of 4.2%, 2.4%, 9.3% and 4.7% for 5, 10, 20 and 30wt% fiber contents, respectively. In contrast, the flexural strengths of the neat SLF/PP/EPDM composites initially increased with SLF loading (5-10wt%), but the rate of strength improvement became less pronounced with further increases in fiber context (Fig. 2.5). This makes sense since SLFs will be less effective in resisting compressive stresses in bending.

Nonetheless, increasing the SLF loading from 5-30wt% resulted in roughly a 46% improvement in flexural strength.

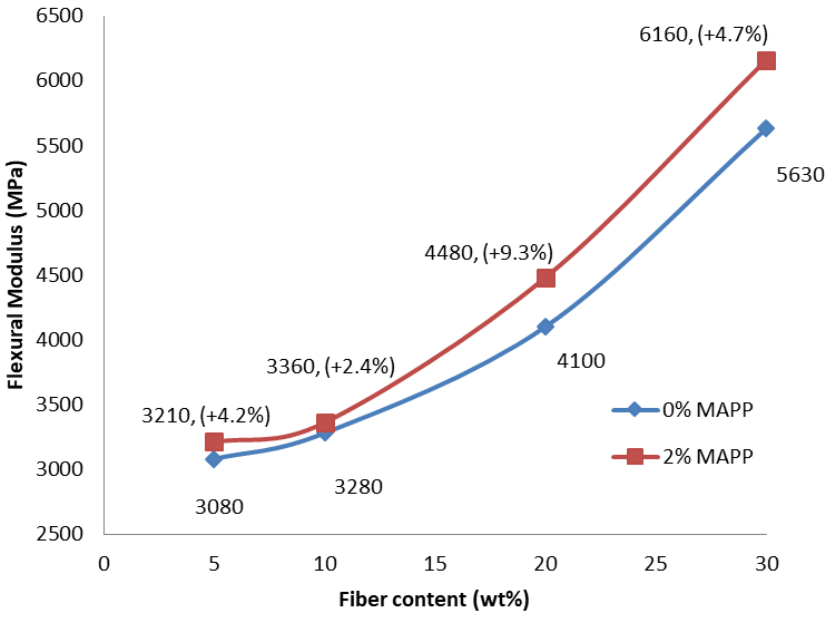

Figure 2.4 Flexural modulus versus fiber content without and with 2wt%. MAPP for SLF/PP/EPDM composites.

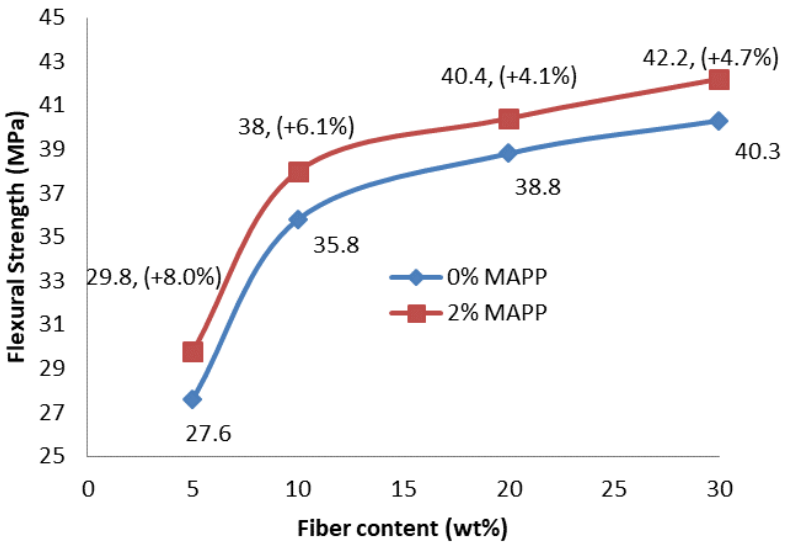

Figure 2.5 Flexural strength versus fiber content without and with 2wt% MAPP for SLF/PP/EPDM composites.

2.5.3 MAPP Influence on the Impact Behavior of SLF/PP/EPDM

ASTM standard D-256 Charpy impact tests were conducted on SLF/PP/EPDM composites with 5, 10, 20, and 30wt% fibers to assess the effect of MAPP on impact properties, and to characterize both energy absorption and fracture morphologies. Figure 2.6 shows the energy absorbed as a function of fiber weight percent for SLF/PP/EPDM composites containing 0-30wt% SLF (no MAPP).

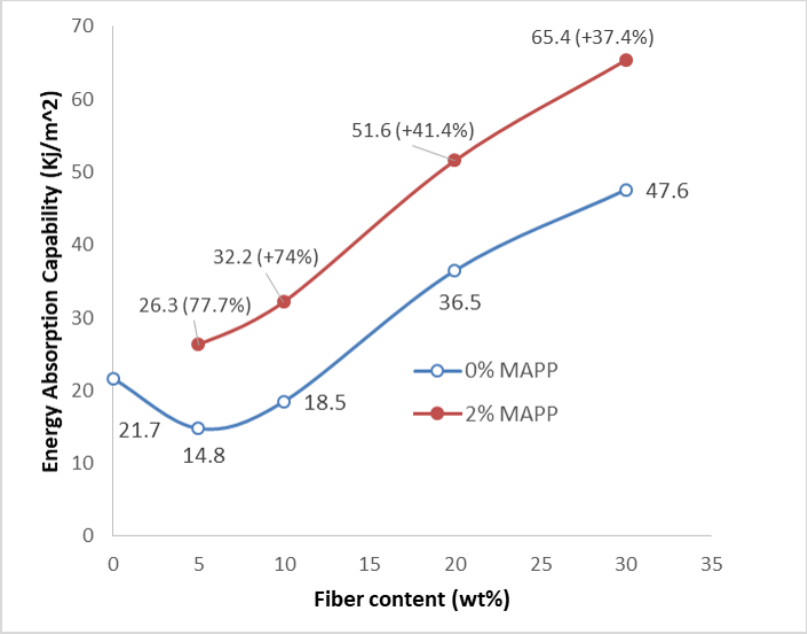

Figure 2.6 Effect of 2wt% MAPP on energy absorption capability for SLF/PP/EPDM composites versus fiber content (The composites with 2wt% MAPP data adapted from Ref. [26])

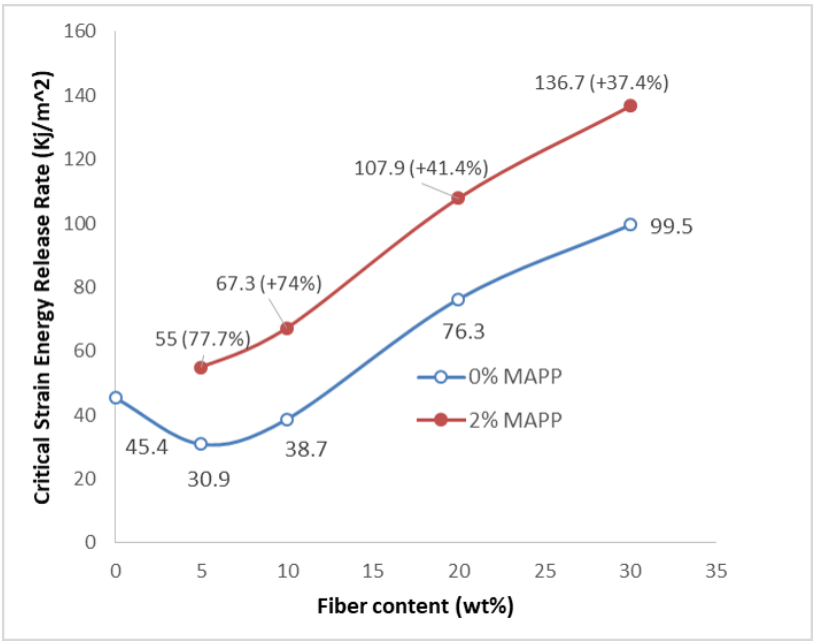

Figure 2.7 Effect of MAPP content on critical strain energy release rate (G_c) for SLF/PP/EPDM composites with different fiber contents (The composites with 2wt% MAPP data adapted from Ref. [26])

For relatively small amounts of SLFs (5-10wt%), the impact energy absorption fell below that for the neat PP/EPDM. At higher fiber loadings (>15wt%), the impact energy absorption exceeded that for the neat matrix and increased significantly with further increases in fiber weight percentages. The initial drop in impact energy absorption at small fiber loadings is consistent with results of Khalili *et al*. [11]; in that study, however, the impact energy absorption was a decreasing function of fiber loading over all fiber weight fractions considered. Figure 2.6 also contains a plot of the impact energy absorbed for SLF/PP/EPDM composites (5-30wt%SLF) containing 2wt% MAPP. The effect of MAPP on the properties of the neat PP/EPDM matrix (0wt% SLF) was not considered. The addition of MAPP improved the impact energy absorption of the composites substantially. For example, inclusion of MAPP led to a 78%, 74%, 41%, and 37% improvements in energy absorption for composites containing 5, 10, 20, and 30wt% SLFs, respectively. As mentioned previously, the relative improvement in composite properties due to the presence of MAPP is more pronounced at lower SLF weight fractions. This suggests that the weight fraction of MAPP should be increased in proportion to the weight fraction total or surface areas of SLFs in order to optimize interfacial adhesion between matrix and fiber. For a given weight fraction of untreated latania fibers, the addition of 2wt% MAPP led to a greater relative improvement in dynamic impact energy absorption (Fig. 2.6) than for quasi-static moduli (Figs. 2.2, 2.4) or strengths (Figs. 2.3, 2.5). This makes sense since MAPP chain disentanglement prior to chain breakage is highly time-dependent. Fiber-to-matrix adhesion also depends on the fiber surface roughness and chemistry, the MAPP chain length at a given fiber surface, and the surface density of MAPPs attached to the fibers. As an aside, Ref. [22] investigated the effect of MAPP on the impact and tensile properties of relatively long flax, hemp, and 30 mm long sisal fiber/PP composites.

Several fracture deformation and failure mechanisms may contribute to these toughness enhancements. They include crack bridging by latania fibers, fiber splitting/fracture/pull-out, and matrix fracture [26, 29, 31, 34]. Fillers (e.g., micro-glass powders) [4-5] or small amounts of non-reinforcing short fibers can either serve as crack propagation barriers that provide increased toughness or stress risers that reduce fracture toughness [5]. SLF/PP/EPDM composites containing 5wt% and 10wt% fibers (no MAPP) absorbed less impact energy at fracture than did PP/EPDM alone (Fig.2.6). Once the fiber content was increased to ≥20wt%, the absorbed impact energy of the composite exceeded that of neat PP/EPDM. At these SLF weight fractions, a greater number of fibers are available to bridge or deflect cracks and to provide physical anchoring. Sawpan *et al*. [35] reported similar Charpy impact test results for 3 mm long hemp natural fiber-reinforced composites with the fiber volume percentages of 30, 40, and 50v%. In that study, the fracture toughness decreased for composites containing 30v% fiber relative to the neat matrix, but increased for composites containing 40v% and 50v% fibers.

Addition of 2wt% MAPP improved the impact energy absorption over the entire range of considered fiber weight fractions (5-30wt%). The use of MAPP provides better fiber/matrix interfacial adhesion and correspondingly more impact energy dissipation. The improved bonding between the fiber and matrix via MAPP's PP interaction with the PP/EPDM matrix enhances the composite fracture toughness, even at low SLF weight fractions (5, 10wt%). As an aside, the impact properties of SLF/PP/EPDM notched specimens with 2wt% MAPP were measured in our previous work [26].

2.5.3.1 G_c determination

Linear elastic fracture mechanics (LEFM) concepts [36] were employed to determine the critical strain energy release rates (G_c) for every Charpy impact test specimen. The total impact energy absorbed (U_c) was measured during each test. The specimens were quasi-brittle with no large-scale viscoelasticity. The use of notched specimens promoted the formation of sharp cracks and subsequent brittle fracture, diminishing the plastic zone ahead of crack tip. Therefore, LEFM can be used to determine the toughness parameters. The critical strain energy release rate (fracture toughness) (G_c) during Charpy impact testing may be expressed as [36]:

$$G_c = \frac{F^2}{2B}\frac{\partial C}{\partial a} \tag{2.1}$$

where F is the force exerted on the middle of specimen by the anvil, a is the crack length, C is the material compliance and B is specimen thickness. From Ref. [36], the fracture toughness may also be expressed as:

$$G_c = \frac{U_c}{BD\theta} \tag{3.2}$$

where U_c is the (measured) energy absorbed at fracture, θ is a geometrical function that depends on the specimen geometry, and D is the specimen width. The specimen thickness for the notched specimen was B=7.1 mm, the specimen width was D=12.7 mm, and the support span was 40 mm. Using the data summarized in [36] for the notched Charpy impact specimens, a value θ=0.369 was adapted here [36].

In this study, the G_c value was based on Eq. (2) for the notched impact samples. Fig.2.7 shows the critical strain energy release rates, G_c, and those calculated for SLF/PP/EPDM composites with and without 2wt% MAPP as a function of fiber content. Not surprisingly, the essential character of the G_c versus fiber content relationship was the same as for the measured energy absorption (Fig. 2.6). The addition of 20wt% MAPP to the composite resulted in a substantial increase (78%-38%) in the absorbed fracture toughness values.

2.5.4 Measurement of Heat Deflection Temperature (HDT)

The HDT is the temperature at which a polymeric specimen deflects through a three-point bending in the edgewise direction under a specific stress as per ASTM D648. The HDT values are strongly influenced by the composite stiffness (i.e., fiber content), matrix hardness, and matrix glass transition temperature [37]. Certain composite product designs and manufacturing require specification of the HDT. Since injection molding is used to produce one third of all polymeric products manufactured by weight in the world [38], characterization of the HDT can be used to establish optimal fabrication procedures and reduce costs. Parts are typically removed from their mold only when the temperature is below or near the HDT. In HDT testing, flexural specimens are subjected to a designated mechanical load while simultaneously increasing the temperature up to the HDT. Fig. 2.8 summarizes and compares the HDT for neat PP/EPDM and for all eight SLF/PP/EPDM composites with and without MAPP.

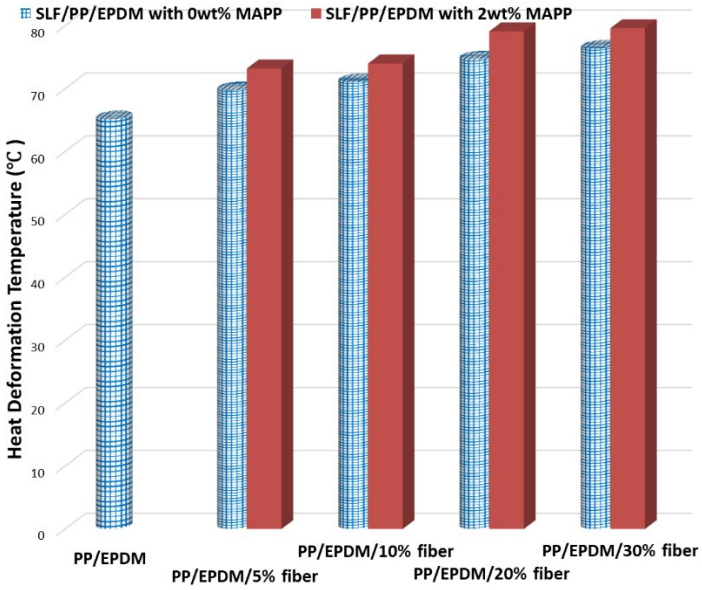

Figure 2.8 Measured HDT for SLF/PP/EPDM composites fabricated with and without 2wt% MAPP with varying fiber contents.

2.6 SEM Images and Fracture Morphology

Fractured surfaces after the tensile, bending and impact testing were observed by SEM. Damage accumulation prior to failure in polymeric composites includes crack initiation/growth and other energy absorption phenomena. The damage progression is governed by complex interactions between constituents, the fiber volume fraction, fiber/matrix interfacial properties and adhesion, stochastic variations in fiber strengths, as well as matrix strengths [41]. Damage to a 20%SLF/PP/EPDM containing 2wt% MAPP during bending testing occurred as fibers resisted crack formation/propagation. Fig. 2.9a shows a microscopic image of the lower (tensile) surface of a bending specimen during the test where fibers and surface crack formation has occurred. In the upper inset, white crazed regions orthogonal to the fibers indicated high strain regions in the matrix where microvoid nucleation/growth and surface crack formation is likely [34]. Fig. 2.9b

shows the lower surface of the bending specimen where subsequent fiber/matrix debonding and surface crack formation has occurred. SLFs in the PP/EPDM composites serve to blunt crack propagation, and the presence of MAPP enhances the adhesive strength between the fiber and the matrix, thus, improving the bending properties. Figures 2.10 and 2.11 show SEM images of brash [42] tensile failures along the fracture surfaces in 30%SLF/PP/EPDM and 20%SLF/PP/EPDM composites subjected to tensile and impact testing, respectively. Fiber breakage is one key indicator of energy absorption because the fibers impede/arrest existing crack propagation, which necessitates additional energy release due to new crack initiation [43]. Figures 2.10 and 2.11 clearly depict the presence of cellulose micro fibrils in the SLF cross section; a single natural fiber may effectively, act as a fiber bundle [43].

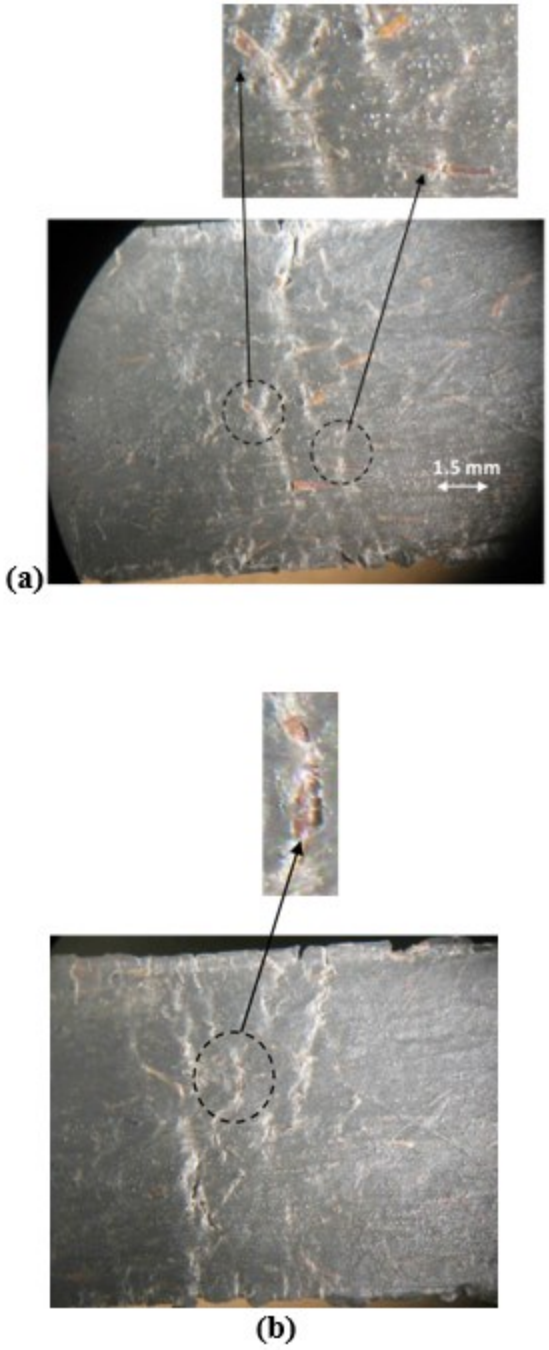

Figure 2.9 (a) Lower surface of 20wt%SLF/PP/EPDM with 2wt% MAPP during bending; the fibers shown resist against crack propagation; (b) Lower surface of 20wt%SLF/PP/EPDM during bending, debonding between fiber and matrix

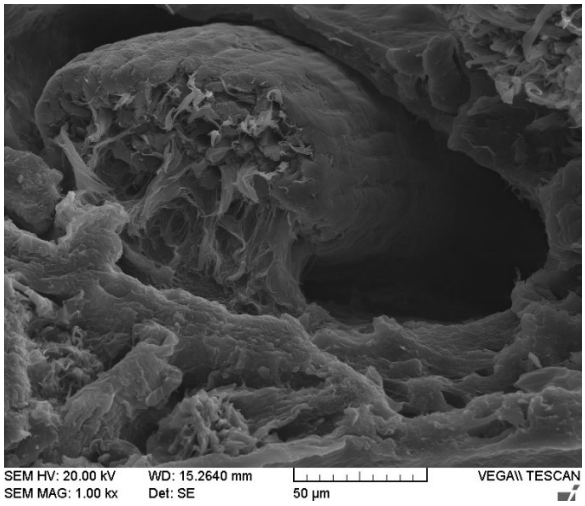

Figure 2.10 Fracture surface of 30wt%SLF/PP/EPDM containing 2wt% MAPP after tensile test (magnification, 1000x)

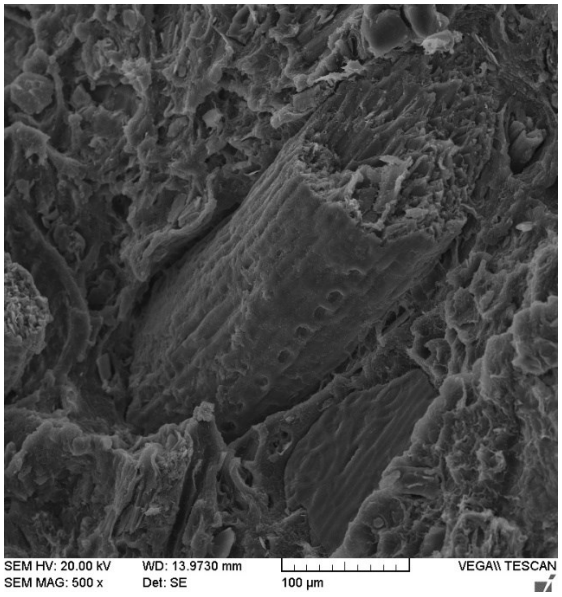

Figure 2.11 Fiber fracture in 20wt%SLF/PP/EPDM containing 2wt% MAPP after an impact test (magnification, 500x)

Fig. 2.12 shows fiber/matrix debonding in 20%SLF/PP/EPDM with 2wt% MAPP. Figures 2.12b and 2.12c show how MAPP entangled in the PP/EPDM matrix enhances fiber-matrix adhesion

through the formation of elongated polymer strands that span the gap between debonded SLFs and the PP/EPDM matrix. As an aside, SEM images of fractured SLF/PP/EPDM composites without MAPP displayed the same fundamental failure mechanisms as those shown in Figs. 2.9-2.12, but these failures occurred at lower applied stress levels.

In short, maleic anhydride functions of MAPP bond to latania fiber surface hydroxyl groups by the formation of covalent ester bonds. These anchor MAPP to the fiber surface while the MAPP's PP chains are compatible and entangle with the PP/EPDM chains of the matrix (cf., Fig.2.12c). Rupturing these adhesive interconnections expends more energy during debonding or pull-out. By and large, the presence of the coupling agent (MAPP) promotes enhanced fiber/matrix adhesion. Chemical bonding by MAPP to the fibers and its entanglement with the PP/EPDM matrix increases the energy revealed during de-cohesion and may also increase the frictional energy associated with fiber-outs. More fracture energy dissipation and consequently more impact energy absorption capability are therefore expected.

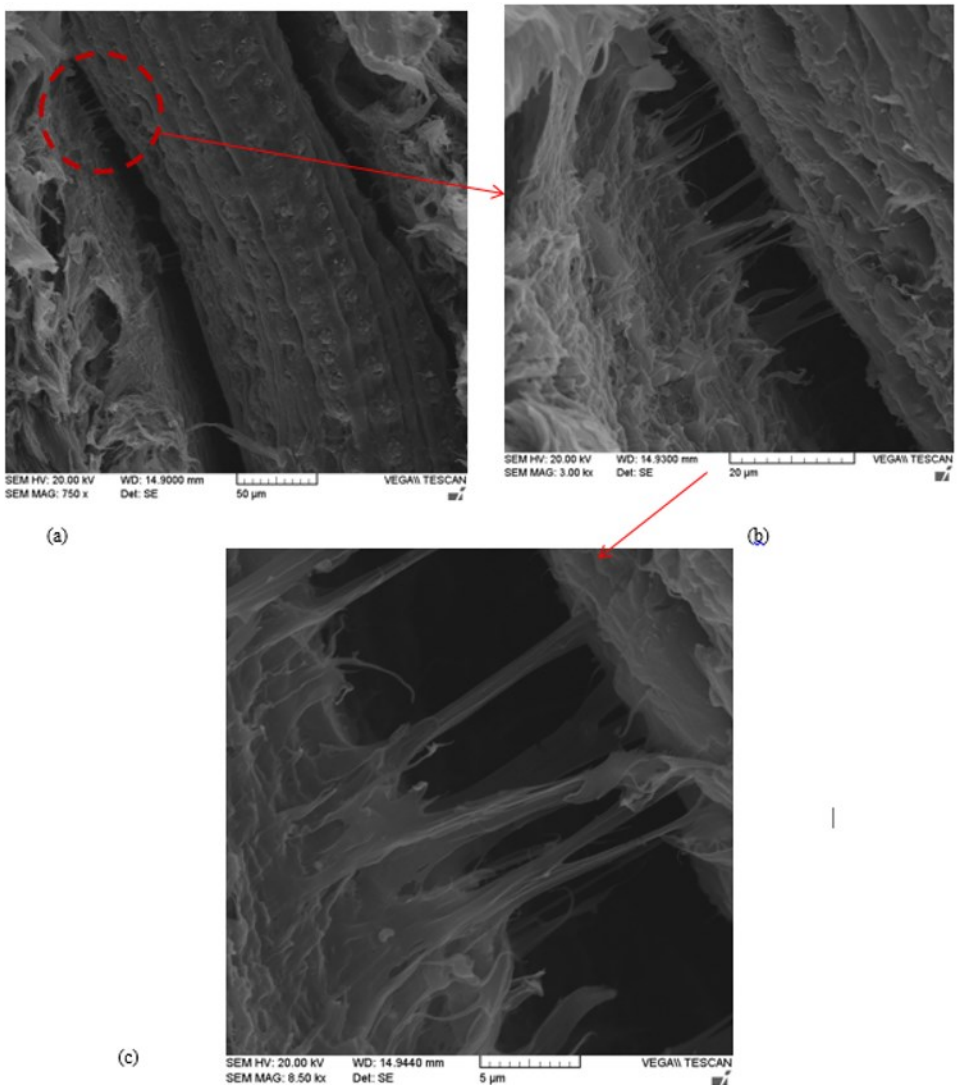

Figure 2.12 Fiber debonding in 20%SLF/PP/EPDM with 2wt% MAPP after tensile test with magnifications of (a) 750x, (b) 3000x, and (c) 8500x.

2.7 Conclusions

The effect of 2wt% MAPP coupling agent on the mechanical behavior of composites comprised of short latania fibers (SLFs) in a PP/EPDM matrix was investigated. SLF/PP/EPDM tensile, flexure, and Charpy impact specimens with 5, 10, 20, and 30wt% fiber loadings were fabricated both with and without 2wt% MAPP. This created MAPP to fiber ratios of 0.4, 0.2, 0.1,

and 0.067, respectively. For a given fiber volume fraction, addition of 2wt% MAPP led to an increase in tensile moduli and strengths of roughly 3-7% and 3-9%, respectively, compared to SLF/PP/EPDM composites with no coupling agent. For a fixed amount of MAPP (2wt%), the relative improvement in mechanical properties generally decreased with increasing SLF weight fraction since the coupling agent must be distributed over a much larger total fiber surface area. Similarly, the composite flexural moduli and strengths increased by 4-9% and 4-8%, respectively, relative to composites prepared without MAPP. Moreover, composites fabricated with 2wt% MAPP displayed a profound improvement (37-78%) in impact energy absorption versus analogous composites with no coupling agent; clearly, use of MAPP provides better fiber/matrix interfacial adhesion and correspondingly more impact energy dissipation. This suggests that MAPP may be used to enhance SLF/PP/EPDM fracture properties for applications where improved energy absorption is of paramount importance (i.e., impact and perhaps crash). Furthermore, addition of 2wt% MAPP increased the composites' heat deflection temperatures (HDTs) by roughly 3.5ºC. A modest increase in HDT can greatly facilitate composite manufacturing by permitting demolding of parts at elevated mold temperatures, thus reducing requisite cool-down times.

Lastly, scanning electron microscopy was used to examine the fracture surfaces of select tensile, bending and impact specimens. The SLF/PP/EPDM failure mechanisms included microvoid nucleation/growth, matrix crazing, matrix cracking, fiber/matrix debonding, SLF pullouts, and SLF brash tensile fractures. Addition of MAPP arguably delays the onset of failure due to improved fiber matrix adhesion associated with the formation of covalent bonds between MAPP and the SLF fiber surfaces, anchoring MAPP to the fibers, combined with the MAPP polymer chain entanglement within the PP/EPDM matrix. These results suggest that

SLF/PP/EPDM composites modified with 2%wt MAPP may serve as a low-cost viable alternative to other natural fiber thermoplastic composites. In the future, this work may be extended to determine the MAPP/SLF ratio necessary to optimize composite mechanical properties for a given fiber loading. In general, differences in natural fiber characteristic sizes, surface chemistries, and surface morphologies make direct comparisons between two different natural fiber composite systems problematic. In addition, MAPP concentrations, MAPP/fiber surface area ratios, MAPP molecular weights, PP/EPDM ratios and molecular weights, and other similar factors all play a crucial role in quasi-static and dynamic composite bulk properties.

2.8 References

[1] Nabi-Saheb B, Jog J.P, Natural fiber polymer composites: A review. Adva in Poly Tech 1999;18(4):351-363.

[2] Daghigh V, Khalili SMR, Eslami-Farsani R. Creep behavior of basalt fiber-metal laminate composites. Comp Part B 2016;91:275-282.

[3] Behnia S, Daghigh V, Nikbin K, Fereidoon A, Ghorbani J. Influence of stacking sequence and notch angle on the Charpy impact behavior of hybrid composites. Mech Comp Mater 2016;52:489-496.

[4] Khalili SMR, Daghigh V, Eslami Farsani R. Mechanical behavior of basalt fiber-reinforced and basalt fiber metal laminate composites under tensile and bending loads. J Reinf Plastics Comp 2011;30(8):647-659.

[5] Eslami-Farsani R, Khalili SMR, Daghigh V. Charpy impact response of basalt fiber reinforced epoxy and basalt fiber metal laminate composites: Experimental study. Int J Damage Mech, 2014;23(6):729-744.

[6] Gurunathan T, Mohanty S, Nayak SK. A review of the recent developments in biocomposites based on natural fibres and their application perspectives. 2015;77:1-25.

[7] Malkapuram R, Kumar V, Yuvraj SN. Recent development in natural fibre reinforced polypropylene composites. J Reinf Plast Comp 2008; 28:1169-89.

[8] Wambua P, Ivens J, Verpoest I. Natural fibres: can they replace glass in fibre reinforced plastics. Comp Sci Tech 2003;63:1259-64.

[9] Cheung H-Y, Ho M-P, Lau K-T, Cardona F and Hui D. Natural fibre-reinforced composite for bioengineering and environmental engineering applications. Compos Part B 2009;40:655-663.

[10] Kandarp Bhatt, Potential for meeting the EU new passenger car CO_2 emissions targets, M.Sc thesis, Massachusetts Institute of Technology, Sep. 2010.

[11] Khalili SMR, Eslami-Farsani R, Rafiezadeh S. An experimental study on the behavior of PP/EPDM/JUTE composites in impact, tensile and bending loadings. J Reinf Plastics Comp 2011;30(16):1341-1347.

[12] Khoathane MC, Vorster OC, Sadiku E.R. Hemp fiber-reinforced 1-Pentene/Polypropylene copolymer: The effect of fiber loading on the mechanical and thermal characteristics of the composites. J Reinf Plastics Comp 2008;27(14):1533-1544.

[13] Niu P, Liu B, Wang X, Yang J, Study on mechanical properties and thermal stability of polypropylene/hemp fiber composites. J Reinf Plastics Compos 2011;30(1):36-44.

[14] Ruksakulpiwat Y, Sridee J, Suppakarn N, Sutapun W. Improvement of impact property of natural fiber-polypropylene composite by using natural rubber and EPDM rubber. Comp Part B 2009;40:619-622.

[15] Du Y, Wu T, Yan N, Kortschot MT, Farnood R. Fabrication and characterization of fully biodegradable natural fiber-reinforced poly(lactic acid) composites. Comp Part B 2014;56:717-723.

[16] Nam TH, Ogihara S, Kobayashi S, Goto K, Effects of surface treatment on mechanical and thermal properties of jute fabric-reinforced poly(butylene succinate) biodegradable composites. Adv Comp Mater 2015;24(2):161-178.

[17] Yang HS, Wolcott MP, Kim HS, Kim S, Kim HJ, Effect of different compatibilizing agents on the mechanical properties of lignocellulosic material filled polyethylene bio-composites. Comp Struc 2007;79(3):369-375.

[18] Karmarkar A, Chauhan SS, Modak JM, Chanda M. Mechanical properties of wood–fiber reinforced polypropylene composites: Effect of a novel compatibilizer with isocyanate functional group. Comp Part A 2007;38(2):227-233.

[19] Kakoua CA, Arrakhiz FZ, Trokoureyb A, Bouhfid R, Qaiss A, Rodrigue D, Influence of coupling agent content on the properties of high density polyethylene composites reinforced with oil palm fibers. Mater Design 2014;63:641-649.

[20] Khimi S.R, Pickering K.L. The effect of silane coupling agent on the dynamic mechanical properties of iron sand/ natural rubber magnetorheological elastomers, Compos Part B 2016;90:115-125.

[21] Wang K, Addiego F, Laachachi A, Kaouache B, Bahlouli N, Toniazzo V, Ruch D. Dynamic behavior and flame retardancy of HDPE/hemp short fiber composites: Effect of coupling agent and fiber loading. Compos Struc 2014;113:74-82.

[22] El-Sabbagh A. Effect of coupling agent on natural fibre in natural fibre/polypropylene composites on mechanical and thermal behaviour. Comp Part B 2014;57:126-135.

[23] Granda L.A, Espinach F.X, Tarrés Q, Méndez J.A, Delgado-Aguilar M, Mutjé P. Towards a good interphase between bleached kraft softwood fibers and poly(lactic) acid. Comp Part B 2016;99:514-520.

[24] Sullins T, Pillay S, Komus A, Ning H. Hemp fiber reinforced polypropylene composites: The effects of material treatments. Comp Part B 2017;114:15-22.

[25] Daghigh V., Haghpanahi M., Nikbin K., Mechanical behavior of novel latania natural fiber reinforced PP/EPDM composites subjected to tensile loads, In: Proceedings of Aerospace Conference, University of Tehran, 2014.

[26] Nasihatgozar M, Daghigh V, Lacy Jr. T.E, Daghigh H, Nikbin K, Simoneau A. Mechanical characterization of novel latania natural fiber reinforced PP/EPDM composites, Poly Test 2016;56:321-328.

[27] Arrakhiz FZ., El-Achaby M, Benmoussa K, Bouhfid R, Essassi EM, Qaiss A, Evaluation of mechanical and thermal properties of Pine cone fibers reinforced compatibilized polypropylene. Mater Design 2012;40:528-535.

[28] Ta Yu, Chang-Mou Wu, Chen-Ju Wang & Syang-Peng Rwi**,** Effects of surface modifications on the interfacial bonding of flax/β-polypropylene composites. Compos Interf 2013;20(7):483-496 .

[29] Samat N., Marini CD, Maritho MA, Sabaruddin FA. Tensile and impact properties of polypropylene/microcrystalline cellulose treated with different coupling agents. Compos Interf 2013;20(7):497-506.

[30] Cerqueira EF, Baptista CARP, Mulinari DR. Mechanical behaviour of polypropylene reinforced sugarcane bagasse fibers composites. Procedia Eng 2011;10:2046-2051, 11th Inter Conf Mech Behavior Mater (ICM11).

[31] Arrakhiz FZ, Achaby MEl, Malha M, Bensalah MO, Fassi-Fehri O, Bouhfid R, Benmoussa K, Qaiss A, Mechanical and thermal properties of natural fibers reinforced polymer composites: Doum/low density polyethylene. Mater Design 2013;43:200-205.

[32] Joseph PV, Joseph K, Thomas S. Short sisal fiber reinforced polypropylene composites: the role of interface modification on ultimate properties. Compos Interf 2002:9(2):171-205.

[33] Quazi TH Shubhra, AKMM Alam and MA Quaiyyum, Mechanical properties of polypropylene composites: A review, Journal of Thermoplastic Composite Materials 2011:26(3):362-391.

[34] Singleton A.C.N., Baillie C.A., Beaumont P.W.R., Peijs T. On the mechanical properties, deformation and fracture of a natural fibre/recycled polymer composite. Compos Part B 2003;34:519-526.

[35] Sawpan MA, Pickering KL, Alan F. Analysis of mechanical properties of hemp fibre reinforced unsaturated polyester composites. J Comp Mater 2013;47(12):1513-1525.

[36] Crawford RJ. Plastics Engineering, Oxford, Butterworth Heinemann, 1998.

[37] Bledzki AK, Mamuna AA, Feldmann M. Polyoxymethylene composites with natural and cellulose fibres: Toughness and heat deflection temperature, Compos Sci Tech 2012;72(15):1870-1874.

[38] Mohanty AK, Misra M, Drzal LT. Natural Fibers, Biopolymers, and Biocomposites**,** Chapter. 3, CRC Press.

[39] Asgari M, Masoomi M. Thermal and impact study of PP/PET fibre composites compatibilized with Glycidyl Methacrylate and Maleic Anhydride. Compos Part B 2012;43(3):1164–1170.

[40] Loureiro N.C., Esteves J.L., Viana J.C., Ghosh S., Development of polyhydroxyalkanoates/poly(lactic acid) composites reinforced with cellulosic fibers. Comp Part B 2014;60:603-611.

[41] Du, Y., Zhang, J., Toghiani, H., Lacy, T. E., Xue, Y., Horstemeyer M.F., Pittman, CU. Kenaf bast fiber bundle-reinforced unsaturated polyester composites. IV: Effects of fiber loadings and aspect ratios on composite tensile properties, Forest Products J 2010;60(3):289-295.

[42] Arthur Koehler, Causes of brashness in wood t, technical bulletin No. 342, Jan. 1933, USA department of agriculture, Washington, D.C. http://naldc.nal.usda.gov/naldc/download.xhtml?id=CAT86200336&content=PDF

[43] Wong KJ, Nirmal U, Lim BK. Impact behavior of short and continuous fiber-reinforced polyester composites. J Reinf Plast Comp 2010;29(23):3463-3474.

CHAPTER III

HEAT DEFLECTION TEMPERATURES OF MULTISCALE BIO-NANO-COMPOSITES USING EXPERIMENTS AND MACHINE LEARNING PREDICTIONS

3.1 Abstract

Biocompatibility, biodegradability, and enhanced properties are remarkable features of bio-composites designed to reduce and replace conventional non-biodegradable polymeric materials. Therefore, it is crucial to propose reliable yet economically efficient new bio-composites. Nano-clays (NCs), short latania fibers (SLFs) and new bio fillers, e.g. pistachio shell powders (PSPs) and date seed powders (DSPs), were used to reinforce poly(propylene)/ethylene-propylene-diene-monomer (PP/EPDM) composites. Heat deflection temperature (HDT) tests were conducted. Then a machine learning (ML)-based prediction tool, the K-Nearest Neighbor Regressor (KNNR), was used to investigate HDTs of various bio-composite compositions. KNNR was employed in this study versus the Decision Tree Regressor (DTR) and Adaptive Boosting Regressor (ABR) ML approaches utilized in the previous study by Daghigh *et al*. [1] for fracture toughness predictions. Furthermore, in contrast to other natural fiber composites, SLF composites have been seldom investigated. Different contents of SLFs, NCs, macro-sized PSPs and macro-sized DSPs were added to the PP/EPDM to investigate the combined effects of bio-fiber, nano-particulate, and macro bio-particulate reinforcements. This research helps develop an understanding of how such low-cost bio-reinforcements influence the HDT of PP/EPDM composites. ML predictions were used to develop lightweight, cost-effective materials

where their use temperatures can be improved. KNNR ML analysis suggested the key factor influencing HDT are SLFs, NCs, DSPs, and PSPs in the order stated.

3.2 Introduction

Many end-use applications in military, medicine, power and energy, and transportation markets attest to the seminal importance of lightweight composites. Global warming and demands for eco-friendly products have motivated the use of bio-composites and natural reinforcements to provide a driving force for sustainable solutions [1-2]. Basalt natural fibers [3-6], hemp, kenaf and flax [7-10], jute [11-12], sisal and coir [13-14], curaua [15], coconut [16], pineapple leaf [17], *etc*. have all been used to reinforce polymer matrix composites. However, reports documenting latania natural fiber-reinforced composites are rare [2, 18]. Latania is a genus of an abundant flowering plant in the palm tree family originating in the Mascarene Islands in the western Indian Ocean. Latania fibers are the skin fibers provided from the phloem or the bast surrounding the plant's stem [18].

In the literature, nanoparticles or microfillers have been added to reinforce composites for final cost and shrinkage reductions, elastic moduli enhancement, performance improvement at higher temperatures, greater hardness, impact improvement, wear resistance, and machinability enhancement [4, 19]. As the average particle size drops for a fixed filler volume fraction, the total surface area of the filler sharply rises. Nano-sized particles have huge specific surface areas. They cause liquid resin viscosities to rise dramatically with increasing filler volume fractions and cause composite properties to drastically change [20]. Large particles are easier to make and to blend; however, they do not influence most bulk properties in the same way as much smaller particles.

Increasing demands to enhance the thermal/mechanical performance of green structural composite materials has led to investigations of new natural reinforcing fillers. Natural powder fillers have received less attention compared to prevalent synthetic fillers such as silica and calcium carbonate [4, 18, 21]. In the present work, new pistachio shell powders (PSPs) and date seed powders (DSPs) are introduced for the first time as filler reinforcements. PSPs, DSP, as well as nano-clays (NCs) and short latania fibers (SLFs) were added into poly(propylene)/ethylene-propylene-diene-monomer (PP/EPDM) composites. These fillers may improve composite thermal and mechanical properties, reduce cost, and enhance recyclability [22]. Since pistachio shells and date seeds are ligno-cellulosic agricultural wastes, their use as reinforcements is a green application. They have no current important industrial usages and are normally incinerated or dumped. Burning agricultural residues may cause environmental air pollution, soil erosion and reduced soil biological activity [23-24].

A few studies have reported thermal/mechanical properties of bio-filler reinforced composites. Ghabeer et al. [21] studied the thermal and mechanical characterization of chicken eggshell/PP composites prepared by melt extrusion containing 10-40wt% untreated and stearic acid-treated eggshells. The crystallization temperature of the composite was increased by adding 10wt% eggshell into PP. However, the impact strength decreased after incorporating eggshell into PP. Essabir et al. [25] studied the effect of both particle size and loading on the mechanical and thermal properties of PP composites reinforced with particulated Argan nut-shells (ANs). Different size ranges from less than 125 μm to a maximum 360 μm diameter were selected. Scanning electron microscopy (SEM), Fourier Transform Infrared Spectroscopy (FT-IR), Thermo Gravimetric Analysis (TGA), Differential Thermal Analysis (DTA) and tensile tests were used to characterize PP composites containing 10, 15, 20 and 25wt% AN particles.

Young's modulus increased up to 43% with particle addition versus neat PP. Also, decreasing AN particle sizes raised the modulus. The composite thermal stability temperature slightly decreased (256–230°C) with particle loading from 10 to 25wt% compared with neat PP (258°C). Later, Essabir et al. [26] used almond shell (AS) particles (100 μm diameter) to reinforce PP. Particle contents of 5, 10, 15, 20, 25, 30wt%, with and without the compatibilizer styrene–(ethylene–butene)–styrene tri-block copolymer grafted with maleic anhydride (SEBS-g-MA), were added to study composite mechanical, thermal and rheological properties. The AN particle addition (30wt%) with MA compatibilizer led to a 35% Young's modulus increase. Initial thermal decomposition temperatures also increased upon adding AS particles.

The key objective of the research herein is to study the influence on thermal properties of adding short latania fibers (SLFs), nano-clays (NCs), pistachio shell powders (PSPs), and fractal date seed particles (DSPs) to poly(propylene)/ethylene-propylene-diene-monomer (PP/EPDM) composites, aided by machine learning (ML) predictions. Maleated polypropylene (MAPP) (2 wt%) was added to all composites to increase the interfacial adhesion between the matrix and each lignocellulosic ingredient. Section 3.2 describes the experimental procedure, and Section 3.3 explains the ML prediction of the composites.

3.3 Experimental Procedure

3.3.1 Materials

In this paper, we used PP/EPDM, MAPP and latania fibers from Ref. [2]. Before and after being chopped, latania fibers are shown in Figures 3.1 [2]. Cloisite 20A nano-clay powders were used (d-Spacing (001) of 31.5 A^o). SEM images were used to assess the morphological structure of pistachio shells and date seeds, respectively. Figures 3.1c and 1d depict the pistachio shell and date seed cross-sections, respectively. The morphological structure appears relatively

constant through the cross-sections based upon SEM imaging (Figures 3.1c and 3.1d). PSPs and the DSPs were produced by grinding pistachio shells and date seeds and using sieve standards to obtain the powders within the range of 5-105 μm. SEM pictures of typical ground PSPs and DSPs are shown (Figures 3.1e and 1f).

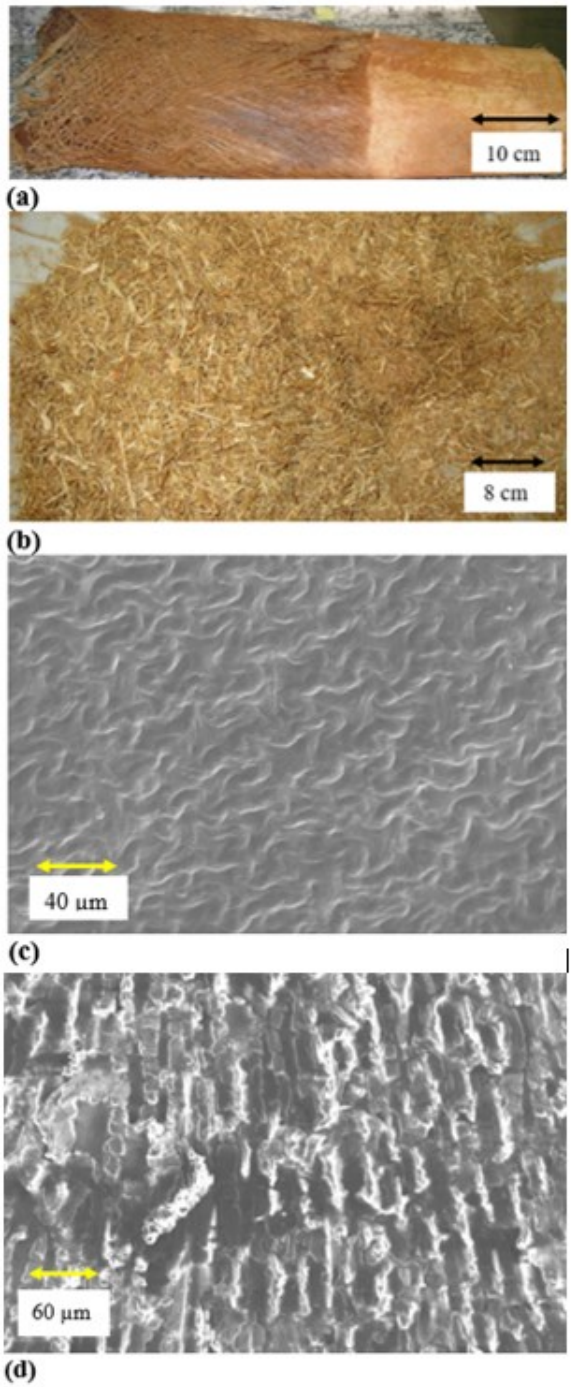

Figure 3.1 (a) Latania fibers before being chopped; (b) Latania fibers after being chopped; (c) SEM picture of a pistachio shell sliced through the thickness (magnification of 1.1kx); (d) SEM picture of a date seed sliced through the thickness (magnification of 521x); (e) SEM picture of a typical pistachio shell powder particle (magnification of 7 kx); (f) SEM picture of a typical date seed powder particle (magnification of 3.61 kx).

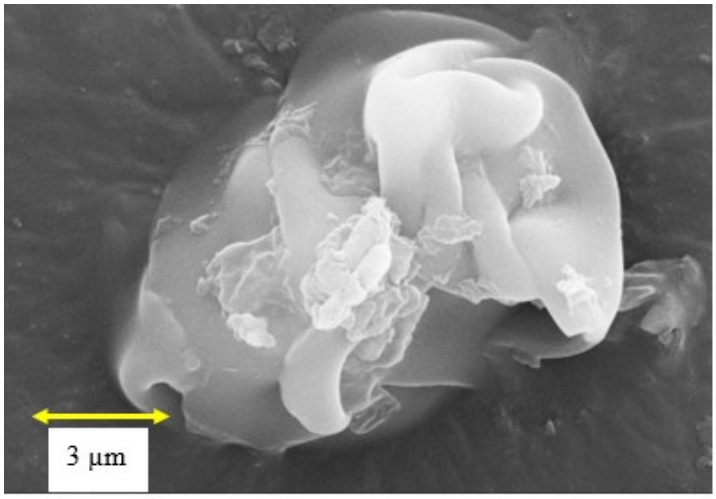

(e)

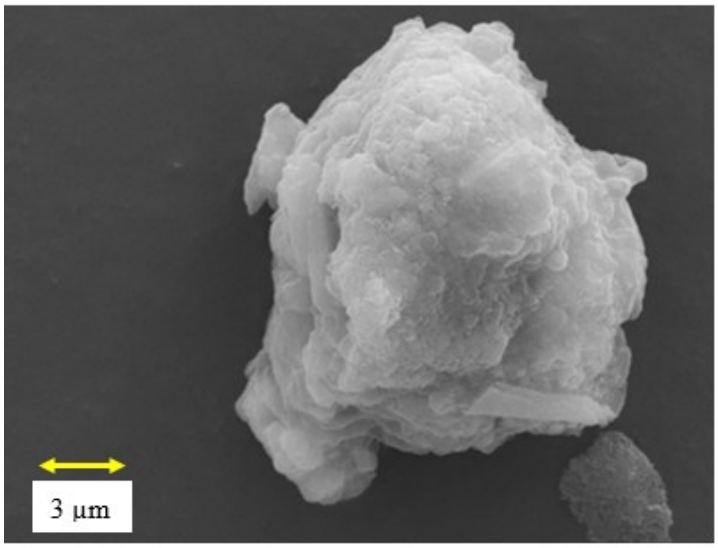

(f)

Figure 3.1 (continued)

3.3.2 Specimen Preparation

Latania fibers were cut into ~10 mm-length short fibers using a guillotine machine (Wiser A-8992 Altaussee, Germany). These were shortened to ~2 mm-lengths when blended in a counter-rotating twin screw extruder with PP/EPDM. Batches containing 0, 5, 10, 20 and 30wt%

of SLF, 0, 1, 3 and 5wt% of NCs, 0, 1, 3 and 5wt% of PSPs, 0, 1, 3 and 5wt% of DSPs were employed to fabricate various combinations of PP/EPDM composites reinforced with SLFs, NCs, PSPs and DSPs. Each batch was prepared using a single extrusion of PP/EPDM into which SLFs, NCs, PSPs and/or DSPs in the appropriate wt% have been added. The extrusions were carried out at T=180°C and by a 60 RPM dual (twin) screw extruder (Collins Extrusions Ltd, Birmingham, UK). To avoid thermal decomposition or burning of the vulnerable lignocellulosic reinforcements (SLFs, DSPs and PSPs), the extruder strands were pulled into a cool water bath. Upon cooling to room temperature, pelletization was performed on these blends followed by drying them out at 80°C for 24 h. Finally, an injection molding machine at T=165-180°C was employed to produce heat deflection temperature (HDT) test specimens [2].

3.3.3 Heat Deflection Temperature (HDT)

Each test was performed according to ASTM D-648 (HDT-Tester HV-2000A, GoTech Co., Taiwan). At least three HDT test repetitions were conducted for each material composition. An imposed stress (1.82 MPa), a temperature ramp rate (2ºC/min), and a maximum deflection (0.25 mm) were applied during these tests. Forty-nine compositions were manufactured. Some of the composites' compositions in each batch and the pertinent HDT values are tabulated in Table 1. A full listing of the input and output values shown partially in Table 1 is given in Appendix (Table A.1).

Table 3.1 The representative composition of each composite blend given and the pertinent experimental HDT values

Input (wt%)	Input (wt%)	Input (wt%)	Input (wt%)	Input (wt%)	Output (°C)
PP/EPDM	SLF	PSP	DSP	NC	HDT
100	0	0	0	0	65.1
97	0	3	0	0	68.9
95	0	5	0	0	69.4
92	5	0	3	0	74.7
90	5	0	5	0	76.3
95	5	0	0	5	77.3
90	10	0	0	0	74
87	10	0	3	0	75.4
80	10	5	0	5	80.5
84	10	3	3	0	79
80	20	0	0	0	79.1
77	20	3	0	0	83.1
75	20	0	5	0	82.3
70	30	0	0	0	79.6
60	30	5	0	5	86
74	30	0	3	3	83.1
74	30	3	3	0	84.9

3.4 Machine Learning-Based Prediction

The K-Nearest Neighbor Regressor (KNNR), an ML approach, was employed to predict the HDT value given for the composition parameters [27]. This ML approach is different from those used in our previous study (Decision Tree Regressor (DTR) and Adaptive Boosting Regressor (ABR) ML approaches) for fracture toughness predictions [1]. K-Fold cross validation was used as an evaluation technique to better estimate the performance of this approach [28]. Following a brief introduction to these methods, the results of experiments will be discussed.

3.4.1 K-Nearest Neighbor Regression

K-Nearest Neighbor (KNN) is an algorithm first proposed by Fix et al. in 1951 [29]. Since then, KNN's variations have been applied to text classification, facial recognition and many other problems [30]. KNN makes a prediction about an unknown point according to the *K* number of data points that are closest to that point. The prediction can be a data point classification of an unknown class, or it can be a regression of an unknown value, associated with that data point [27].

Given a data set of *n* covariates, $X = x_1, x_2, \ldots, x_n$, and their corresponding response values, $Y = y_1, y_2, \ldots, y_n$, we intend to predict the response value of a given covariate *x*, where *x* is not present in our data set X. The steps employed by the KNNR algorithm can be summarized as follows:

1. Calculate the distances d_i of each data point x_i from *x* by using the Euclidean distance:

$$d_i(x_i, x) = \sqrt{(x_1 - x)^2 + (x_2 - x)^2 + \cdots + (x_n - x)^2} \tag{3.1}$$

2. Sort the distances d_i in an increasing order and among all the points in the data set. Then, choose the *k* points that are closest to *x* and put them in a set of nearest neighbors, *C*.
3. The estimated value of the response value of $\hat{y}$ (here is HDT value) is calculated by averaging the response values of data points in set C.

$$\hat{y} = \frac{1}{k} \sum_{y_i \epsilon \, \mathrm{C}} y_i \tag{3.2}$$

In Step 3 of this algorithm, the inverse of distances and Gaussian distribution are used as weights for calculating the mean value. In such a case, the closer points are assumed to be more influential on the estimated response value ($\hat{y}$). Nonetheless, the uniform distribution of weights is more common.

3.4.2 K-Fold Cross Validation

To assess the capability of a model in generalization, the data set is randomly split into *K* segments of the same size. As depicted in Fig. 3.2 across *K* iterations, the training is performed using *K*- 1 segments of the data set and the testing is performed on the remaining segment of the data. This approach is particularly useful in situations where a limited set of data is available as in the case of our study. Following the K-Fold cross validation approach, an estimation of the model performance is used to predict the outcomes of a given data set that has not been available during the model training.

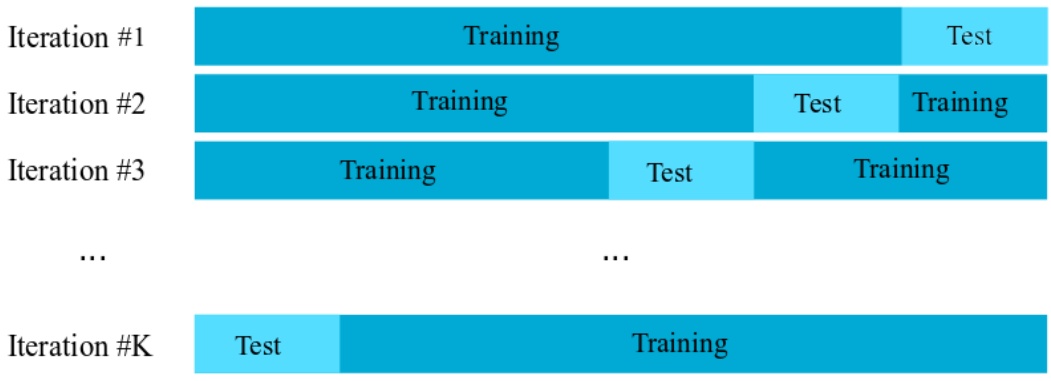

Figure 3.2 The visualization of split segments in each of the K iterations.

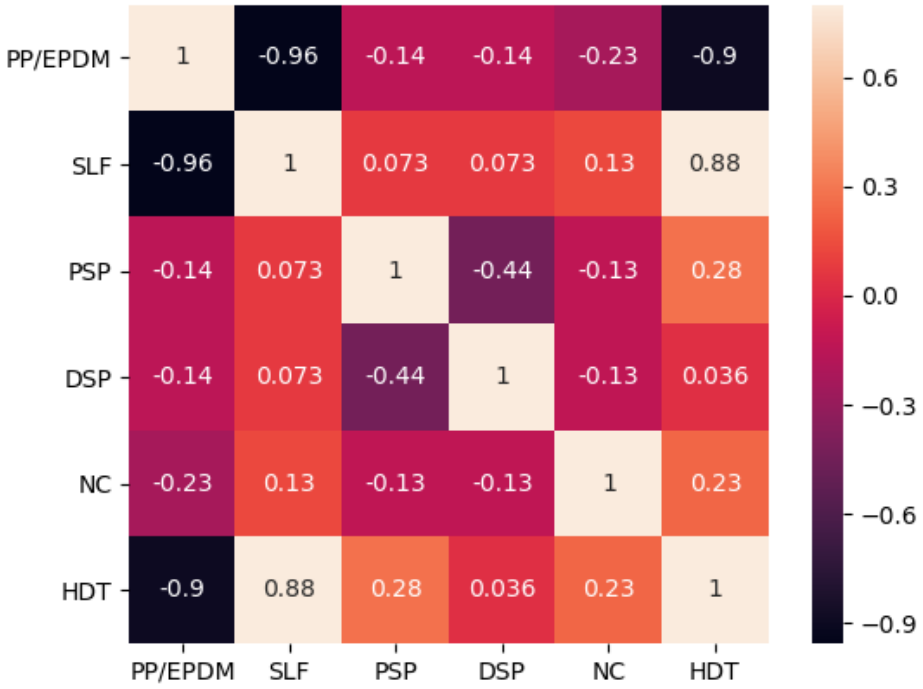

Figure 3.3 Correlation of the features (PP/EPDM, SLF, PSP, DSP and NC) and HDT

Table 3.2 Comparison of performance evaluations using two KNNR methods: UD and ID

Neighbors (k)	UD_R^2	ID_R^2	UD_MAE	ID_MAE	UD_RMSE	ID_RMSE	UD_RMSE/AV (%)	ID_RMSE/AV (%)
2	0.882	0.892	1.348	1.372	1.815	1.722	2.311	2.194
3	0.900	0.898	1.400	1.240	1.7355	1.583	2.209	2.017
4	0.892	0.859	1.283	1.461	1.704	1.884	2.170	2.400
5	0.843	0.884	1.403	1.360	1.691	1.685	2.153	2.146
6	0.867	0.857	1.513	1.463	2.002	1.813	2.550	2.310

UD: Uniform distribution of weights
ID: Inverse of distances of weights.

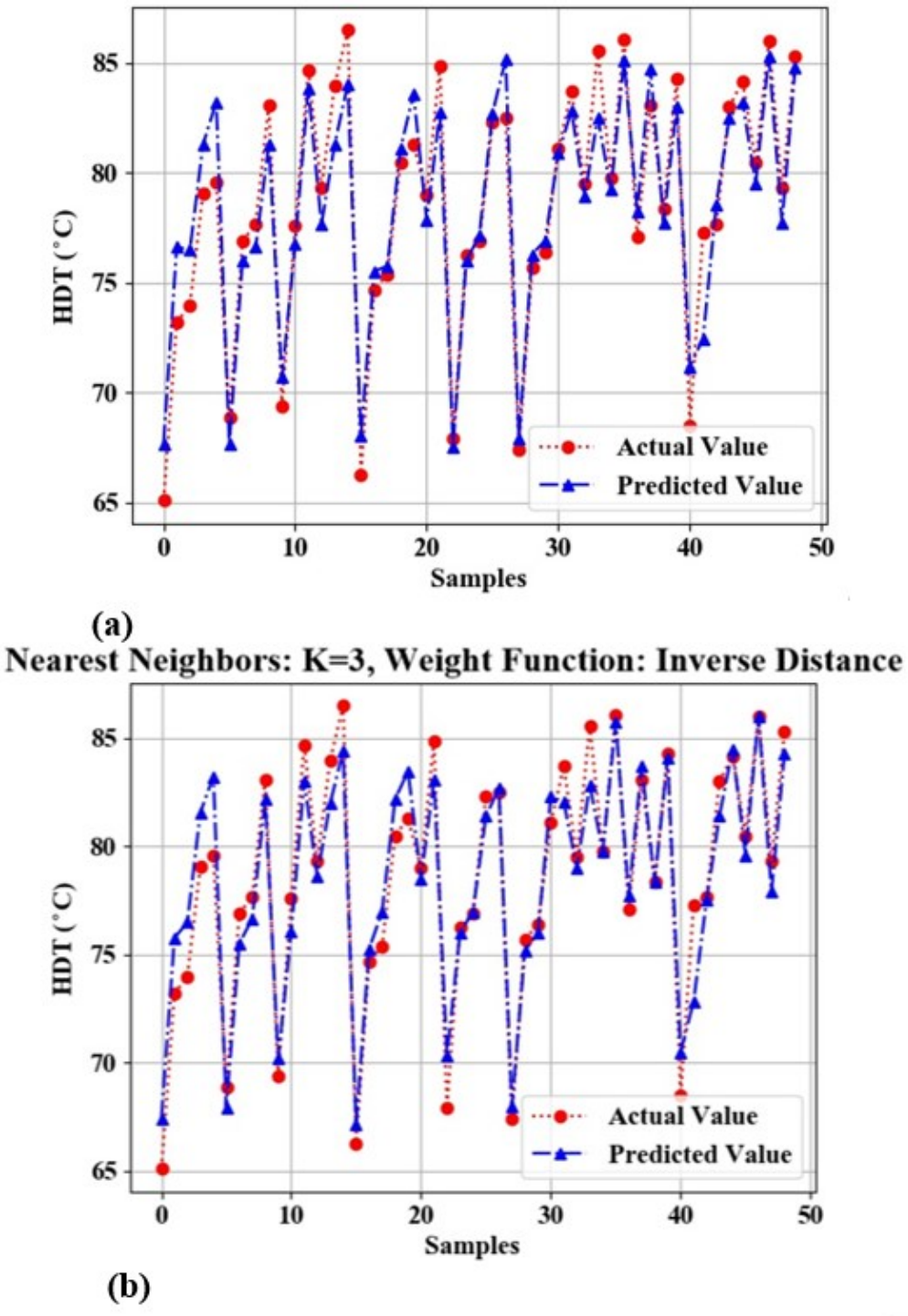

Figure 3.4 Actual (in red) versus predicted (in blue) HDT values (horizontal axis represents the number of samples and the vertical axis represents the HDT values in centigrade degrees) (K=3).

3.4.3 Performance Evaluation Metrics

To evaluate the performance of this ML approach, three evaluation metrics are considered. The following are the three commonly reported metrics of regression models:

Mean Absolute Error (MAE): calculated by Equation (3.3) from the *m* predicted samples:

$$MAE = \frac{1}{m}\sum_{i=1}^{m}\left|\hat{y}_i - y_i\right| \tag{3.3}$$

where $\hat{y}_i$ is the predicted value, and y_i is the actual value of *i-th* sample in the test set.

Root Mean Squared Error (RMSE): calculated by equation (3.4):

$$RMSE = \sum_{i=1}^{m}\sqrt{\frac{1}{m}\left(\hat{y}_i - y_i\right)^2} \tag{3.4}$$

where the parameters are the same as in the MAE. However, the RMSE is more sensitive to large errors. In other words, if the errors of the predictions have higher variance, then RMSE would report a greater value compared to a more uniformly distributed error.

R-Squared: R^2 is defined as below:

$$R^2 = 1 - \frac{\sum_{i=1}^{m}\left(\hat{y}_i - y_i\right)^2}{\sum_{i=1}^{m}\left(y_{ave} - y_i\right)^2} \tag{3.5}$$

where y_{ave} is the mean of the actual response values (y_i). More accurate predictions result in a value of R^2 closer to 1. Table 3.2 shows a comparison of performance evaluations using two KNNR methods: Uniform distribution of weights (UD) and Inverse of distances of weights (ID) indicating the acceptable accuracy of the ML-based-predictive model used in this study. Comparing R^2, *MAE*, *RMSE*, *RMSE/AV* for each *K* in Table 3.2 suggests that choosing *K*=3 offers the best model for HDT predictions.

3.5 Results and Discussion

3.5.1 Measurement of Heat Deflection Temperature (HDT)

The ASTM D648 method was used for HDT testing in this work. HDT is measured as a temperature at which the specimen is deflected under a specific flexural load indicating short-term stiffness [31] of the materials at elevated temperatures. Matrix glass transition temperatures, matrix hardness, and the stiffness are factors that can seriously affect the HDT amplitudes [32]. More than 30% of all polymeric components in the world are produced through injection molding [33]. The temperature of the injection mold is often about 200ºC or higher during the production, and the temperature of the mold at the time of removal should be below the HDT. Obviously, increasing the HDT has a significant effect on reducing the production time per component and the cost of mass production.

Fig. 3.3 shows the correlation of data and the role of each constituent on the HDTs. The meaningful associations in this figure are those of HDT (as an output) with PP/EDPM, SLF, PSP, DSP and NC (each as an input). Positive or negative values show the direct or reverse associations between the output and each input. Fig. 3.4 shows the actual and predicted data using the ML method (Neighbor number *K*=3). Full representation of Fig. 3.4 (*K*= 2 to 6) is shown in Fig. A.3.1 (see Appendix). As can be seen in Fig. 3.3, the correlation of HDT value and

SLF wt% value is 0.88. Thus, SLF has the highest effect on HDTs compared to the wt% values of PSP, DSP and NC. Improvement in the composite flexural stiffness is likely the main reason behind an increase in HDTs. Similar enhancements in HDT upon the fiber addition have been reported by other researchers [2, 32, 34]. Furthermore, Daghigh *et al.* [2] showed that there is a correlation between tensile/flexural stiffness and HDT values upon SLF additions to PP/EPDM composites. The correlation between HDT and PSP is 0.28 indicating PSP's second rank of the reinforcement to produce HDT improvement. A number of studies have been conducted to show the effect of micro and nano fillers on the stiffness of composites. A rigid phase addition into a polymer matrix can enhance the composite stiffness [4, 18, 35-38]. Shuhadah and Supri [39] reported that adding egg shell powers (an average particle size of 63 μm) into polymer matrix composites raised the stiffness.

By and large, adding NCs to composites can enhance stability and permeability properties compared with the bulk polymer [3, 40-42]. If hybrid composites can exert a synergy between bio-based natural fibers in a nano-reinforced polymer, this may provide improved properties with environmental advantages [3]. The current study shows that NCs addition into PP/EPDM composites has a significant effect on the HDT enhancement (The correlation is 0.23; see Fig. 3.3). The NCs have high surface areas which can restrict polymer segmental motion at their solid surfaces, effectively reducing flow in these surface regions and raising HDTs.

A high-quality specific surface offered by nanoparticles requires a good interaction between nanoparticles and the polymer matrix. NC polymer composites can be defined into three general types of NC/polymer interactions which vary with the degree of exfoliation achieved: (a) typical composites, in which the NC performs as a conventional small-sized filler; (b) intercalated nanocomposites, where some portion of polymer enters into the gallery spacing

between the clay layers; and (c) exfoliated nanocomposites, where the bulk polymer surrounds highly exfoliated clay platelets [43]. In fact, the well-ordered parallel platelets of NC particles need to be separated to get a high-quality interaction. Increasing the d-spacing between the NC platelets facilitates the required interaction between the clay and the polymer chains [44-46].

There is an interesting difference between the effect of PSP and DSP on the HDT values. PSP exerts a stronger HDT enhancement than DSP. It is likely due to the difference between the hardness of PSP and DSP. PSP is harder than DSP. In addition, a slower value of change with temperature in PSP hardness versus DSP hardness may be another reason behind higher effectiveness of PSP than DSP on HDT. Bledzki et al. [32] reported that long cellulose fiber-reinforced polyoxymethylene (POM) composites enjoyed a higher HDT than abaca fiber-reinforced POM composites, due to slower change in the cellulose fibers hardness versus abaca fibers. In addition, stronger bonding between PSP and the matrix versus bonding between DSP and the matrix may be another reason behind greater HDT enhancement properties of PSP versus DSP.

The inclusion sizes are large (SLF length ~2 mm, DSP diameter ~70 um, PSP diameter ~5-105 um) relative to the ASTM test thickness dimension of 6.3 mm. Thus, having a representative composite composition throughout the thickness, with a suitable number of all inclusions and their orientations independent of the thickness, is unlikely to be possible during HDT testing. Far thicker specimens are required to assure this. For example, if the HDT test were conducted on specimens that were 10x or 100x the ASTM standard thickness and size, and with representative length and width, at some point the specimens would be of their material composite representative. Subsequently, the ML method might end up with different predicted results. Nevertheless, the ASTM test and specimen size are standard for the field and used for

these inclusion sizes. For instance, Essabir et al. [25] used three different particle size ranges, while the mechanical and thermal specimen sizes were the same for all particle size ranges. This article is among the few articles which investigated the effect of particle size. However, the specimen size is standard (ISO 527-1) and the same for all samples. Therefore, to the best of the authors' knowledge, no literature discusses relating particle size to the needed specimen size with a representative material in the smallest (usually thickness) dimension.

This study suggests PSPs and DSPs could be promising low-cost reinforcements for composites while consuming agricultural wastes. These particles are compatible with PP/EPDM and probably a myriad of other matrix systems. If the possible negative impacts of these sized particles on high and low cycle fatigue, creep, and impact strength of composites can be tolerated in selected end uses, their very low cost could warrant their use.

3.6 Conclusions and Recommendations

An approach based on machine learning (ML) predictions was used for predicting the thermal behavior of a new set of hybrid composites containing short latania fibers (SLFs), nano-clays (NCs), date seed powders (DSPs) and pistachio shell powders (PSPs) reinforcements. Various weight fractions of PP/EPDM matrix polymer, SLFs, NCs, PSPs, and DSPs were blended using a counter rotating twin-screw extruder. All combinations contained 2 wt% of MAPP to enhance the interfacial properties. The heat deflection temperatures (HDTs) of these composites depended in a complicated manner on properties and relative sizes of each ingredient (SLF, NC, DSP and PSP) and their interactions. About 50 different composites with various constituent combinations were fabricated and their HDTs were determined. This data was used to establish an ML-based prediction model using the K-Nearest Neighbor Regressor (KNNR)

method. A cross validation was successfully conducted to show the accuracy of the ML-based-predictive model. SLFs, PDPs and NCs were found to be the most influencing factors, respectively, at enhancing the HDT. The DSPs showed the smallest effect on HDT values likely due to its less hardness and weaker interfacial adhesion with the matrix. Hence, they promoted less increase in stiffness. This research is an illustration of how machine learning can be employed routinely to facilitate the improved properties and costs when substituting bio-derived components into materials. This research will continue to investigate other thermal properties such as dynamic mechanical analysis (DMA) and thermogravimetric analysis (TGA). The roles of SLF, NC, PSP and DSP in the thermal property enhancement (HDT, DMA and TGA) will be compared and discussed to get an in-depth understanding of thermal behaviors of this set of bio-nano-composites.

3.7 References

[1] V. Daghigh ,T. E. Lacy Jr., H. Daghigh, G. Gu, K. T. Baghaei, M. F. Horstemeyer, C. U. Pittman Jr., "Fracture toughness machine learning predictions on short fiber, nano- and micro-particle reinforced composites," *Composite Structures,* vol. Submitted, 2019.

[2] V. Daghigh, T. E. Lacy Jr., C. U. Pittman Jr., H. Daghigh, "Influence of maleated polypropylene coupling agent on mechanical and thermal behavior of latania fiber-reinforced PP/EPDM composites," *Polymer Composites,* vol. doi.org/10.1002/pc.24752, 2018.

[3] R. Eslami-Farsani, S.M.R. Khalili, Z. Hedayatnasab, N. Soleimani, "Influence of thermal conditions on the tensile properties of basalt fiber reinforced polypropylene–clay nanocomposites," *Materials and Design,* vol. 53, pp. 540-549, 2014.

[4] R.E. Farsani, S.M.R. Khalili, V. Daghigh, "Charpy impact response of basalt fiber reinforced epoxy and basalt fiber metal laminate composites: experimental study," *International Journal of Damage Mechanics,* vol. 23, no. 6, pp. 729-744, 2014.

[5] V. Daghigh, S.M.R. Khalili, R.E. Farsani, "Creep behavior of basalt fiber metal laminate composites," *Composites Part B: Engineering,* vol. 91, pp. 275-282, 2016.

[6] S. Behnia, V. Daghigh, K. Nikbin, A.B. Fereidoon, J. Ghorbani, "Influence of stacking sequence and notch angle on the Charpy impact behavior of hybrid composites," *Mechanics of Composite Materials,* vol. 52, no. 4, pp. 489-496, 2016.

[7] G. Cicala, G. Cristaldi, G. Recca, G. Ziegmann, A. El-Sabbagh, M. Dickert, "Properties and performances of various hybrid glass/natural fibre composites for curved pipes," *Materials and Design,* vol. 30, no. 7, pp. 2538-2542, 2009.

[8] N. Saba, M.T. Paridah, M. Jawaid, "Mechanical properties of kenaf fibre reinforced polymer composite: a review," *Construction and Building Materials,* vol. 76, pp. 87-96, 2015.

[9] A. El-Sabbagh, L. Steuernagel, G. Ziegmann, "Processing and modeling of the mechanical behavior of natural fiber thermoplastic composite: flax/polypropylene," *Polymer Composites,* vol. 30, no. 4, pp. 510-519, 2009.

[10] A. El-Sabbagh, L. Steuernagel, G. Ziegmann, "Characterisation of flax polypropylene composites using ultrasonic longitudinal sound wave technique," *Composites Part B: Engineering ,* vol. 45, no. 1, pp. 1164-1172, 2013.

[11] M.A. Gunninga, L.M. Geevera, J.A. Killiona, J.G. Lyonsa, C.L. Higginbothama, "Mechanical and biodegradation performance of short natural fibre polyhydroxybutyrate composites," *Polymer Testing ,* vol. 32, pp. 1603-1611, 2013.

[12] H.N. Dhakal, V. Arumugam, A. Aswinraj, C. Santulli, Z.Y. Zhang, A. Lopez-Arraiza, "Influence of temperature and impact velocity on the impact response of jute/UP composites," *Polymer Testing,* vol. 35, pp. 10-19, 2014.

[13] P. Wambua, J. Ivens, I. Verpoest, "Natural fibres: can they replace glass in fibre reinforced plastics?," *Composite Science and Technology,* vol. 63, no. 9, pp. 1259-1264, 2013.

[14] D. V. O. de Moraes, R. Magnabosco, G. H. B. Donato, S. H. P. Bettini, M. C. Antunes, "Influence of loading frequency on the fatigue behaviour of coir fibre reinforced PP composite," *Polymer Testing,* vol. 41, pp. 184-190, 2015.

[15] D.O. Castro, A. Ruvolo-Filho, E. Frollini, "Materials prepared from biopolyethylene and curaua fibers: composites from biomass," *Polymer Testing,* vol. 31, no. 7, pp. 880-888, 2012.

[16] C. Merlini, G. M.O. Barra, D. P. Schmitz, S. D.A.S. Ramôa, A. Silveira, T. Medeiros Araujo, A. Pegoretti, "Polyaniline-coated coconut fibers: structure, properties and their use as conductive additives in matrix of polyurethane derived from castor oil," *Polymer Testing,* vol. 38, pp. 18-25, 2014.

[17] U. Wisittanawat, S. Thanawan, T. Amornsakchai, "Mechanical properties of highly aligned short pineapple leaf fiber reinforced – nitrile rubber composite: effect of fiber content and Bonding Agent," *Polymer Testing,* vol. 35, pp. 20-27, 2014.

[18] M. Nasihatgozar, V. Daghigh, T. E. Lacy Jr., H. Daghigha, K. Nikbin, A. Simoneau, "Mechanical characterization of novel latania natural fiber reinforced PP/EPDM composites," *Polymer Testing,* vol. 56, pp. 321-328, 2016.

[19] S. Vigneshwaran, M. Uthayakumar, V. Arumugaprabu, R. D. Joel Johnson, S. Vigneshwaran, M. Uthayakumar, V. Arumugaprabu, R. D. Joel Johnson, "Influence of filler on erosion behavior of polymer composites: A comprehensive review," *Journal of Reinfroced Plastcis and Composites,* pp. 1-9, 2018.

[20] L. Sun, R. F. Gibson, F. Gordaninejad, J. Suhr, "Energy absorption capability of nanocomposites: A review," *Composites Science and Technology,* vol. 69, no. 14, pp. 2392-2409, 2009.

[21] T. Ghabeer, R. Dweiri, S. Al-Khateeb, "Thermal and mechanical characterization of polypropylene/eggshell biocomposites," *Journal of Reinforced Plastics and Composites ,* vol. 32, no. 6, p. 402–409, 2013.

[22] H. Ismail and R. Ramli, "Organoclay filled natural rubber nanocomposites: The effects of filler loadingand mixing method," *Journal of Reinforced Plastics and Composites,* vol. 27, no. 16-17, pp. 1909-1924, 2008.

[23] G. Tepić, T. Pejakov, B. Lalić, V. Vukadinović, S. Milisavljević, "The application of recycled aluminum and plastics in environmental protection," *Metalurgija,* vol. 52, no. 3, pp. 395-398, 2013.

[24] S.M. Lee, D.W. Cho, W.H. Park, S.G. Lee, S.O. Han, L.T. Drzal, "Novel silk/poly(butylenes succinate) biocomposites: the effect of short fiber content on their mechanical and thermal properties," *Composite Science and Technology,* vol. 65, no. 3-4, pp. 647-657, 2005.

[25] H. Essabir, E. Hilali, A. Elgharad, H. El Minor, A. Imad, A. Elamraoui, O. Al Gaoudi, , "Mechanical and thermal properties of bio-composites based on polypropylene reinforced with Nut-shells of Argan particles," *Materials and Design ,* vol. 49, pp. 442-448, 2013.

[26] H. Essabir, S. Nekhlaoui, M. Malha, MO. Bensalah, FZ. Arrakhiz, A. Qaiss, R. Bouhfid , "Bio-composites based on polypropylene reinforced with Almond Shells particles: Mechanical and thermal properties," *Materials and Design,* vol. 51, pp. 225-230., 2013.

[27] D. Yankov, D. DeCoste, E. Keogh, "Ensembles of nearest neighbor forecasts," pp. 545-556, 2006.

[28] T. Fushiki, "Estimation of prediction error by using K-fold cross-validation," *Statistics and Computing,* vol. 21, no. 2, pp. 137-146, 2011.

[29] E. Fix, J. L. Hodges, Jr., "Discriminatory Analysis: Nonparametric Discrimination: Consistency Properties. International Statistical Review," *International Statistical Review,* vol. 57, no. 3, pp. 238-247, 1989.

[30] N. Bhatia, SSCS Vandana, "Survey of Nearest Neighbor Techniques," *International Journal of Computer Science and Information Security,* vol. 8, no. 2, pp. 302-305, 2010.

[31] N. K. MacVarish, "Understanding Your Data Sheet: Heat Deflection Temperature," http://blog.impactplastics-ct.com/blog/understanding-your-data-sheet-heat-deflection-temperature, 2018.

[32] AK. Bledzki, AA. Mamun, M. Feldmann, "Polyoxymethylene composites with natural and cellulose fibres: Toughness and heat deflection temperature," *Composites Science and Technology,* vol. 72, no. 15, pp. 1870-1874, 2012.

[33] A.K. Mohanty, M. Misra, L.T. Drzal, Natural fibers, biopolymers, and biocomposites, Boca Raton: CRC Press, 2005.

[34] M. Asgari, M. Masoomi, "Thermal and impact study of PP/PET fibre composites compatibilized with Glycidyl Methacrylate and Maleic Anhydride," *Composites Part B: Engineering,* vol. 43, no. 3, pp. 1164-1170, 2012.

[35] S.M.R. Khalili, V. Daghigh, R.E. Farsani, "Mechanical behavior of basalt fiber-reinforced and basalt fiber metal laminate composites under tensile and bending loads," *Journal of Reinforced Plastcis and Composites,* vol. 30, no. 8, pp. 647-659, 2011.

[36] R. Eslami Farsani, SMR Khalili, V. Daghigh, R. Fazaeli, "Creep Behavior of Basalt and Glass Fiber Reinforced Epoxy Composites," *Journal of Mechanical Research and Application ,* vol. 3, no. 1, pp. 29-36, 2011.

[37] M. Nasihatgozar, V. Daghigh, M. Eskandari, K. Nikbin, A. Simoneau, "Buckling analysis of piezoelectric cylindrical composite panels reinforced with carbon nanotubes," *International Journal of Mechanical Sciences,* vol. 107, pp. 69-79, 2016.

[38] H. Daghigh, V. Daghigh, "Free vibration of size and temperature-dependent carbon nanotube (CNT)-reinforced composite nanoplates with CNT agglomeration," *Polymer Composites,* vol. 40, no. S2, pp. E1479-E1494, 2019.

[39] S. Shuhadah, A.G. Supri, "LDPE-Isophthalic Acid-Modified Egg Shell Powder Composites (LDPE/ESPI)," *Journal of Physical Science,* vol. 20, no. 1, pp. 87-98, 2009.

[40] A.K. Subramaniyan, C.T. Sun, "Interlaminar fracture behavior of nanoclay reinforced glass fiber composites," *Journal of Composite Materials,* vol. 42, no. 20, pp. 2111-2122, 2008.

[41] M. Zanetti, S. Lomakin, G. Camino, "Polymer layered silicate nanocomposites," *Macromolecular Materials and Engineering ,* vol. 279, pp. 1-9, 2000.

[42] D. Garcı, A. López, O. Picazo, J.C. Merino, J.M. Pastor, "Polypropylene–clay nanocomposites: effect of compatibilizing agents on clay dispersion," *European Polymer Journal,* vol. 39, no. 5, pp. 945-950, 2003.

[43] M. L. López-Quintanilla, S. Sánchez-Valdés, S. Sánchez-Valdés, S. Sánchez-Valdés, "Effect of some compatibilizing agents on clay dispersion of polypropylene-clay nanocomposites," *Journal of Applied Polymer Science,* vol. 100, no. 6, pp. 4748-4756, 2006.

[44] FC. Chiu, SM. Lai, JW. Chen, PH. Chu, "Combined effects of clay modifications and compatibilizers on the formation and physical properties of melt-mixed polypropylene/clay

nanocomposites," *Journal of Polymer Science Part B Polymer Physics ,* vol. 42, pp. 4139-4150, 2004.

[45] C.O. Rohlmann, MD. Failla, LM. Quinzani, "Linear viscoelasticity and structure of polypropylene–montmorillonite nanocomposites," *Polymer ,* vol. 47, no. 22, pp. 7795-7804, 2006.

[46] J. Pascual, E. Fages, O. Fenollar, D. García, R. Balart, "Influence of the compatibilizer/nanoclay ratio on final properties of polypropylene matrix modified with montmorillonite-based organoclay," *Polymer Bulletin,* vol. 62, no. 3, pp. 367-380, 2009.

CHAPTER IV

FRACTURE TOUGHNESS MACHINE LEARNING PREDICTIONS ON SHORT FIBER, NANO- AND MICRO-PARTICLE REINFORCED COMPOSITES

4.1 Abstract

Tailorability is an important advantage of composites. Incorporating new bio-reinforcements into composites can contribute to using agricultural wastes and creating tougher and more reliable materials. Nevertheless, the huge number of possible natural material combinations works against finding optimal composite designs. Here, machine learning (ML) was employed to effectively predict fracture toughness properties of multiscale bio-nano-composites. Charpy impact tests were conducted on composites with various combinations of two new bio fillers, pistachio shell powders and fractal date seed particles, as well as nano-clays (NCs) and short latania fibers, all which reinforce a poly(propylene)/ethylene-propylene-diene-monomer matrix. The measured energy absorptions obtained were used to calculate strain energy release rates as a fracture toughness parameter using linear elastic fracture mechanics and finite element analysis (FEA) approaches. Despite the limited number of training data obtained from these impact tests and FEA, the ML results were accurate for prediction and optimal design. This study applied the Decision Tree Regressor and Adaptive Boosting Regressor ML methods in contrast to the K-Nearest Neighbor Regressor ML approach used in our previous study for heat deflection temperature predictions [1]. Scanning electron microscopy, optical microscopy and transmission electron microscopy were used to study the NC dispersion and impact fracture morphology.

4.2 Introduction

Poly(propylene) (PP) is a widely used thermoplastic matrix in natural composite materials. PP has been utilized in packaging, automotive, textile, and non-structural applications [2]. Nevertheless, its relatively low impact strength, particularly at lower temperatures, has motivated addition of various elastomeric modifiers to reinforce and toughen PP [3-4]. The ethylene–propylene–diene terpolymer (EPDM) is a widely used modifier [2, 5-10] which significantly improves PP's impact behavior [11-12].

The natural fibers basalt [13-17], hemp, kenaf and flax [18-21], jute [22-23], sisal [24], coir [24-25], curaua [26], coconut [27], pineapple leaf [28], *etc.* have been used to reinforce polymer matrix composites, but latania natural fiber-reinforced composites have only been reported rarely [29]. In addition to using natural fibers, nano-particles or micro-fillers are often added to reinforce composites [30]. Micro- and nano-powder fillers are mostly used to enhance hardness, elastic moduli, impact, wear and thermal resistance, while reducing cost and mechanical shrinkage [14]. For example, micron-sized rigid glassy spheres, elastic rubber particles, rigid nano-sized $CaCO_3$ [31], Al_2O_3 [32], SiO_2, [33] and TiO_2 [34] powders, carbon nano-tubes (CNTs) [35-37] and nano-clay (NC) platelets [38] have been used as reinforcements.

4.2.1 Effects of Particle Stiffness

Adding micro soft/elastic fillers increases polymer composite impact toughness, but reduces the modulus of elasticity [39]. On the other hand, increasing the amount of micro or nano (one dimension must be 100 nm or less [40]) hard/rigid fillers enhances both impact toughness and modulus of elasticity [39, 41]. As an example, adding rigid 0.6 μm $CaCO_3$ particles (0.2vol%) into high density polyethylene (HDPE) leads to a two-fold increase in the impact strength [31]; Al_2O_3 nano-particle (13 nm diameter) addition (1–2vol.%) into epoxy resin

enhances stiffness, impact energy and failure strain [32]. Adding 2.5, 5.5 and 8.5wt% of micro-glass powder spheres (53-62 μm diameters) to basalt fiber polymer composites increases Young's modulus, flexural stiffness and strength, creep stiffness and energy absorption capability particularly at elevated temperatures [14, 42-43].

Using core shell rubber (CSR) nano-particles (500 nm diameter) with a soft rubber core and a glassy shell increased an epoxy vinyl ester resin's fracture toughness considerably more than the same weight fraction of montmorillonite (MMT) NC particles [44]. However, when NC platelets were aligned along the fiber axis to reinforce glass fiber-reinforced composites, the interlaminar fracture toughness dropped compared to the composite without the NC [45].

4.2.2 Effects of Particle Size

Micro- versus nano-scale sized fillers may affect mechanical properties of composites differently. TiO_2 particle (32 nm diameter)/epoxy nano-composites showed higher tensile failure strains versus those with micron-size TiO_2 (0.24 μm) [46]. Micro- and nano-silica fillers affected the mechanical properties of rigid and flexible polyurethane foams differently [47]. Nano-silica filler additions increased the compressive strength of flexible polyurethane foams, while the rebound resilience decreased [47]. In contrast, micro-filler addition to flexible foams reduced compressive strength and hardness, suggesting greater energy dissipation in nano-silica-filled foams [47]. Glass beads and spherical alumina (Al_2O_3, aluminum dioxide) particles in sizes from the macro- (0.5 mm) to the nano- (15 nm) scales were used to reinforce vinyl ester resin. Tensile tests showed that the interfacial fracture toughness depended on the particle size where nano sizes gave greater interfacial fracture toughness [48]. The sliding mode fracture occurring in these samples significantly enhanced the interfacial fracture toughness of polymer composites which incorporated nano-size particles [48].

It is important to know more about the simultaneous effects of combining both natural fibers with nano- and macro-powders in composites, but few such studies exist. Farsani et al. [13] added NC powders to short basalt fiber (SBF)-reinforced PP to investigate SBF-PP nano-composites under tensile loads. Young's modulus and yield strength were improved by NC addition. Ashik et al. [49] added nano-silicon dioxide (0, 5 and 10wt%) to jute fiber/epoxy composites. Young's modulus, ultimate tensile strength, peak load, and ultimate number of fatigue cycles were higher after 5wt% nano-silicon dioxide addition. Patnaik *et al.* [50] reported an industrial flyash (80-100 μm diameter) that provided superior flexural strength enhancements compared to those of alumina and SiC particles in glass reinforced polyesters.

The mechanical effects of adding both nano- and macro-scale powders to a polymer matrix reinforced with short natural fibers have not been reported in the literature [1]. Therefore, in this research, NC and the new bio micro-scale powders (pistachio shell powder (PSP) and date seed powder (DSP)) were added simultaneously to short latania natural fiber (SLF)-reinforced PP/EPDM. The cost of making nano-sized or small micro-sized (diameter less than 50 μm) PSPs, DSPs, or mineral powders by top-down grinding or other size-reduction methods is much higher than making large amounts of macro-sized particles (diameters > 50 μm). Extensive energy is expended exposing large new surface areas as particle dimensions are reduced. Thus, if macro-sized particles can improve a target property while other properties remain useable and costs are lowered, this is worthwhile investigating.

4.3 Experimental Procedure

4.3.1 Materials

PP/EPDM, MAPP and latania fibers were the same as those used previously [1, 51]. Cloisite 20A nano-clay (NC) powders were used as received (d-Spacing of 31.5 A^o). The

pillaring agent originally used to induce the large d-spacing in the Closite 20 is the mixture of dimethyl(ditallow) quaternary ammonium salts synthesized from tallow-based fats. These salts had been intercalated into the clay and these positive counter-ions replaced the interlayer Na^+, K^+, *etc*. cations originating in the clay. These changes are counter-balanced by the negative charges in the aluminosilicate layers. Therefore, the (+) charged pillaring agents are now intercalated between the clay layers and have pushed them apart prior to the NC incorporation into the composite by twin-screw extrusion. The morphological structures of pistachio shells (PSs) and date seeds (DSs) were observed through SEM images taken from PS and DS cross sections (Figures 1a and 1b). PSPs and DSPs within the range of 5-105 μm were obtained by grinding PSs and DSs and passing the powders through standard sieves. SEM pictures of typical ground PSP and DSP are shown (Figs. 4.1c and 1d).

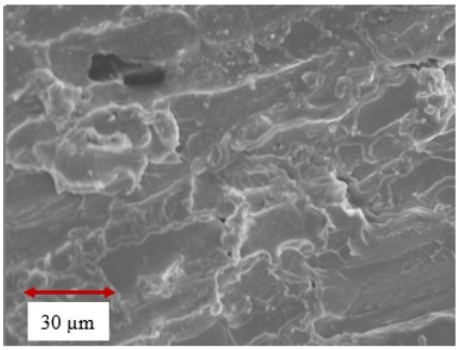

(a)

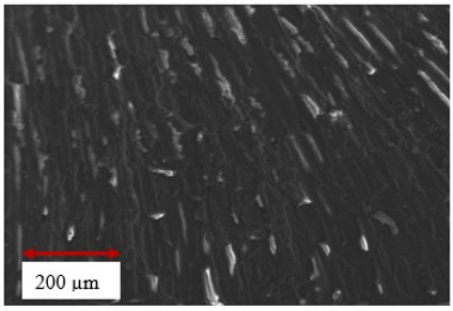

(b)

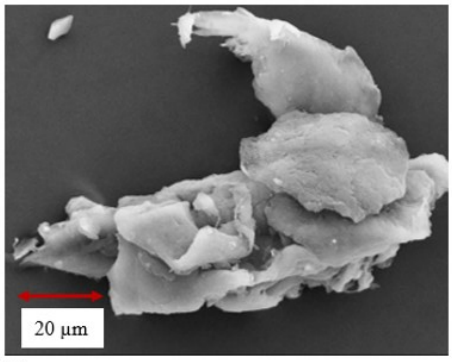

(c)

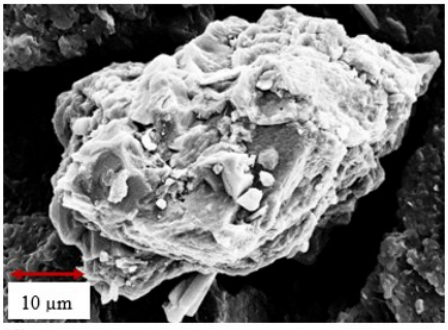

(d)

Figure 4.1 (a) SEM picture of a pistachio shell sliced through the thickness (magnification of 1.86 kx); (b) SEM picture of a date seed sliced through the thickness (magnification of 400 x); (c) SEM picture of a typical pistachio shell powder particle; (d) SEM picture of a typical date seed powder particle (magnification of 1.6 kx).

4.3.2 Specimen Preparation

The entire specimen preparation process was exactly the same as those in Refs. [1, 51]. SLFs (0, 5, 10, 20, and 30 wt%), NCs (0, 3, and 5 wt%), PSPs (0, 3, and 5 wt%), and DSPs (0, 3, and 5 wt%) were incorporated into ~ 50 different batches to fabricate ~ 50 combinations of PP/EPDM composites reinforced with SLFs, NCs, PSPs and/or DSPs. All batches contained 2 wt% MAPP [51]. Finally, Charpy impact test specimens were produced using an injection molding machine at 165-180°C [51] having the nominal ASTM standard dimensions: length, 63.7 mm; width, 12.7 mm; thickness, 7.1 mm; depth of notch, 3.8 mm; notch angle, 45° [29, 51].

4.3.3 Mechanical Testing Procedure and Equipment

ASTM D-256 Charpy impact tests were carried out on the composites. The Charpy impact testing machine was employed for dynamic three-point flexural tests on beams with or without a notch [3, 16, 29]. Three to five replications were performed on each material composition. After testing, the failure surfaces of specimens were examined by a high magnification optical microscope, and a SEM/EDX (40 FE-SEM Zeiss Supra 40, USA) to see the fracture morphology and the reinforcement(s)/matrix interfaces. Select specimens containing NC were studied using a TEM (JEOL 2100 TEM, USA) to examine the NC distribution and exfoliation. Gold coatings were used for clarity enhancement for SEM. SEM/EDX and TEM investigations were performed without gold coating to avoid the change in the surface chemical compositions.

4.3.4 G_c Determination

The critical strain energy release rate (G_c) was calculated for every Charpy impact test specimen using linear elastic fracture mechanics (LEFM) [29, 51-52]. The total impact energy

absorbed (U_c) was measured during each test. The specimens were quasi-brittle with no large-scale viscoelasticity. The use of notched specimens intensified the sharp crack formation and subsequent brittle fracture, minimizing the plastic zone formation ahead of crack tip [51]. Therefore, LEFM is eligible for determining the toughness parameters. The critical strain energy release rate (fracture toughness) (G_c) during Charpy impact testing may be expressed as [29, 51-52]:

$$G_c = \frac{F^2}{2B}\frac{\partial C}{\partial a} \tag{4.1}$$

where F is the anvil force exerted on the specimen middle, a is the crack length, C is the material compliance and B is the specimen thickness. The fracture toughness may also be expressed as [29, 51-52]:

$$G_c = \frac{U_c}{BD\theta} \tag{5.2}$$

where U_c is the (measured) energy absorbed at fracture, θ is a geometrical parameter that depends on the specimen geometry, and D is the specimen width. The specimen geometries were: thickness B = 7.1 mm, and width F = 12.7 mm; the support span was 40 mm. A value of θ = 0.369 was calculated using the finite element method and was selected here considering the data summarized in [52] for the notched Charpy impact specimens [29, 51-52]. The measured energies absorbed at fracture (U_c) obtained from the experiments were converted to fracture toughness (G_c) values based on Eqs. 1 and 2. These are *partly* tabulated in Table 1. A full table

of these values is available in Table A.1 (Appendix). “Input (wt%)” is component wt% of each composite.

Table 4.1 The representative composition of each composite blend and the pertinent experimental fracture toughness (G_c) values

Input (wt%)	Input (wt%)	Input (wt%)	Input (wt%)	Input (wt%)	Output (KJ/m^2)
PP/EPDM	SLF	PSP	DSP	NC	Fracture Toughness
100	0	0	0	0	45.4
97	0	3	0	0	52
95	0	5	0	0	57.1
92	5	3	0	0	64.8
90	5	0	5	0	77.3
95	5	0	0	5	74.8
90	10	0	0	0	67.3
82	10	0	5	3	102.8
80	10	0	5	5	114.3
80	20	0	0	0	107.9
77	20	0	0	3	125.2
75	20	0	0	5	137.5
70	30	0	0	0	136.7
62	30	0	5	3	177.7
74	30	3	0	3	170.3

4.4 Machine Learning Prediction

Our earlier paper [1] investigated heat deflection temperatures of the same class of composites using the K-Nearest Neighbor Regressor (KNNR) [53] machine learning (ML) method. In the current paper, the G_c values were obtained from the experiments and FEA. Then, two ML regression methods were used to predict the fracture toughness values of the composites: a) The Decision Tree Regressor (DTR) [54] and b) Adaptive Boosting Regressor (ABR) [55]. The performances of these two ML methods were evaluated by performing K-Fold

cross validation. We benchmarked several algorithms; DTR and ABR gave us the best results. Therefore, a brief description is given below of these algorithms and the performance metrics.

4.4.1 Decision Tree Regressor (DTR)

DTR is a ML method proposed by Breiman et al. [54]. This algorithm iteratively creates a tree that divides data points based on the feature that caused the highest disparity in the output (Here is fracture toughness). In this article, DTR from the Scikit Learn library [56] was implemented for the regression purpose.

4.4.2 Adaptive Boosting Regression (ABR)

ABR is the process of training several weak learners sequentially in order to create a single strong predictor from them [55]. In each iteration, a weak learner is added to the set of learners and it is trained on the part of data that the previous learner had performed poorly when using. In this way, a group of models are trained. This group of models decide if an input belongs to class +1 or -1. The collection of weak learners constitutes a single strong learner. In this article, a group of DTRs has been used as the internal learners of the ABR [55].

4.4.3 K-Fold Cross Validation

Given a data set of m data points, these m points were randomly broken into K segments and then, in K iterations, the model was trained on all segments except one. This way, a less optimistic estimation of the model's ability in prediction of unseen samples was obtained [57]. This concept is illustrated by Fig. 4.2.

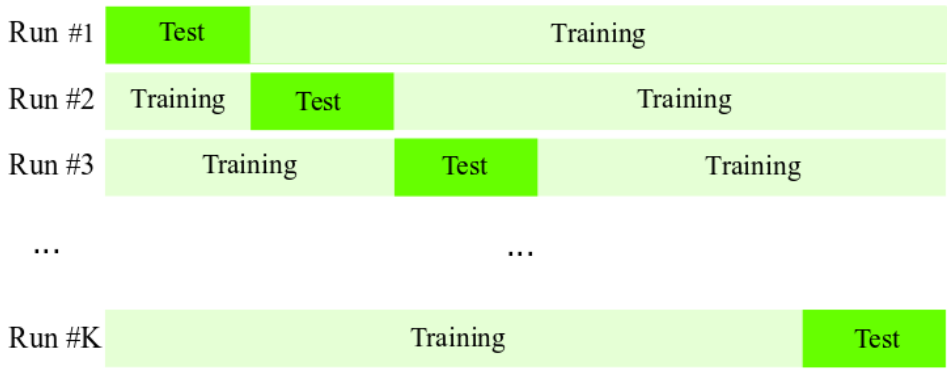

Figure 4.2 Split segment visualization in each *K* run

4.4.4 Performance Metrics

The performance of the predictions was evaluated using four different metrics which are commonly used for evaluation of regression models.

Mean Absolute Error (MAE): Given a data set of *m* input points $\{x_1,x_2,...,x_m\}$, their true outputs $\{ y_1,y_2,...,y_m\}$ and the corresponding predictions of the outputs by the model: $\{\hat{y}_1,\hat{y}_2, \dots , \hat{y}_m\}$,

MAE is calculated by Eq. (4.3):

$$MAE = \frac{1}{m}\sum_{i=1}^{m}\|\hat{y}_i - y_i\| \tag{4.3}$$

Root Mean Squared Error (RMSE): The square root of the average of the error squared. The *m,* $\hat{y}_i$, and y_i hold the same values as in Eq. (4.4).

$$RMSE = \sqrt{\frac{1}{m}\sum_{i=1}^{m}(\hat{y}_i - y_i)^2} \tag{4.4}$$

R-Squared: A measure of comparing the variance of the true value of the data with the errors of predictions. The smaller the variance, the better the results. The model is more accurate if the R^2 is closer to 1.

$$R^2 = 1 - \frac{\sum_{i-1}^{m}(y_i - \hat{y}_i)^2}{\sum_{i-1}^{m}(y_i - \bar{y}_i)^2} \tag{4.5}$$

4.5 Results and Discussion

ASTM D-256 Charpy impact tests were conducted on composites containing varying amounts of SLFs, NCs, PSPs, and DSPs to investigate the effect of these ingredients on fracture toughness and fracture morphology of the composites. Figure 3 summarizes the correlation of data and role of each constituent (PP/EPDM, SLF, NC, PSP, and DSP) on the fracture toughness. The meaningful associations in this figure are those of fracture toughness (as an output) with PP/EPDM, SLF, NC, PSP, and DSP (each as an input). Positive or negative values indicate the direct or reverse associations between the output and each input. The SLF wt% correlation with the fracture toughness value is 0.97. Thus, the amount of SLF is the most effective factor for increasing fracture toughness. This can be compared to the wt% correlation values for PSP (0.11), DSP (0.16) and NC (0.26). In total, this reflects the importance of stiffness enhancement upon SLF addition to the composites. Several reports have suggested stiffness enhancement and

impact improvement associated with short fibers addition to the composites [51, 58-59]. This improvement is based on crack deflection, and physical anchoring creation [51, 60].

Other factors improving fracture toughness are the NC, DSP and PSP weight percentages with the fracture toughness correlations of 0.26, 0.16, 0.11, respectively (Fig. 4.3). The greater effect of NC on fracture toughness compared with those of DSP and PSP is attributed to the greater surface area of NC compared with those of DSP and PSP. The thicknesses of NC are in the range of 7-40 nm after twin screw extrusion blending of the composites (See section 5. "Optical microscope, and SEM/TEM images and fracture morphology" as well as the Appendix (Fig. 4.A.1). The purchased Closite 20 nano-platelets were readily sheared into successively thinner platelets with fewer stacked individual clay layers (exfoliated clay) during the twin-screw manufacturing process. The high shear generates the resulting exfoliated/intercalated nano-clay composites. Many similar results exist for adding NC to polymers [61-62].

The impact behavior of fiber and particle composites is governed by the fabrication method, fiber/matrix interface strength, constituent physical and mechanical properties, specimen geometry and the test conditions [13, 16, 29]. Generally, fillers have two concurrent roles in composites. The first is acting as a hole/defect provider causing stress concentration points, which leads to a pre-damaged material. The second is serving as a physical barrier against crack propagations [14]. Both PSP and DSP have mildly improved the fracture toughness (Fig. 4.3) within the composition range probed. This suggests that the positive (second) role outweighs the negative (first) role when incorporating DSP and PSP in the polymer matrix. The role of these particles is indeed similar to the aggregates in reinforced concretes, where the fillers behave as frictional materials and the matrix as an adhesive [14].

Correlations of DSP and PSP wt% values with the fracture toughness values are 0.16 and 0.11, respectively (Fig. 3). This noticeable difference is likely due to lower rigidity of DSP versus PSP. Several publications have confirmed that particles with a lower modulus of elasticity, when present in composites, resulted in greater composite toughness [63-64].

The SLF, DSP and PSP inclusions are large (SLF lengths ~ 2mm, SLF diameters ~70 μm), DSP (diameters 5-105 μm), PSP (diameters 5-105 μm), and the ASTM test thicknesses are small (7.1 mm). Therefore, the specimens' through-thickness dimensions will not contain a representative specimen composition (independent of change in thickness versus inclusion sizes and number of inclusions present), when testing is performed. This was emphasized and discussed in our previous publication on ML predictions of the heat deflection temperatures of this same composite series [1]. If Charpy impact tests were conducted on specimens that were 10x or 100x the ASTM thickness and size, with all lengths and widths kept in the same ratio, at some point the specimens would then always contain a representative material across the composite thickness. Subsequently, the ML method might end up with different predicted results. However, ASTM Charpy Impact tests are the standard throughout the composite industry. Hence, optimizing processes based on ASTM procedures is standard practice.

Use of PSPs and DSPs in this composite series had beneficial effect on heat deflection temperature [1]. This is now shown for fracture toughness. Furthermore, DSPs and PSPs are made from low cost agricultural wastes. Nevertheless, probable deleterious effects may occur on properties like high and low cycle fatigue, creep, and vibrating and dynamic strength. As long as these negatives can be tolerated in the anticipated end uses, the application of these low-cost fillers is justified.

Figure 4.3 Correlation of the features (PP/EPDM, SLF, PSP, DSP and NC) and fracture toughness

Figure 4.4 shows the actual results and the ML predictions using AdaBoost and Regression Tree. The performance evaluation of Adaboost and Regression Tree are, for simplicity, only partly tabulated in Table 4.2. Adaptive boosting was used as a predictor with a number range of estimators from 2 to 50. To show the overall performance trend with respect to the estimator numbers, a few graphs are provided in Fig. 4.4 and many others are given in the Appendix (Fig. 4.A.1). The more estimators that are used, the greater the ability of the model becomes in regression. Nevertheless, the chance of overfitting increases with a larger number of estimators. Therefore, over 50 estimator numbers are not considered for the estimator population size. The optimum number of estimators in this case study is 10 (depth 4) (Fig.4 and Table 4.2). Table 4.2 shows only a partial summary of the performance evaluations. The complete performance evaluation values from ML are presented in the Appendix (Table 4.A.2).

Table 4.2 Performance evaluations using AdaBoost and Regression Tree

No.	depth	estimators	regtree_R^2	adaboost_R^2	regtree_MAE	adaboost_MAE
0	2	5	0.909	0.912	10.176	10.029
1	3	5	0.834	0.833	11.611	11.438
2	4	5	0.939	0.953	8.447	7.334
3	2	10	0.879	0.896	10.390	9.264
4	3	10	0.938	0.947	8.278	7.725
5	4	10	0.950	0.943	7.119	7.979
6	4	15	0.930	0.930	8.286	8.340
7	4	20	0.929	0.938	8.315	7.805

regtree_R^2: R^2 in the Regression Tree method; adaboost_R^2: R^2 in the Adaboost method
regtree_MAE: MAE in the Regression Tree method; adaboost_MAE: MAE in the Adaboost method

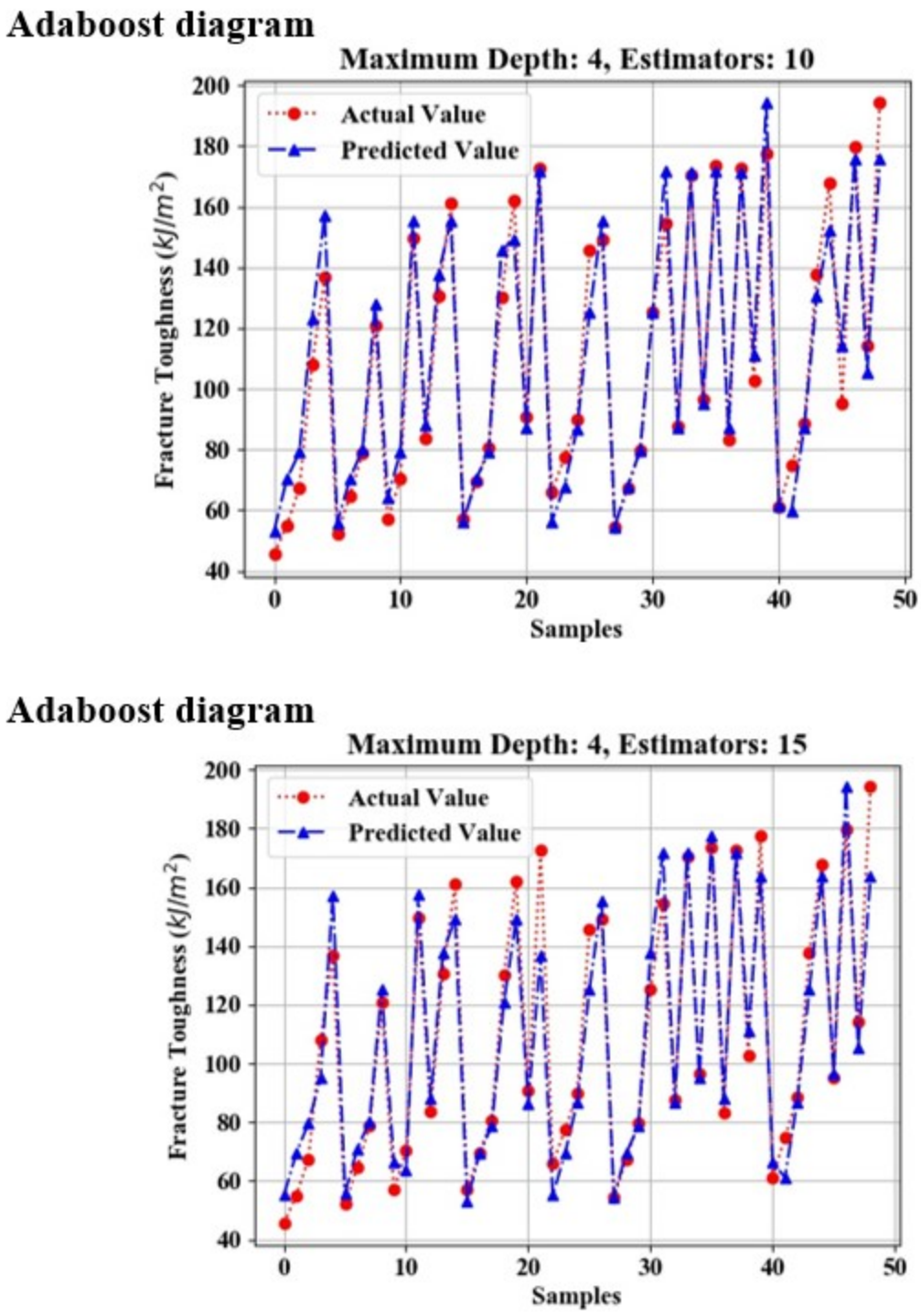

Figure 4.4 Actual and predicted fracture toughness (Gc) values (horizontal axis represents the number of samples and the vertical axis represents the Gc values.

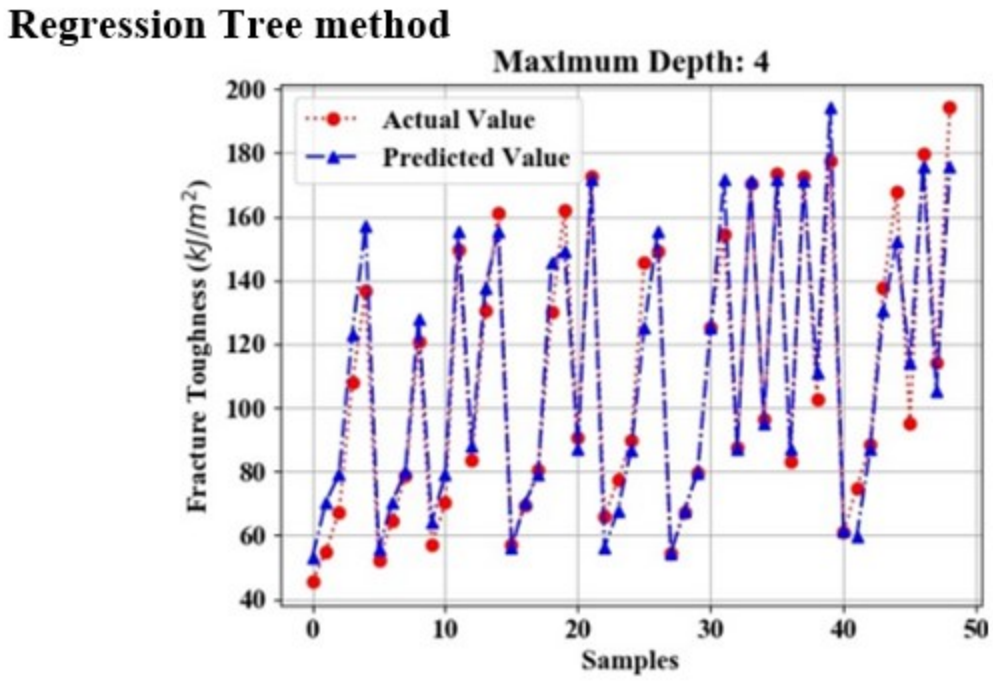

Figure 4.4 (continued)

4.6 Optical Microscope, and SEM/TEM Images and Fracture Morphology

Impacted specimens were inspected to investigate fracture morphology using optical microscopy (OM) and SEM. The damage progression is governed by complex interactions between constituents, the fiber volume fraction, fiber/matrix interfacial properties and adhesion, stochastic variations in fiber strengths, filler particle sizes, filler interfacial bonding as well as matrix strengths [41]. Figures 4.5a and b show the 20wt%SLF/3%DSP/PP/EPDM composite where fiber fracture and fiber/matrix debonding are the main failure mechanisms. Figures 4.5c and d depict the fracture surfaces of the 5wt%DSP/PP/EPDM and 5wt%PSP/PP/EPDM composites, respectively. DSPs and PSPs in the matrix can act as microcrack propagation obstacles and increase the fracture surface area, leading to increases the ductility and energy absorption capability. Enhancing the pistachio-to-matrix adhesion will benefit these effects. In

general, these composite matrix fracture surfaces had rougher surfaces and more crack deflection phenomenon compared with matrices without (or with less) SLF, NC, PSP, and DSP [51, 65], indicating more ductility is afforded by adding SLF, NC, PSP, and DSP.

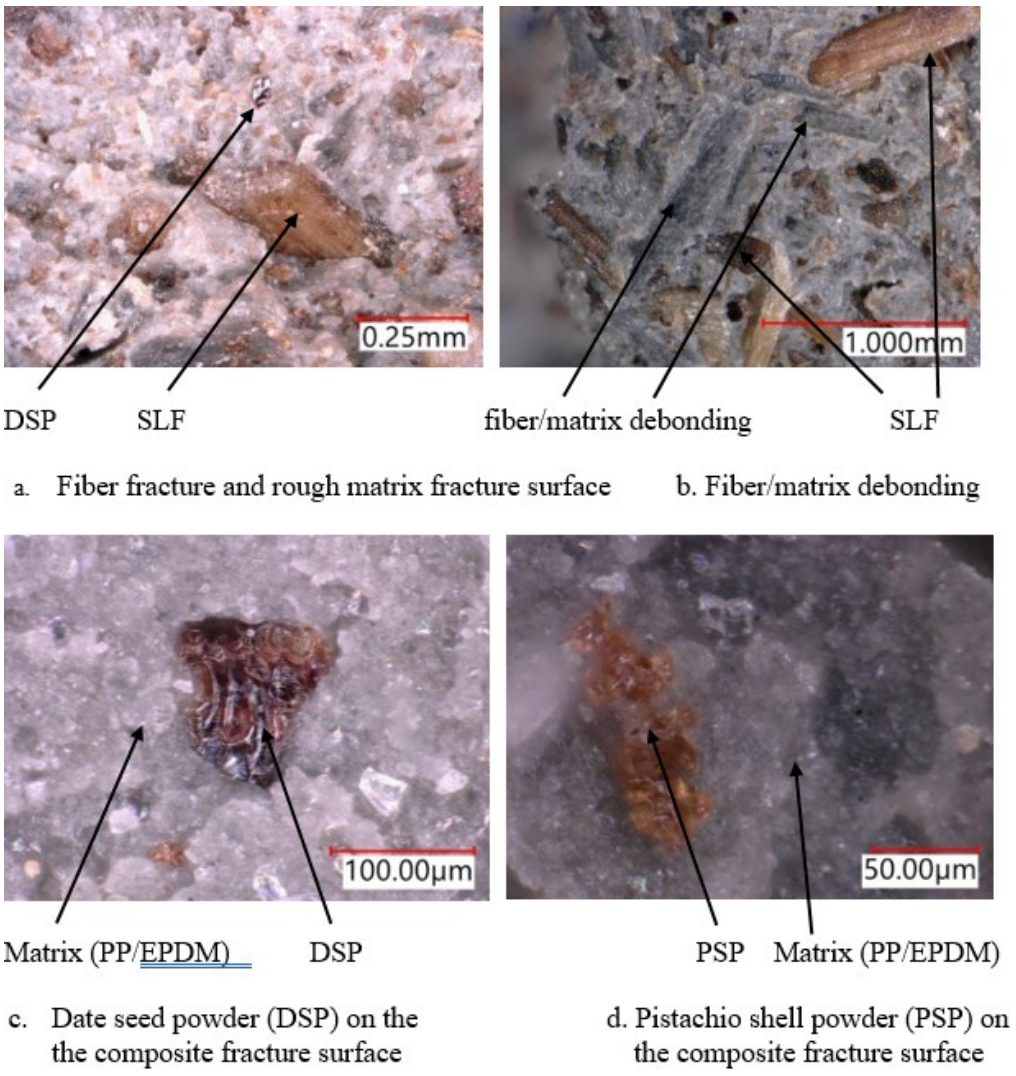

Figure 4.5 Optical microscope images of (a and b) (a and b) the 20wt%SLF/3wt%DSP/PP/EPDM Composite with 2wt% MAPP; (c) the 5wt%DSP/PP/EPDM composite with 2wt% MAPP and (d) the 5wt%PSP/PP/EPDM composite with 2wt% MAPP

MAPP's maleic anhydride function covalently bonds to form ester groups at the hydroxyls on SLF, PSP and DSP surfaces while MAPP's PP chains move into the PP/EPDM matrix. This enhances inclusion-to-matrix adhesion and compatibility. Figure 4.6 depicts this improved adhesion as particles pull away and are detached. The matrix has been deformed into a very rough surface until the MAPP chains, bound to PSP, untangle from the matrix. This leads to higher energy dissipation during PSP/matrix debonding.

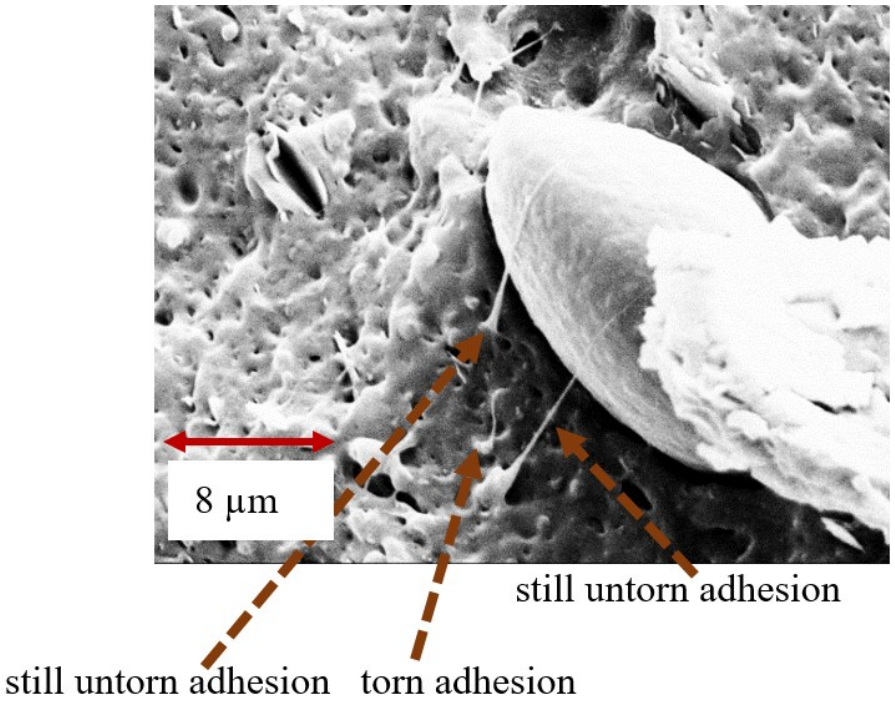

Figure 4.6 Partially debonded pistachio shell powder (PSP) on the fracture surface of 3wt%PSP/PP/EPDM with 2wt% MAPP after a Charpy impact test (magnification, 3.0 kx).

Fiber pull-out and fiber/matrix debonding release considerable frictional energy during Charpy impact test (Fig. 4.7). As expected, matrix cracking and crazing are ubiquitous failure mechanisms in these investigated specimens.

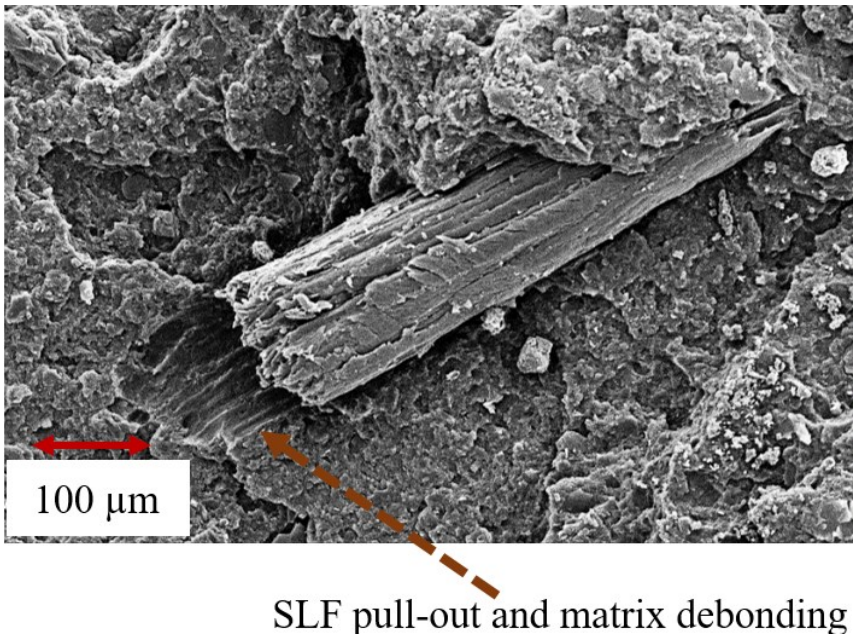

Figure 4.7 Fiber pull-out and fiber/matrix debonding during Charpy impact test of 20wt%SLF/3wt%NC/PP/EPDM with 2wt% MAPP (magnification, 150 x).

SEM/EDX and TEM views of NC particles in the exfoliated/intercalated nano-clay composites (20wt%SLF/3wt%NC/PP/EPDM) are depicted by Figs. 4.8a, b, c and d. NC participates in improving toughness. Figure 4.8a shows an SEM view of several NC platelet faces. The range of *xy* dimensions observed over the composite samples is 300-600 nm. All EDX spectra confirm these are NC particles by exhibiting their aluminasilicate structure with substantial magnesium present from their Al, Si, and Mg EDX peaks. Figure 4.8b is a different SEM of the same sample showing another NC particle and the EDX analysis. The EDX analysis exhibits carbon, calcium, potassium and iron in various amounts. The carbon is from PP/EDPM matrix material in the vicinity, iron is a known impunity in the Closite 20a platelets, and calcium and potassium are likely present between the clay platelets as original interlayer cations which were never replaced by the pillaring agent. Figure 4.8c illustrates some NC edges where the NC particles are observed close enough to perpendicular to the micrograph's surface to measure the platelet

thicknesses. Figure 4.8d gives a NC edge observed by the TEM. The average NC platelet thickness shown in Fig. 4.8d is ~ 16 nm. At least 19 NC platelet thicknesses from SEM were measured and tabulated in Table 3 in the Appendix (Table 4.3.A). The average is 23 nm, however some platelet stacks that are up to 60 nm thick were observed after examining many locations by SEM.

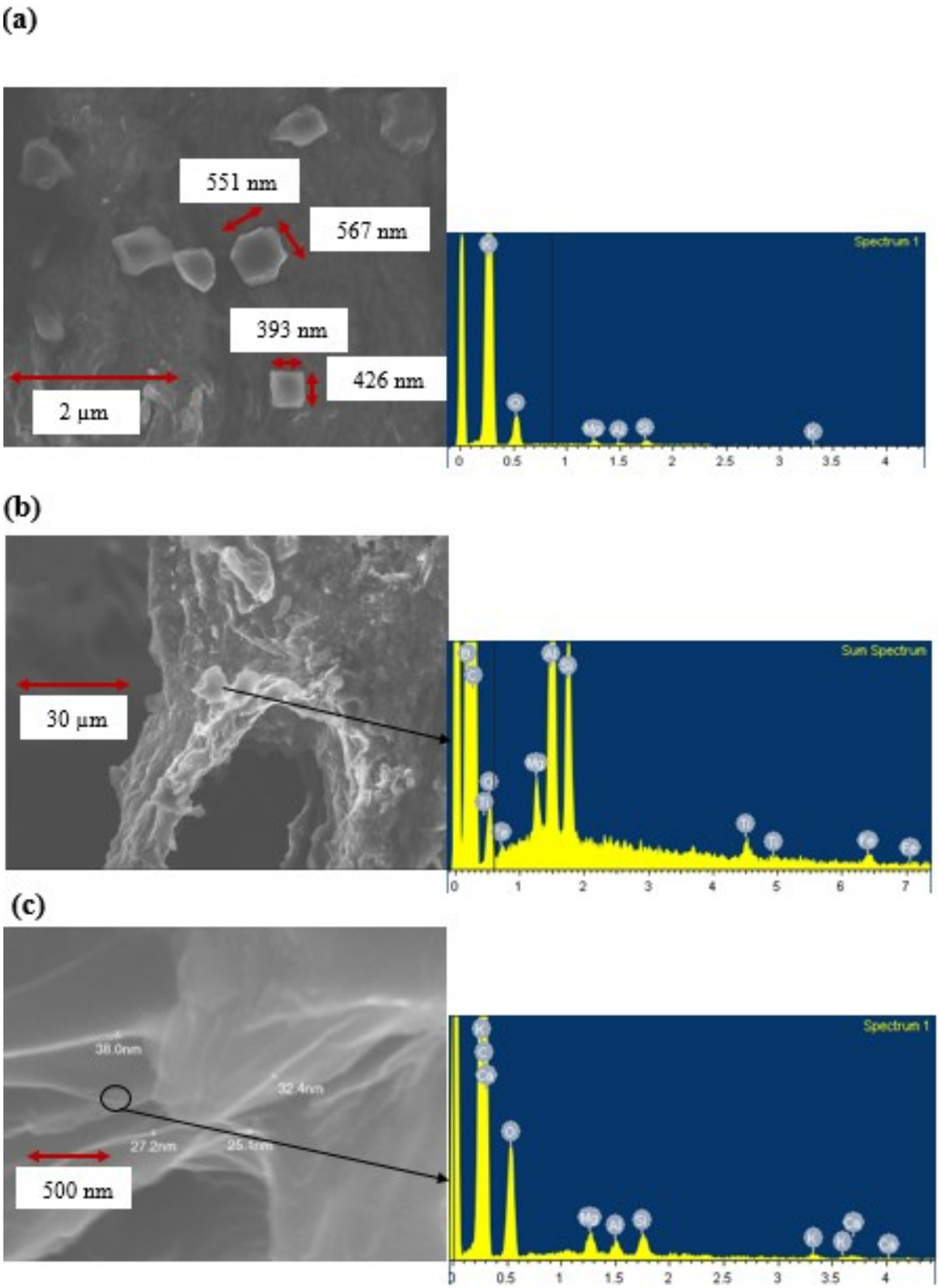

Figure 4.8 SEM/EDS (a), (b) and (c), TEM (d) observations of Nano-clay particles 20wt%SLF/3wt%NC/PP/EPDM with 2wt% MAPP.

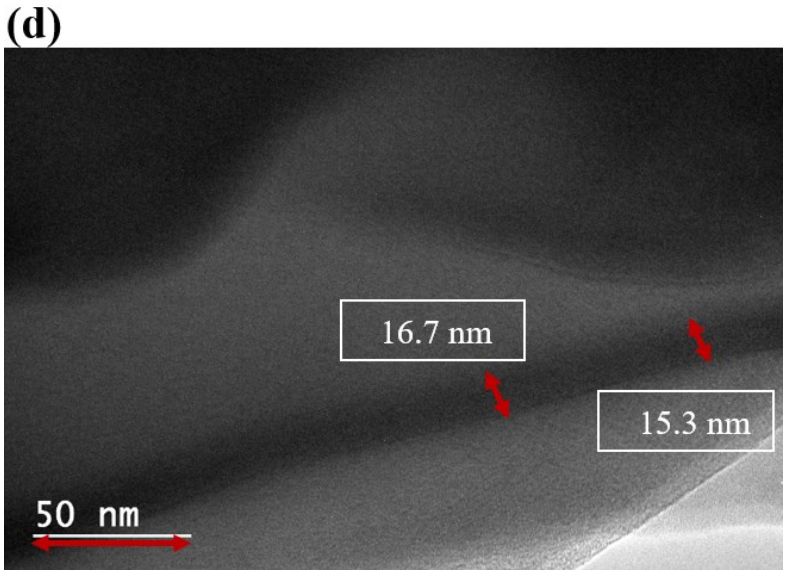

Figure 4.8 (continued)

4.7 Conclusions

PP/EPM composites containing various amounts of SLF, PSP, DSP, and NC inclusions and MAPP as a coupling agent were fabricated. The TEM/SEM/EDS results suggested the NC thicknesses were in the range of 7-40 nm indicating the success of twin-screw extruder method in NC layers expansions which led to fracture toughness enhancements. The specimens fracture toughness was determined by Charpy impact testing and FEA. Then, Adaboost and Regression Tree machine learning (ML) methods were employed to model and predict the fracture toughness properties of these very complex composite formulations. Cross validation was performed to successfully validate the accuracy of the ML prediction models. Fracture toughness values were simultaneously affected by SLF, NC, DSP, and PSP, respectively. Two new bio-fillers, PSP and DSP, showed promising participation in the composite fracture toughness improvement. Less rigid DSP contributed to its higher toughness enhancement capability compared with that of PSP. The matrix cracking, fiber/matrix debonding, fiber pull out, fiber

fracture, pistachio shell and date seed powder/matrix deboding as well as the microvoid growth were contributing failure mechanisms. MAPP contributed to the energy absorption increase during the impact test by improving PSP and DSP/matrix interfacial adhesion. How the multiple reinforcing components and their widely varying sizes might influence the fracture toughness of these composites is extremely complex. Thus, ML predictions could provide a way to assist in the prediction and optimization of fracture toughness by varying compositions.

References

[1] V. Daghigh, T. E. Lacy Jr., H. Daghigh, G. Gu, K. T. Baghaei, M. F. Horstemeyer, C.U. Pittman, Jr., "Heat deflection temperatures of bio-nano-composites using experiments and machine learning prediction," *Materials Today Communications ,* no. https://doi.org/10.1016/j.mtcomm.2019.100789, 2019.

[2] H.M. da, V.D. Costa, M. Ramos, C.G. Rocha, "Analysis of thermal properties and impact strength of PP/SRT, PP/EPDM and PP/SRT/EPDM mixtures in single screw extruder," *Polymer Testing,* vol. 25, pp. 498-503, 2006.

[3] SMR Khalili, RE Farsani, V Daghigh, "Aging Influence on Charpy Impact Behavior of Basalt Fiber Reinforced Epoxy Composites," *International Journal of Advanced Design and Manufacturing Technology ,* vol. 6, no. 2, pp. 81-85, 2013.

[4] R.D. Anandjiwala, S. Blouw, "Composites from bast fibres – prospects and potential in the changing market environment," *Journal of Natural Fibers,* vol. 4, pp. 91-109, 2007.

[5] B.Z. Jang, D.R. Uhlmann, J.B. Vander Sande, "Crystalline morphology of polypropylene and rubber-modified polypropylene," *J. App. Poly Sci.,* vol. 29, pp. 4377-4393, 1984.

[6] J. Karger-Kocsis, A. Kallo, A. Szafner, G. Bodor, Z. Senyei, "Morphological study on the effect of elastomeric impact modifiers in polypropylene systems," *Polymer,* vol. 20, pp. 37-43, 1979.

[7] K. Dao, "Rubber phase dispersion in polypropylene," *Polymer,* vol. 25, pp. 1527-1533, 1984.

[8] J. Karger-Kocsis, V.N. Kuleznev, "Dynamic mechanical and impact properties of polypropylene/EPDM blends," *Polymer,* vol. 23, pp. 699-705, 1982.

[9] K.A. Dubey, S.K. Sinha, Y.K. Bhardwaj, L. Panicker, L. Varshney, "Carbon black-filled PE/PP/EPDM blends: phase selective localization of carbon black and EPDM-induced phase stabilization," *Polymer-Plastics Technology and Engineering,* vol. 53, pp. 442-450, 2014.

[10] B.Z. Jang, D.R. Uhlmann, J.B. Vander Sande, "Ductile–brittle transition in polymers," *Journal of Applied Polymer Science ,* vol. 29, no. 11, pp. 3409-3420, 1984.

[11] G.A.O. Xiang, M.A.O. Li-xin, J.I.N. Ri-guang, Z.H.A.N.G. Li-qun, T.I.A.N. Ming, "Structure and mechanical properties of PP/EPDM/attapulgite ternary blends," *Polymer Journal,* vol. 39, no. 10, pp. 1011-1017, 2007.

[12] H.M. da Costa, V.D. Ramos, W.S. da Silva, A.S. Sirqueira, "Analysis and optimization of polypropylene (PP)/ethylene–propylene– diene monomer (EPDM)/scrap rubber tire (SRT) mixtures using RSM methodology," *Polymer Testing,* vol. 29, no. 5, pp. 572-578, 2010.

[13] R. Eslami-Farsani, S.M.R. Khalili, Z. Hedayatnasab, N. Soleimani, "Influence of thermal conditions on the tensile properties of basalt fiber reinforced polypropylene–clay nanocomposites," *Materials and Design,* vol. 53, pp. 540-549, 2014.

[14] R.E. Farsani, S.M.R. Khalili, V. Daghigh, "Charpy impact response of basalt fiber reinforced epoxy and basalt fiber metal laminate composites: experimental study," *International Journal of Damage Mechanics,* vol. 23, no. 6, pp. 729-744, 2014.

[15] V. Daghigh, S.M.R. Khalili, R.E. Farsani, "Creep behavior of basalt fiber metal laminate composites," *Composites Part B: Engineering,* vol. 91, pp. 275-282, 2016.

[16] S. Behnia, V. Daghigh, K. Nikbin, A.B. Fereidoon, J. Ghorbani, "Influence of stacking sequence and notch angle on the Charpy impact behavior of hybrid composites," *Mechanics of Composite Materials,* vol. 52, no. 4, pp. 489-496, 2016.

[17] M. Lamea, V. Daghigh, M. Soroush, K. Nikbin, "The buckling behavior of vacuum-infused open-hole unidirectional basalt fiber composites-experimental and numerical investigations," *Mechanics of Composite Materials ,* vol. 55, no. 5, pp. 1-17, 2019.

[18] G. Cicala, G. Cristaldi, G. Recca, G. Ziegmann, A. El-Sabbagh, M. Dickert, "Properties and performances of various hybrid glass/natural fibre composites for curved pipes," *Materials and Design,* vol. 30, no. 7, pp. 2538-2542, 2009.

[19] N. Saba, M.T. Paridah, M. Jawaid, "Mechanical properties of kenaf fibre reinforced polymer composite: a review," *Construction and Building Materials,* vol. 76, pp. 87-96, 2015.

[20] A. El-Sabbagh, L. Steuernagel, G. Ziegmann, "Processing and modeling of the mechanical behavior of natural fiber thermoplastic composite: flax/polypropylene," *Polymer Composites,* vol. 30, no. 4, pp. 510-519, 2009.

[21] A. El-Sabbagh, L. Steuernagel, G. Ziegmann, "Characterisation of flax polypropylene composites using ultrasonic longitudinal sound wave technique," *Composites Part B: Engineering ,* vol. 45, no. 1, pp. 1164-1172, 2013.

[22] M.A. Gunninga, L.M. Geevera, J.A. Killiona, J.G. Lyonsa, C.L. Higginbothama, "Mechanical and biodegradation performance of short natural fibre polyhydroxybutyrate composites," *Polymer Testing ,* vol. 32, pp. 1603-1611, 2013.

[23] H.N. Dhakal, V. Arumugam, A. Aswinraj, C. Santulli, Z.Y. Zhang, A. Lopez-Arraiza, "Influence of temperature and impact velocity on the impact response of jute/UP composites," *Polymer Testing,* vol. 35, pp. 10-19, 2014.

[24] P. Wambua, J. Ivens, I. Verpoest, "Natural fibres: can they replace glass in fibre reinforced plastics?," *Composite Science and Technology,* vol. 63, no. 9, pp. 1259-1264, 2013.

[25] D. V. O. de Moraes, R. Magnabosco, G. H. B. Donato, S. H. P. Bettini, M. C. Antunes, "Influence of loading frequency on the fatigue behaviour of coir fibre reinforced PP composite," *Polymer Testing,* vol. 41, pp. 184-190, 2015.

[26] D.O. Castro, A. Ruvolo-Filho, E. Frollini, "Materials prepared from biopolyethylene and curaua fibers: composites from biomass," *Polymer Testing,* vol. 31, no. 7, pp. 880-888, 2012.

[27] C. Merlini, G. M..O. Barra, D. P. Schmitz, S. D. A. S. Ramôa, A. Silveira, T. M. Araujo, A. Pegoretti, "Polyaniline-coated coconut fibers: structure, properties and their use as conductive additives in matrix of polyurethane derived from castor oil," *Polymer Testing,* vol. 38, pp. 18-25, 2014.

[28] U. Wisittanawat, S. Thanawan, T. Amornsakchai, "Mechanical properties of highly aligned short pineapple leaf fiber reinforced – nitrile rubber composite: effect of fiber content and Bonding Agent," *Polymer Testing,* vol. 35, pp. 20-27, 2014.

[29] M. Nasihatgozar, V. Daghigh, T. E. Lacy Jr., H. Daghigh, K. Nikbin, A. Simoneau, "Mechanical characterization of novel latania natural fiber reinforced PP/EPDM composites," *Polymer Testing,* vol. 56, pp. 321-328, 2016.

[30] S. Vigneshwaran, M. Uthayakumar, V. Arumugaprabu, R. Deepak Joel Johnson, S. Vigneshwaran, M. Uthayakumar, V. Arumugaprabu, R. Deepak Joel Johnson, "Influence of filler on erosion behavior of polymer composites: A comprehensive review," *journal of Reinfroced Plastcis and Composites,* pp. 1-9, 2018.

[31] Z.H. Liu, K.W. Kwok, R.K.Y. Li, C.L. Choy, "Effect of coupling agent and morphology on the impact strength of high density polyethylene/CaCO3 composites," *Polymer,* vol. 43, no. 8, pp. 2501-2506, 2002.

[32] B.D. Wetzel, F. Haupert, M. Zhang, "Epoxy nanocomposites with high mechanical and tribological performance," *Composite Science and Technology,* vol. 63, no. 14, pp. 2055-2067, 2003.

[33] P. Rosso, L. Ye, K. Friedrich, S. Sprenger, "A toughened epoxy resin by silica nanoparticle reinforcement," *J Appl Polym Sci, 100 (3) (2006), pp. 1849-1855,* vol. 100, no. 3, pp. 1849-1855, 2006.

[34] B. Wetzel, P. Rosso, F. Haupert, A. Friedric, "Epoxy nanocomposites – fracture and toughening mechanisms," *Eng Fract Mech, 73 (16) (2006), pp. 2375-2398,* vol. 73, no. 16, pp. 2375-2398, 2006.

[35] V. D. M. E. K. N. A. S. M. Nasihatgozar, "Buckling analysis of piezoelectric cylindrical composite panels reinforced with carbon nanotubes," *International Journal of Mechanical Sciences,* vol. 107, pp. 69-79, 2016.

[36] V. D. H. Daghigh, "Free vibration of size and temperature-dependent carbon nanotube (CNT)-reinforced composite nanoplates with CNT agglomeration," *Polymer Composites,* vol. 40, no. S2, pp. E1479-E1494, 2019.

[37] H. Daghigh, V. Daghigh, A. Milani, D.D. Tannant, T.E. Lacy Jr., J.N. Reddy, "Nonlocal Bending and Buckling of Agglomerated CNT-Reinforced Composite Nanoplates," *Composite Part B,* vol. Accepted for Publication , 2019.

[38] N. Gupta, R. Maharsia, "Enhancement of energy absorption in syntactic foams by nanoclay incorporation for sandwich core applications," *Applied Composite Materials,* vol. 12, no. 3-4, pp. 247-261, 2005.

[39] V. J.C., "Polymeric materials for impact and energy dissipation," *Plastics, Rubber and Composites,* vol. 35, no. 6-7, pp. 260-267, 2006.

[40] Cristina Buzea, Ivan I. Pacheco2, b), and Kevin Robbie, "Nanomaterials and nanoparticles: Sources and toxicity," *Biointerphases,* vol. 2, no. 4, p. https://doi.org/10.1116/1.2815690, 2007.

[41] Z. Bartczak, A.S. Argon, R.E. Cohen, M. Weinberg, "Toughness mechanism in semi-crystalline polymer blends: II high-density polyethylene toughened with calcium carbonate filler particles," *Polymer,* vol. 40, no. 9, pp. 2347-2365, 1999.

[42] S.M.R. Khalili, V. Daghigh, R.E. Farsani, "Mechanical behavior of basalt fiber-reinforced and basalt fiber metal laminate composites under tensile and bending loads," *Journal of Reinforced Plastcis and Composites,* vol. 30, no. 8, pp. 647-659, 2011.

[43] R. Eslami Farsani, SMR Khalili, V. Daghigh, R. Fazaeli, "Creep Behavior of Basalt and Glass Fiber Reinforced Epoxy Composites," *Journal of Mechanical Research and Application ,* vol. 3, no. 1, pp. 29-36, 2011.

[44] A.K. Subramaniyan, C.T. Sun, "Toughening polymeric composites using nanoclay: crack tip scale effects on fracture toughness," *Composites Part A,* vol. 38, no. 1, pp. 34-43, 2007.

[45] A.K. Subramaniyan, C.T. Sun, "Interlaminar fracture behavior of nanoclay reinforced glass fiber composites," *Journal of Composite Materials,* vol. 42, no. 20, pp. 2111-2122, 2008.

[46] C.B. Ng, L.S. Scbadler, R.W. Siegel, "Synthesis and Mechanical properties of TiO2–epoxy nanocomposites," *Nanostructure Materials,* vol. 12, no. 1, pp. 507-510, 1999.

[47] I. Javni, W. Zhang, V. Karajkov, Z.S. Petrovic, V. Divjakovic, "Effect of nano- and micro-silica fillers on polyurethane foam," *Journal of Cellular Plastics,* vol. 38, no. 3, pp. 229-239, 2002.

[48] J. Cho, M.S. Joshi, C.T. Sun, "Effect of inclusion size on mechanical properties of polymeric composites with micro and nano particles," *Composite Science and Technology,* vol. 66, no. 13, pp. 1941-1952, 2006.

[49] K.P. Ashik, R. S. Sharma, N. Raghavendra, "Effect of Filler on Mechanical Properties of Natural Fiber Reinforced Composites," *Asian Journal of Chemistry,* vol. 29, no. 8, pp. 1697-1701, 2017.

[50] A. Patnaik, A. Satapathy, S.S. Mahapatra, R.R. Dash, "A Comparative Study on Different Ceramic Fillers Affecting Mechanical Properties of Glass—Polyester Composites," *Journal of Reinforced Plastics and Composites ,* vol. 28, no. 11, pp. 1305-1314, 2009.

[51] V. Daghigh, T. E. Lacy Jr., C. U. Pittman Jr., H. Daghigh, "Influence of maleated polypropylene coupling agent on mechanical and thermal behavior of latania fiber-reinforced PP/EPDM composites," *Polymer Composites,* vol. 39, no. S3, pp. E1751-E1759, 2018.

[52] R. Crawford, Plastics Engineering, Oxford: Butterworth Heinemann, 1998.

[53] D Yankov, D DeCoste, E. Keogh, "Ensembles of nearest neighbor forecasts," in *Lecture notes in computer science*, European Conference on Machine Learning, 2006, pp. 545-556.

[54] L. Breiman, and H. Friedman, C.J. Stone, R.A. Olshen, Breiman, L., and H. Friedman. "J., A. Olshen, R., & J. Stone, C. 1984, Classification and Regression Trees. (Wadsworth and Brooks), 1984.

[55] R. Schapire, "Explaining AdaBoost," *Empirical Inference,* pp. 37-52, 2013.

[56] F. Pedregosa, G. Varoquaux, A. Gramfort, V. Michel, B. Thirion, O. Grisel, M. Blondel, P. Prettenhofer, R. Weiss, V. Dubourg, J. Vanderplas, A. Passos, D. Cournapeau, M. Brucher, M. Perrot, "Scikit-learn: Machine Learning in Python," *Journal of Machine Learning Research,* vol. 12, no. Oct, pp. 2825-2830, 2011.

[57] T. Fushiki, "Estimation of prediction error by using k-fold cross-validation," *Statistics and Computing,* vol. 21, pp. 137-146, 2011.

[58] H. Anuar, N.A. Hassan, F. Mohd Fauzey, "Compatibilized PP/EPDM-kenaf fibre composite using melt blending method," *Advanced Materials Research ,* Vols. 264-265, pp. 743-747, 2011.

[59] H. Anuar, A. Zuraida, "Improvement in mechanical properties of reinforced thermoplastic elastomer composite with kenaf bast fibre," *Composites Part B Engineering,* vol. 42, no. 3, pp. 462-465, 2011.

[60] M.A. Sawpan, K.L. Pickering, and F. Alan, "Analysis of mechanical properties of hemp fibre reinforced unsaturated polyester composites," *Journal of Composite Materials,* vol. 47, no. 12, pp. 1513-1525, 2013.

[61] H. Miyagawa, L.T. Drzal, "The effect of chemical modification on the fracture toughness of montmorillonite clay/epoxy nanocomposites," *J Adhesion Sci Technol,* vol. 18, no. 13, pp. 1571-1588, 2004.

[62] H. Miyagawa, A.K. Mohanty, L.T. Drzal, M. Misra, "Effect of clay and alumina-nanowhisker reinforcements on the mechanical properties of nanocomposites from biobased epoxy: a comparative study," *Ind Eng Chem Res,* vol. 43, no. 22, pp. 7001-7009, 2004.

[63] Z. Bartczak, A.S. Argon, R.E. Cohen, M. Weinberg, "Toughness mechanism in semi-crystalline polymer blends: II. High-density polyethylene toughened with calcium carbonate filler particles," *Polymer,* vol. 40, no. 9, pp. 2347-2365, 1999.

[64] J. Viana, "Polymeric materials for impact and energy dissipation," *Plastics Rubber and Composites,* vol. 35, no. 6-7, pp. 260-267, 2006.

[65] S. U. Khan, K. Iqbal, A. Munir, J. K. Kim, "Quasi-static and impact fracture behaviors of CFRPs with nanoclay-filled epoxy matrix," *Composites Part A: Applied Science and Manufacturing,* vol. 42, no. 3, pp. 253-264, 2011.

CHAPTER V

CONCLUDING REMARKS AND FUTURE WORK

5.1 Concluding Remarks

Natural short latania fiber (SLF)-reinforced poly(propylene)/ethylene-propylene-diene-monomer (SLF/PP/EPDM) bio-composites reinforced with nano-clays (NCs), pistachio shell powders (PSPs), and/or date seed particles (DSPs) were characterized by mechanical and thermal tests using experiments and machine learning (ML) predictions. Three related research topics were included in this dissertation: (1) an investigation of maleated polypropylene (MAPP) coupling agent on mechanical and thermal behavior of SLF/PP/EPDM composites, (2) heat deflection temperature (HDT) of bio-nano-composites using experiments and ML predictions, and (3) fracture toughness ML predictions of short fiber, nano- and micro-particle reinforced composites. The first project deals with the MAPP effect on tensile, bending, Charpy impact and HDT of SLF/PP/EPDM composites with various SLF contents. The second project introduces two novel bio-powder-additives (DSP and PSP) and assesses the HDT of PP/EPDM composites using experiments and K-Nearest Neighbor Regressor (KNNR) ML predictions. The composites are made of various contents of SLF (0, 5, 10, 20, and 30wt%), NCs (0, 1, 3, 5wt%), micro-sized PSPs (0, 1, 3, 5wt%) and micro-sized DSPs (0, 1, 3, 5wt%). The third project investigated the fracture toughness of the same composite series used in the second project, using Charpy impact tests, finite element analysis, and ML approach using Decision Tree Regressor (DTR) and Adaptive Boosting Regressor (ABR). The tensile/flexural moduli and strengths' composites were

improved up to 9% upon 2 wt% MAPP addition compared with the composites with zero MAPP. Additionally, 2 wt% MAPP addition to composites highly improved energy impact absorption (up to78%) and HDT (up to 4 C^o). SLF, NC, DSP and PSP all could enhance HDT and fracture toughness values. KNNR ML approach could well predict the composite's HDT values and, Decision Tree Regressor (DTR) and Adaptive Boosting Regressor ML algorithms worked well with fracture toughness predictions. These ML models can be used for further predictions of HDT and fracture toughness results to find optimized compositions. Pictures taken through transmission electron microscope, scanning electron microscope and X-Ray proved the NC dispersion and exfoliation as one of the factors in HDT and fracture toughness improvements.

5.2 Future Work

The composites and ML model developed in this work may be further developed 1) by considering the effect of fiber and filler geometries, 2) by considering possible optimized compositions, and 3) by including more mechanical and thermal characterizations. *First*, the current ML models do not consider the influence of changes in the fiber and filler geometries. These changes may lead to a remarkable increase or decrease in the HDT and fracture toughness results. *Second*, the current ML modes have capabilities to predict HDT and fracture toughness results for every possible composition of PP/EPDM, SLF, NC, PSP, and DSP within the range of available experimental data. Thus, the present ML models can be employed to find the optimized composition of composites with maximum HDT and fracture toughness results. *Lastly*, thermogravimetric analysis (TGA) and dynamic mechanical analysis (DMA) tests are being carried out to get further information on thermal properties of the composites containing PP/EPDM, SLF, NC, PSP, and DSP. Further thermal properties ML predictions from these bio-nano-composites will be discussed in a separate manuscript.

APPENDIX A

SUPPLEMENTARY MATERIALS FOR CHAPTER 3

Table A.1 3.1.A_1 (Full format of Table 3.1). The composition of each composite blend and the pertinent experimental heat deflection temperature (HDT) values

Input	Input	Input	Input	Input	Output
PP/EPDM	SLF (wt%)	PSP (wt%)	DSP (wt%)	NC (wt%)	HDT (°C)
100	0	0	0	0	65.1
97	0	3	0	0	68.9
95	0	5	0	0	69.4
97	0	0	3	0	66.3
95	0	0	5	0	67.9
97	0	0	0	3	67.4
95	0	0	0	5	68.5
95	5	0	0	0	73.2
92	5	3	0	0	76.9
90	5	5	0	0	77.6
92	5	0	3	0	74.7
90	5	0	5	0	76.3
92	5	0	0	3	75.7
95	5	0	0	5	77.3
90	10	0	0	0	74
87	10	0	3	0	75.4
85	10	0	5	0	76.9
87	10	3	0	0	77.7
85	10	5	0	0	79.3
87	10	0	0	3	76.4
85	10	0	0	5	77.7
82	10	5	0	3	79.8
82	10	0	5	3	78.4

Table A.2 3.1.A_2 (Continuation of Full format of Table 3.1). The composition of each composite blend and the pertinent experimental HDT values

Input	Input	Input	Input	Input	Output
PP/EPDM	SLF (wt%)	PSP (wt%)	DSP (wt%)	NC (wt%)	HDT (°C)
80	10	5	0	5	80.5
80	10	0	5	5	79.3
84	10	3	0	3	79.5
84	10	0	3	3	77.1
84	10	3	3	0	79
80	20	0	0	0	79.1
77	20	3	0	0	83.1
75	20	5	0	0	84
77	20	0	3	0	80.5
75	20	0	5	0	82.3
77	20	0	0	3	81.1
75	20	0	0	5	83
70	30	0	0	0	79.6
67	30	3	0	0	84.7
65	30	5	0	0	86.5
67	30	0	3	0	81.3
65	30	0	5	0	82.5
67	30	0	0	3	83.7
65	30	0	0	5	84.2
62	30	5	0	3	86.1
62	30	0	5	3	84.3
60	30	5	0	5	86
60	30	0	5	5	85.3
74	30	3	0	3	85.6
74	30	0	3	3	83.1
74	30	3	3	0	84.9

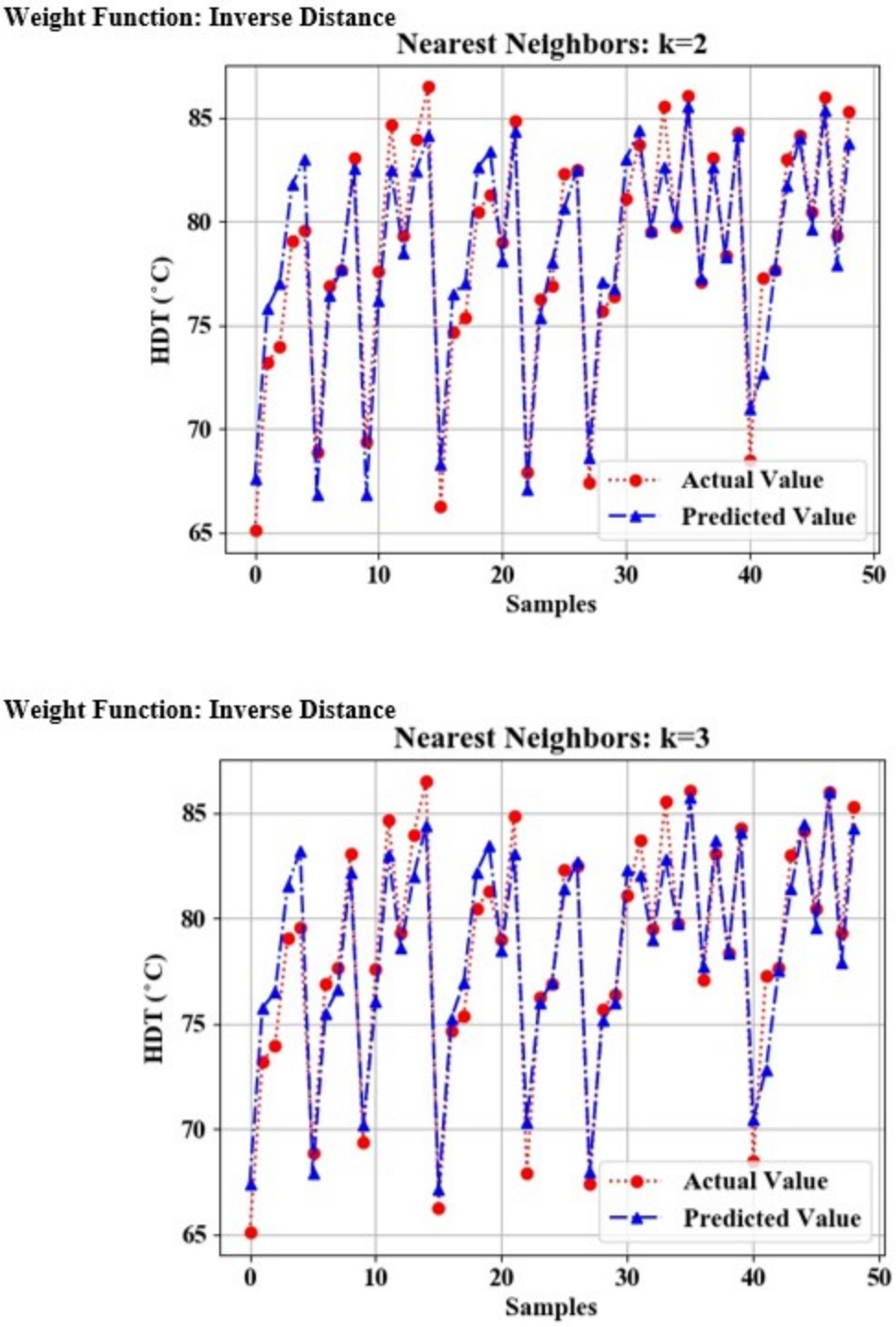

Figure A.1 (Full format of Fig. 3.4). Actual (in red) and predicted (in blue) HDT values (horizontal axis represents the number of samples and the vertical axis represents the HDT values in centigrade degrees

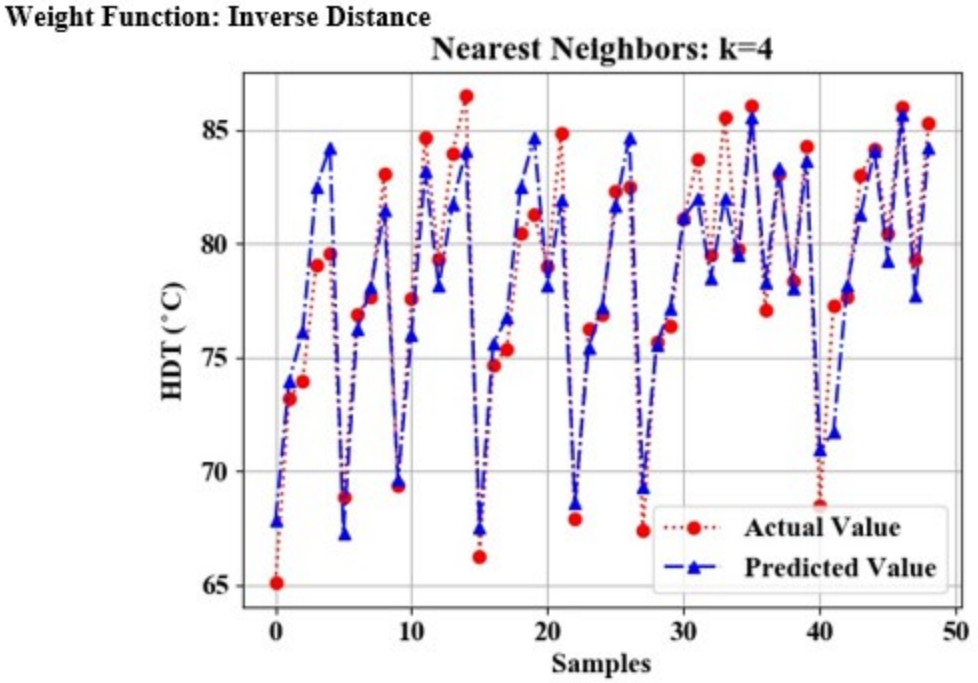

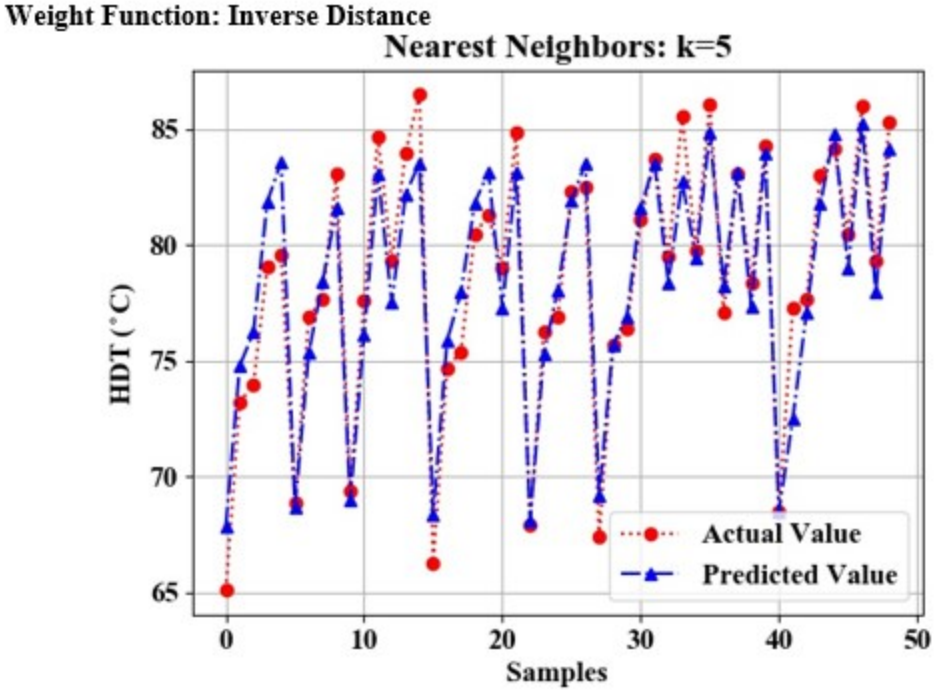

Figure A.1 (continued)

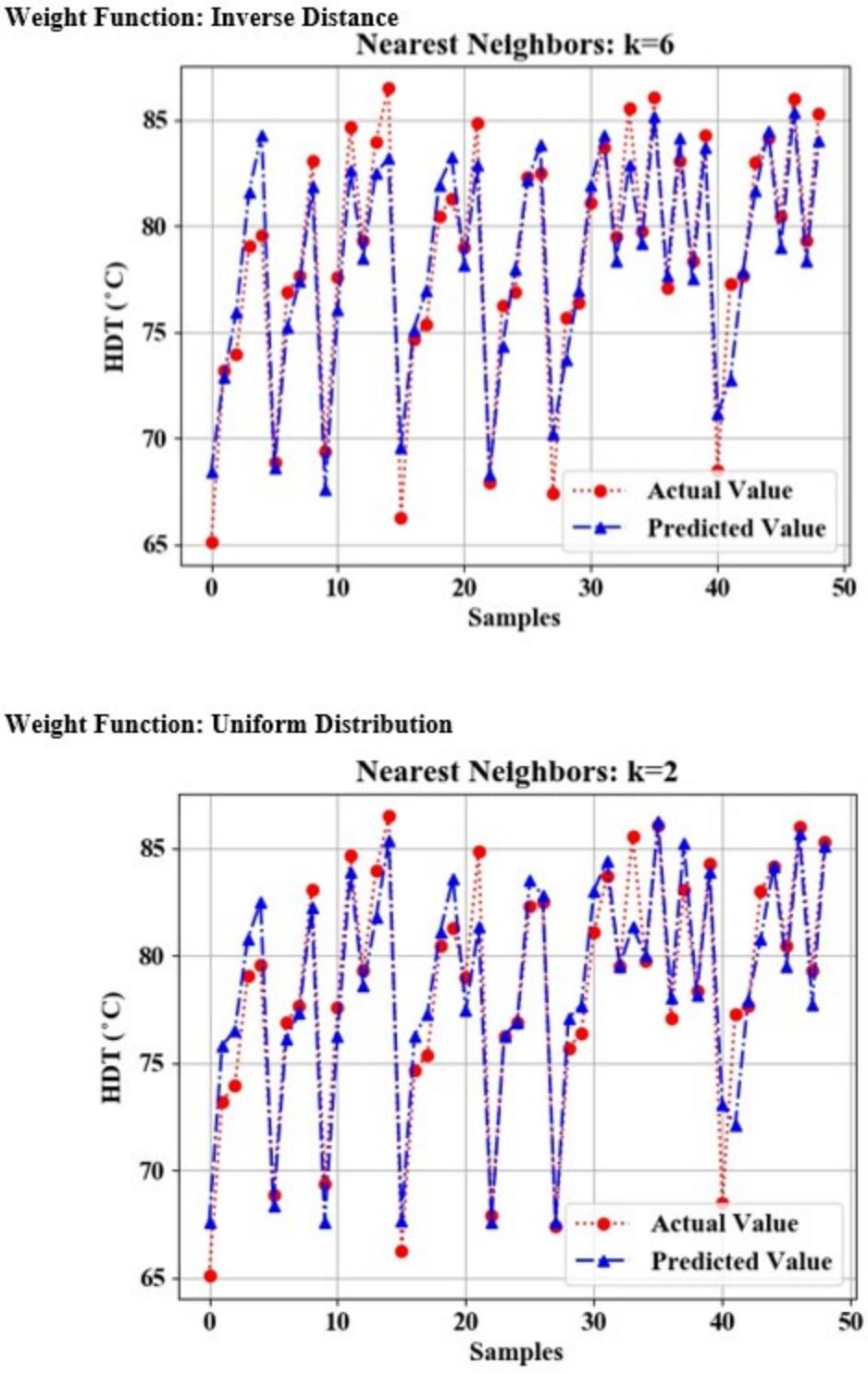

Figure A.1 (continued)

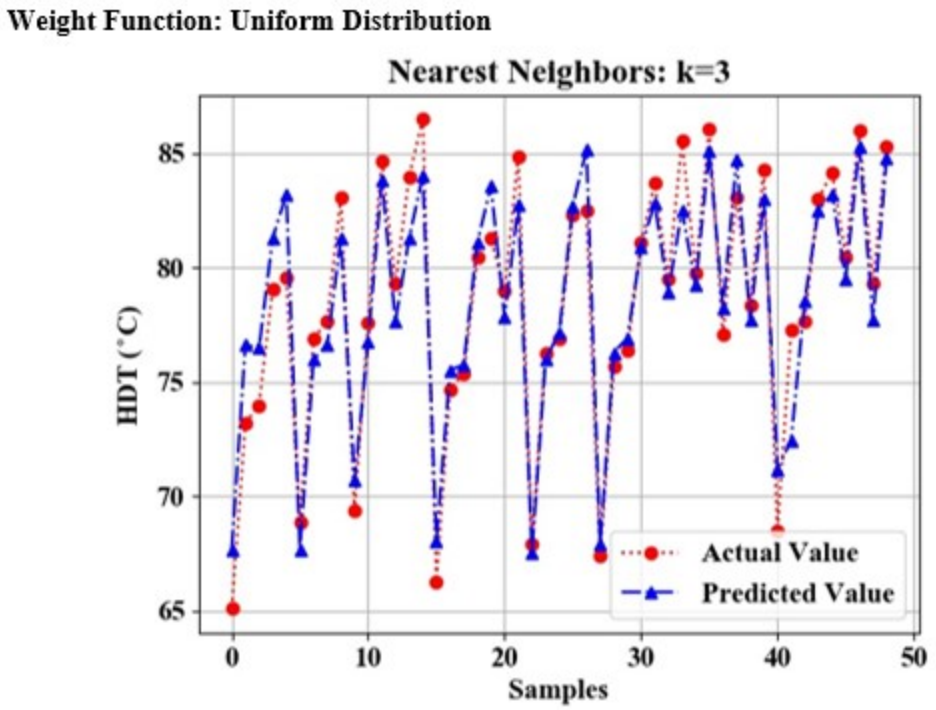

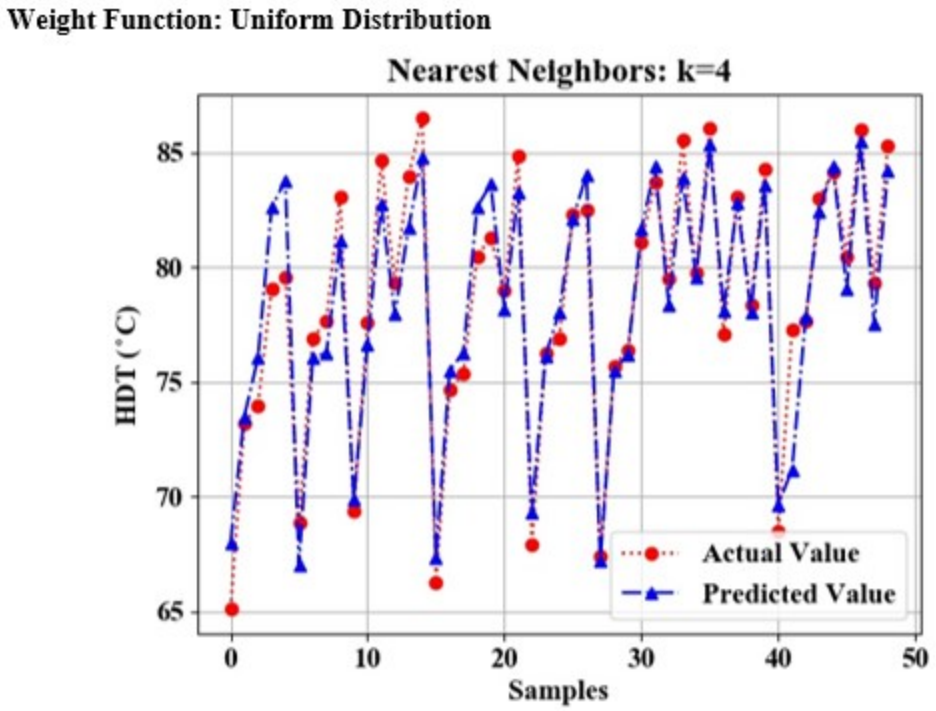

Figure A.1 (continued)

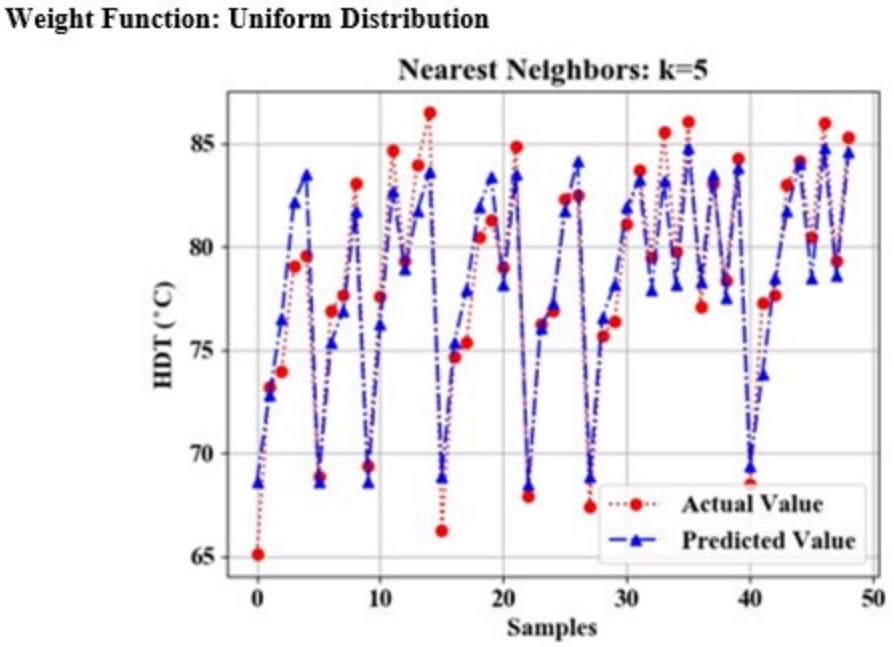

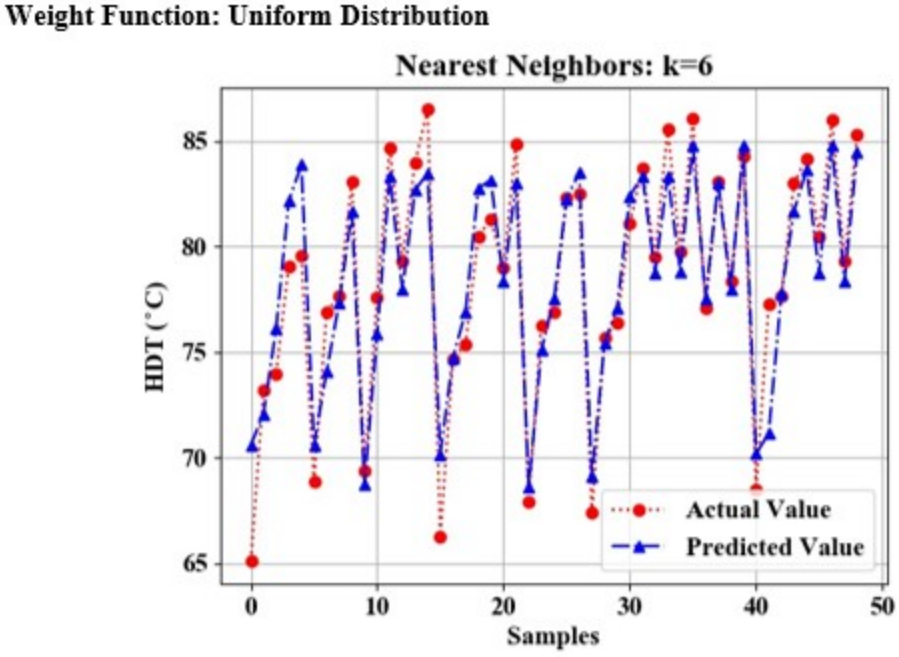

Figure A.1 (continued)

APPENDIX B

SUPPLEMENTARY MATERIALS FOR CHAPTER 4

Table B.1 Table 4.1.B_1 (Full format of Table 4.1). The composition of each composite blend and the pertinent experimental fracture toughness (G_c) values

Input (wt%)	Input (wt%)	Input (wt%)	Input (wt%)	Input (wt%)	Output
PP/EPDM	SLF	PSP	DSP	NC	Fracture Toughness (KJ/m^2)
100	0	0	0	0	45.4
97	0	3	0	0	52
95	0	5	0	0	57.1
97	0	0	3	0	57.3
95	0	0	5	0	66
97	0	0	0	3	54.5
95	0	0	0	5	61.2
95	5	0	0	0	55
92	5	3	0	0	64.8
90	5	5	0	0	70.2
92	5	0	3	0	69.4
90	5	0	5	0	77.3
92	5	0	0	3	67.1
95	5	0	0	5	74.8
90	10	0	0	0	67.3
87	10	0	3	0	80.7
85	10	0	5	0	89.7
87	10	3	0	0	78.6
85	10	5	0	0	83.6
87	10	0	0	3	79.6
85	10	0	0	5	88.4
82	10	5	0	3	96.3
82	10	0	5	3	102.8

Table B.1 (continued)

Input (wt%)	Input (wt%)	Input (wt%)	Input (wt%)	Input (wt%)	Output
PP/EPDM	SLF	PSP	DSP	NC	Fracture Toughness (KJ/m^2)
80	10	5	0	5	95.1
80	10	0	5	5	114.3
84	10	3	0	3	87.6
84	10	0	3	3	83.4
84	10	3	3	0	90.9

Table B.2 Table 4.1.A_2 (Continuation of Full format of Table 4.1). The composition of each composite blend and the pertinent experimental fracture toughness (Gc) values

Input (wt%)	Input (wt%)	Input (wt%)	Input (wt%)	Input (wt%)	Output
PP/EPDM	SLF	PSP	DSP	NC	FT (KJ/m^2)
80	20	0	0	0	107.9
77	20	3	0	0	120.8
75	20	5	0	0	130.6
77	20	0	3	0	130
75	20	0	5	0	145.7
77	20	0	0	3	125.2
75	20	0	0	5	137.5
70	30	0	0	0	136.7
67	30	3	0	0	149.6
65	30	5	0	0	161.1
67	30	0	3	0	162.2
65	30	0	5	0	149
67	30	0	0	3	154.5
65	30	0	0	5	167.8
62	30	5	0	3	173.7
62	30	0	5	3	177.7
60	30	5	0	5	179.7
60	30	0	5	5	194.2
74	30	3	0	3	170.5
74	30	0	3	3	172.8
74	30	3	0	3	170.3
74	30	3	3	0	172.8

FT: Fracture Toughness

Table B.3 Table 4.2.A_1 (Full format of Table 4.2). Performance evaluations using AdaBoost and Regression Tree.

No.	depth	estimators	regtree_rmse	adaboost_rmse	regtree_rmse/av	adaboost_rmse/av
0	2	5	12.3835	12.2295	11.3840	11.2425
1	3	5	15.9964	15.2483	14.7053	14.0176
2	4	5	10.9673	9.2124	10.0821	8.4689
3	2	10	12.8908	11.9351	11.8504	10.9718
4	3	10	10.4743	9.6675	9.6289	8.8872
5	4	10	9.4482	9.9636	8.6856	9.1594
6	2	15	14.4455	11.7106	13.2796	10.7655
7	3	15	9.6444	10.7684	8.8660	9.8993
8	4	15	11.0664	11.2425	10.1733	10.3351
9	2	20	12.4226	11.5621	11.4100	10.6289
10	3	20	10.0951	9.6927	9.2803	8.9104
11	4	20	10.9024	10.4047	10.0224	9.5649

regtree_rmse: RMSE in the Regression Tree method;
adaboost_rmse: RMSE in the Adaboost method;
regtree_rmse/av: RMSE average in the Regression Tree method;
adaboost_rmse/av: RMSE average in the Adaboost method

Table B.4 Table 4.2.A_2 (Continuation of Full format of Table 4.2). Performance evaluations using AdaBoost and Regression Tree.

No.	depth	estimators	regtree_R^2	adaboost_R^2	regtree_mae	adaboost_mae
0	2	5	0.9092	0.9119	10.1760	10.0289
1	3	5	0.8337	0.8334	11.6114	11.4376
2	4	5	0.9390	0.9533	8.4469	7.3338
3	2	10	0.8788	0.8961	10.3903	9.2639
4	3	10	0.9384	0.9473	8.2781	7.7252
5	4	10	0.9492	0.9435	7.1186	7.9789
6	2	15	0.8536	0.9079	11.8761	9.4281
7	3	15	0.9423	0.9288	7.7148	8.6314
8	4	15	0.9299	0.9299	8.2856	8.3400
9	2	20	0.9084	0.9220	10.1200	9.5113
10	3	20	0.9428	0.9477	8.0560	8.1841
11	4	20	0.9286	0.9378	8.3154	7.8055

regtree_R^2: R^2 in the Regression Tree method; adaboost_R^2: R^2 in the Adaboost method
regtree_MAE: MAE in the Regression Tree method; adaboost_MAE: MAE in the Adaboost method

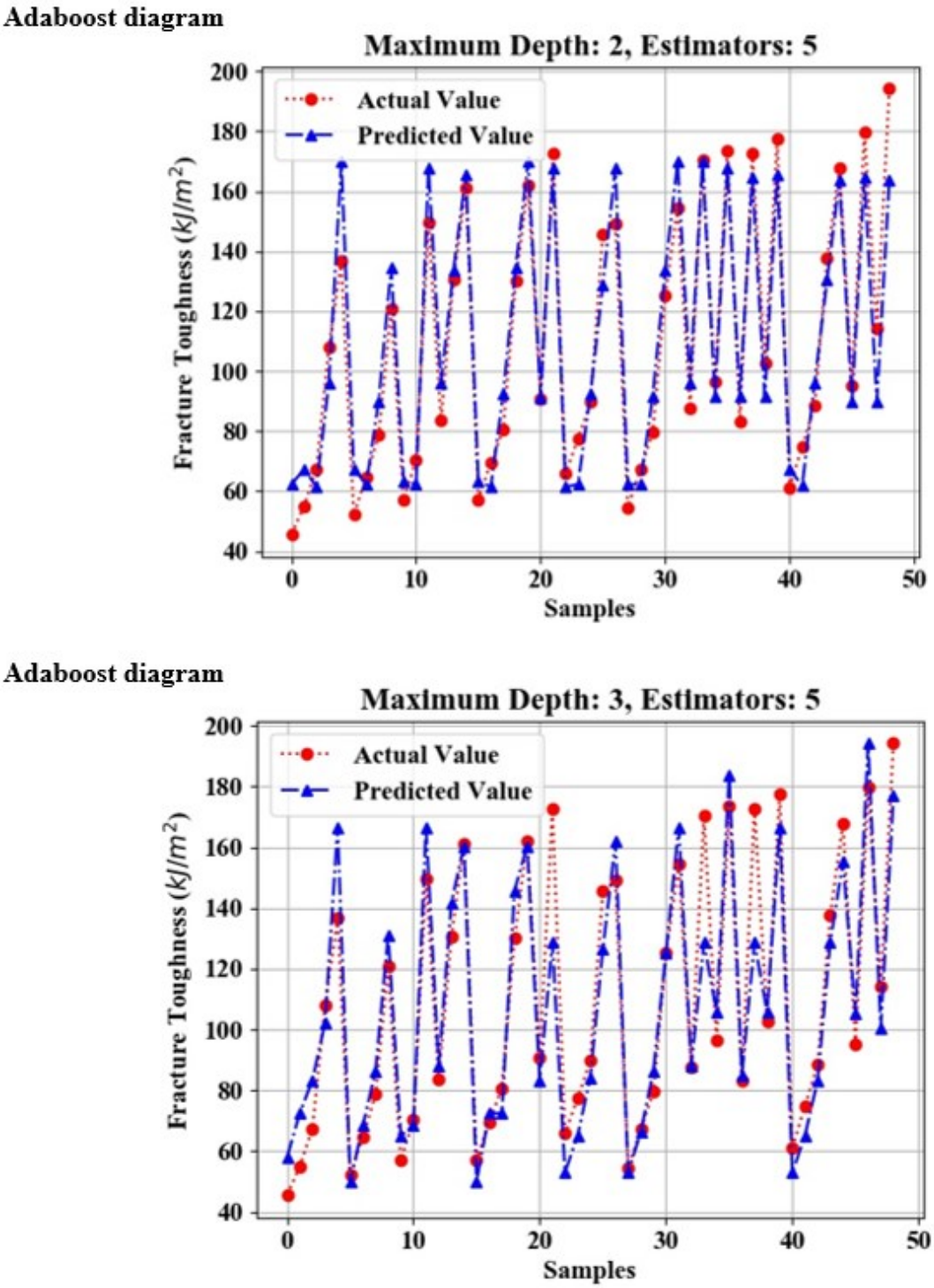

Figure B.1 Fig. 4.1.A (Full format of Fig. 4.1). Actual and predicted fracture toughness (Gc) values (horizontal axis represents the number of samples and the vertical axis represents the Gc values.

Adaboost diagram

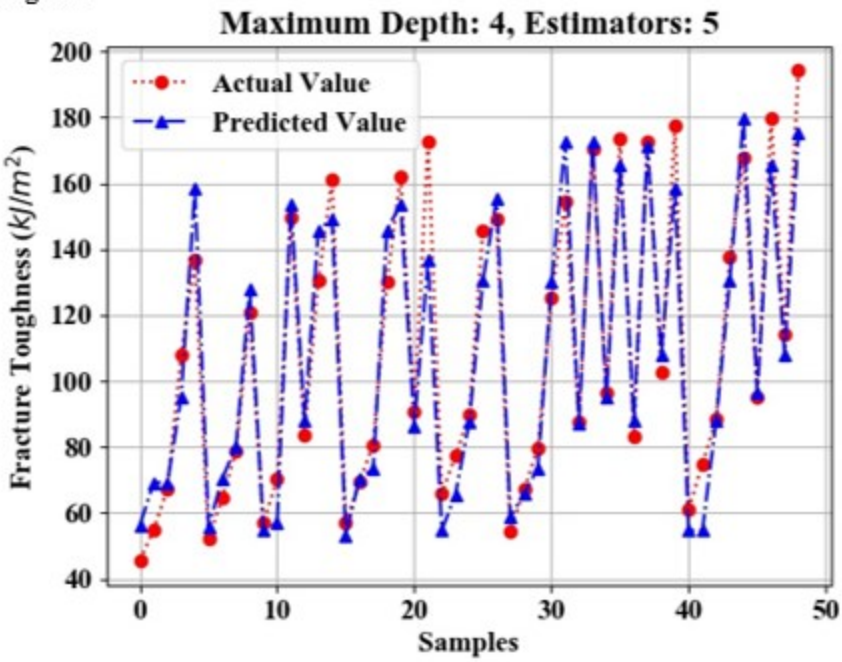

Adaboost diagram

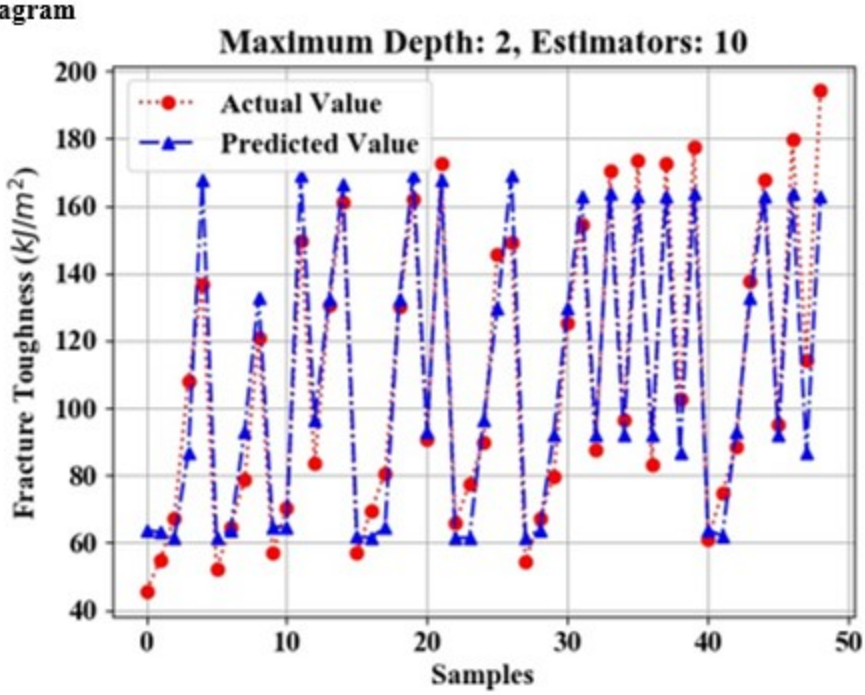

Figure B.1 (continued)

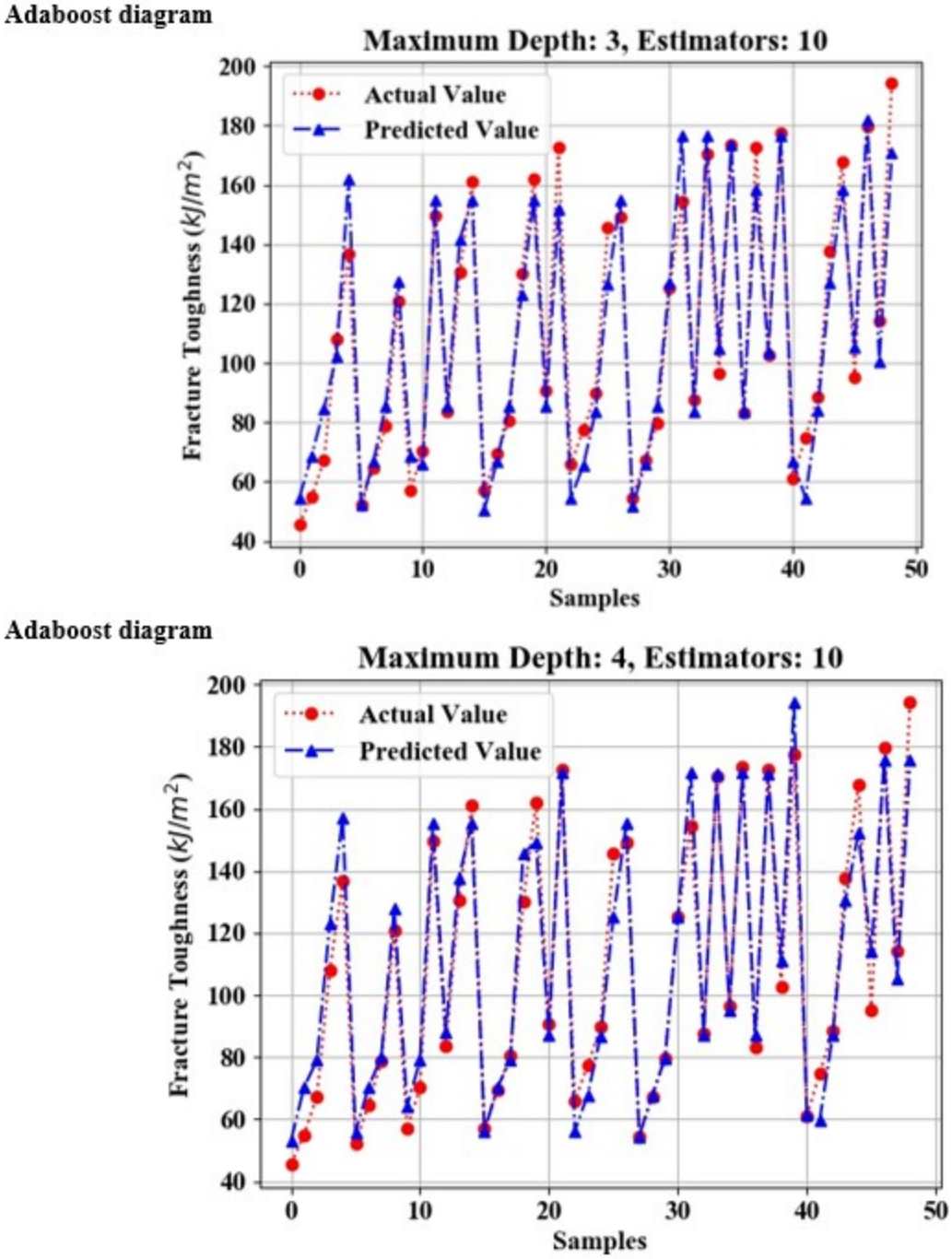

Figure B.1 (continued)

Adaboost diagram

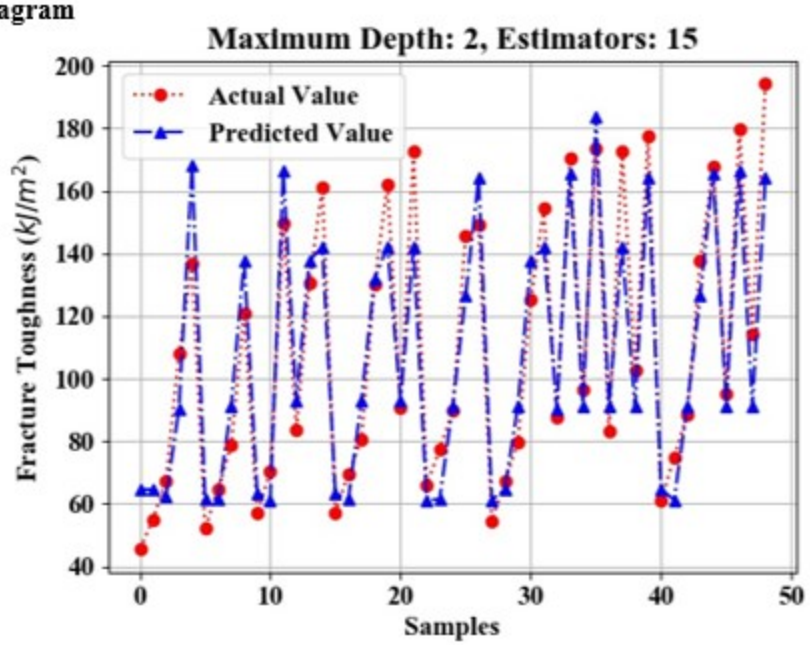

Adaboost diagram

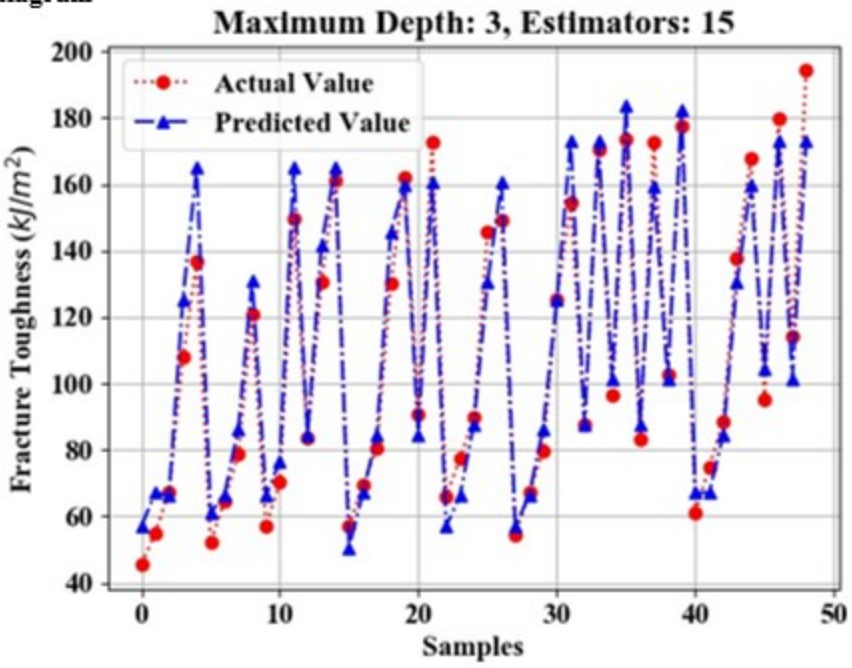

Figure B.1 (continued)

Adaboost diagram

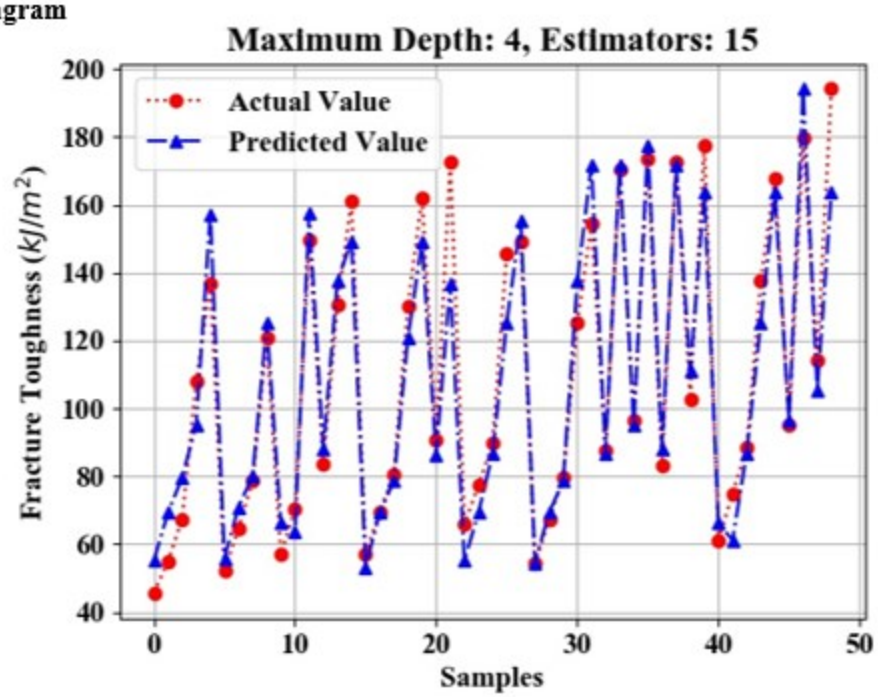

Adaboost diagram

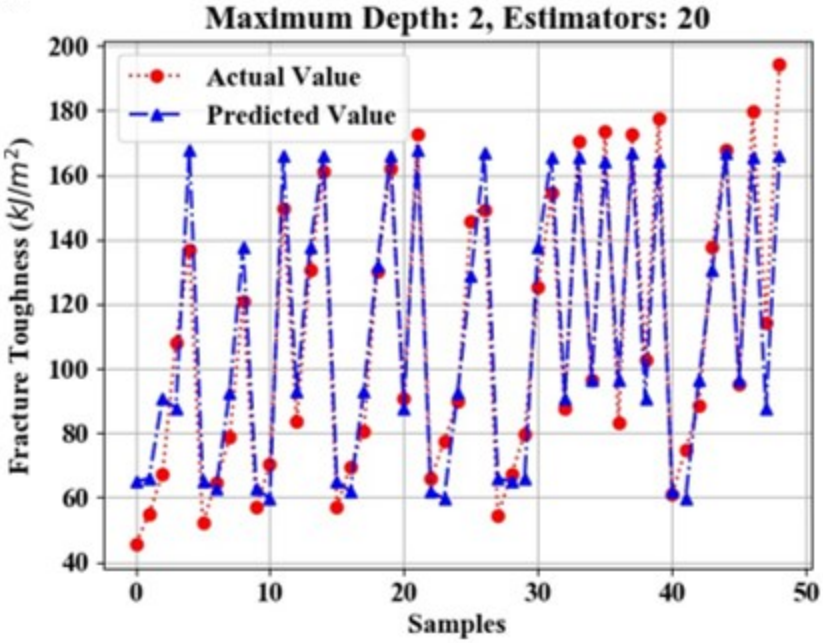

Figure B.1 (continued)

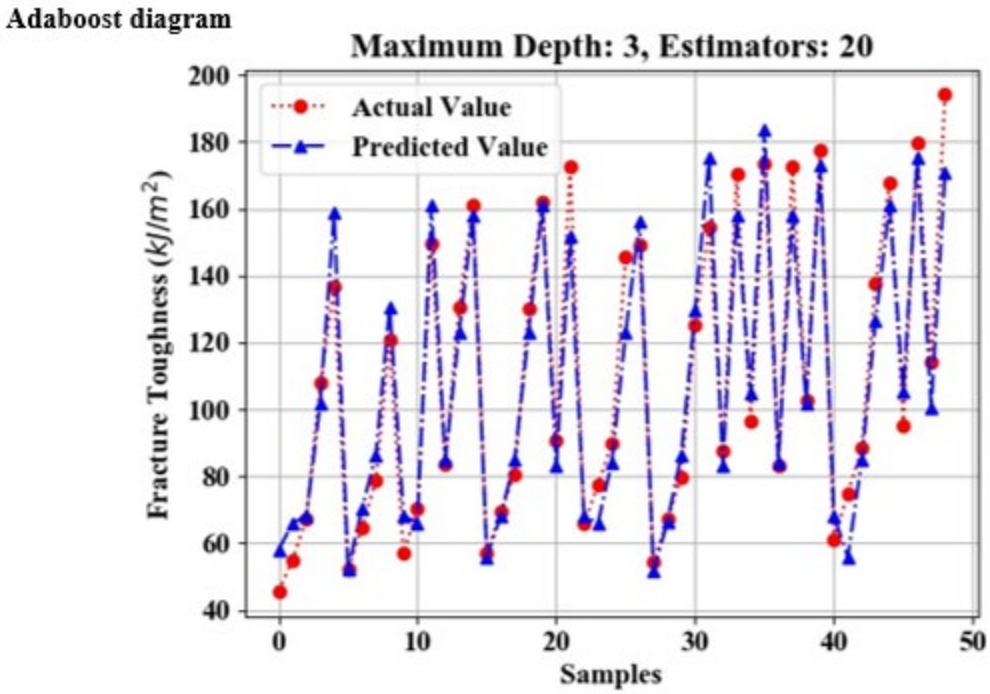

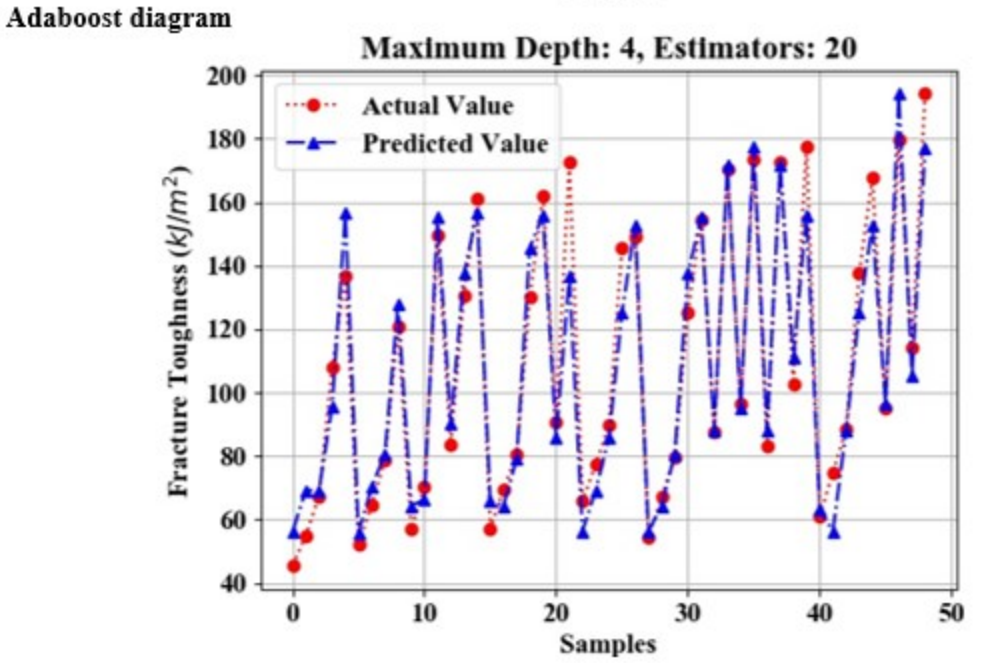

Figure B.1 (continued)

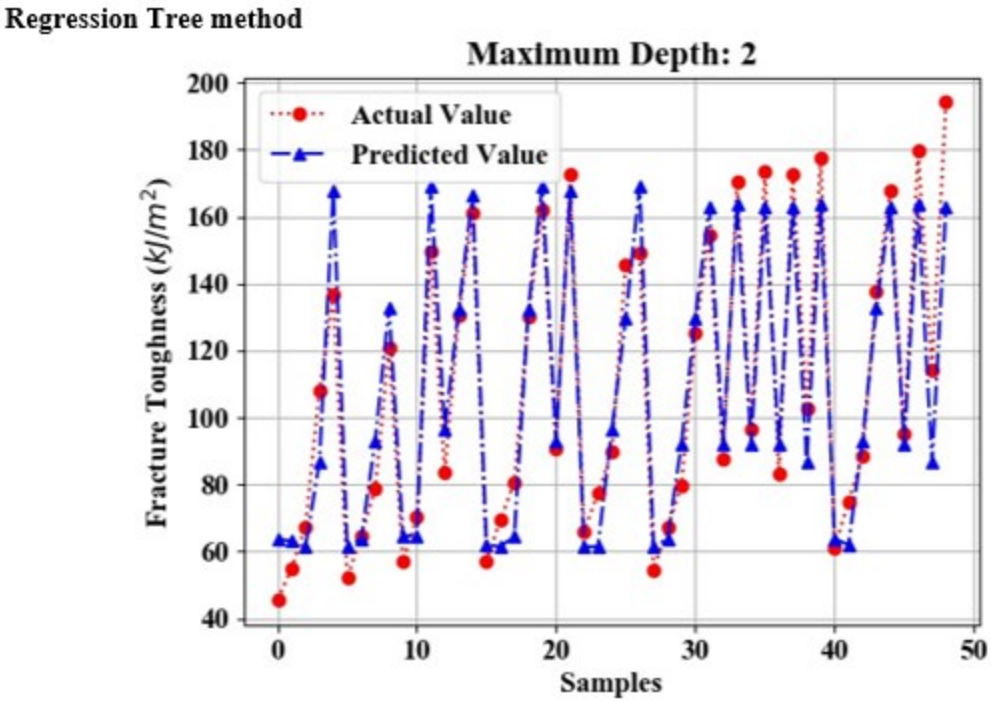

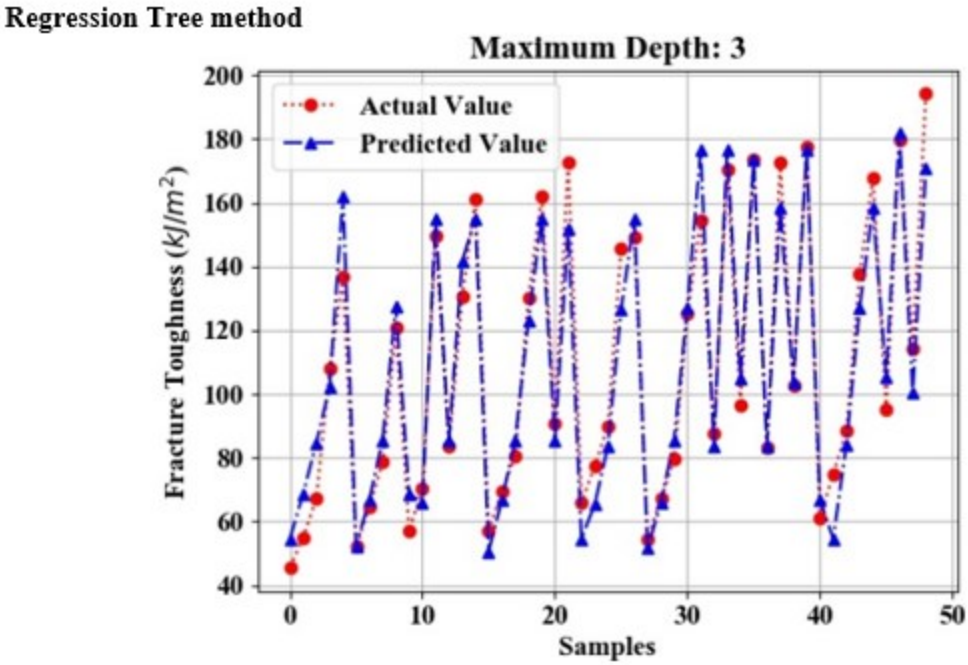

Figure B.1 (continued)

Regression Tree method

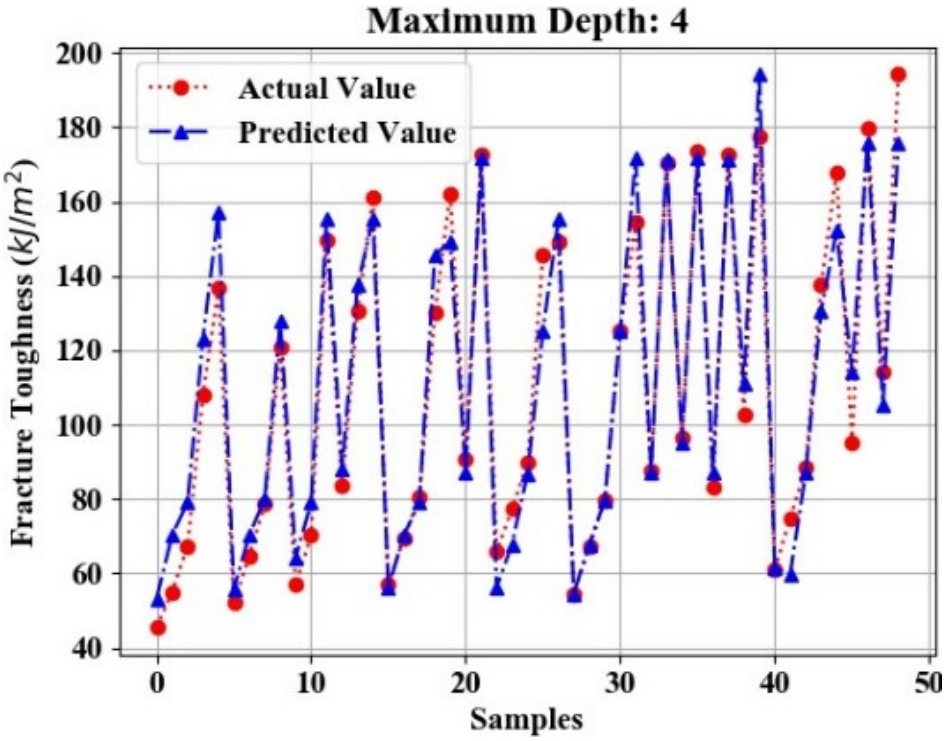

Figure B.1 (continued)

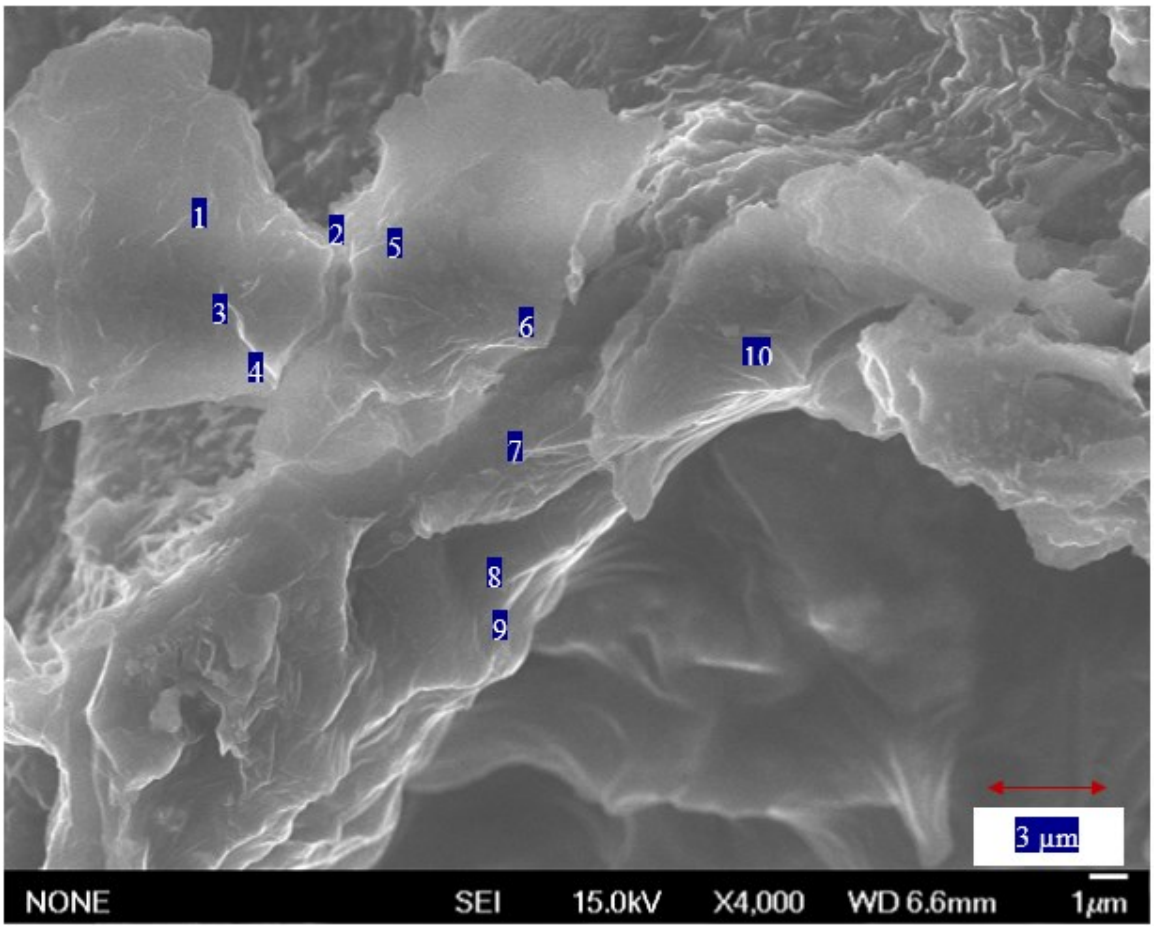

Figure B.2 Fig. 4.2.A._a (magnification of 4 kx).

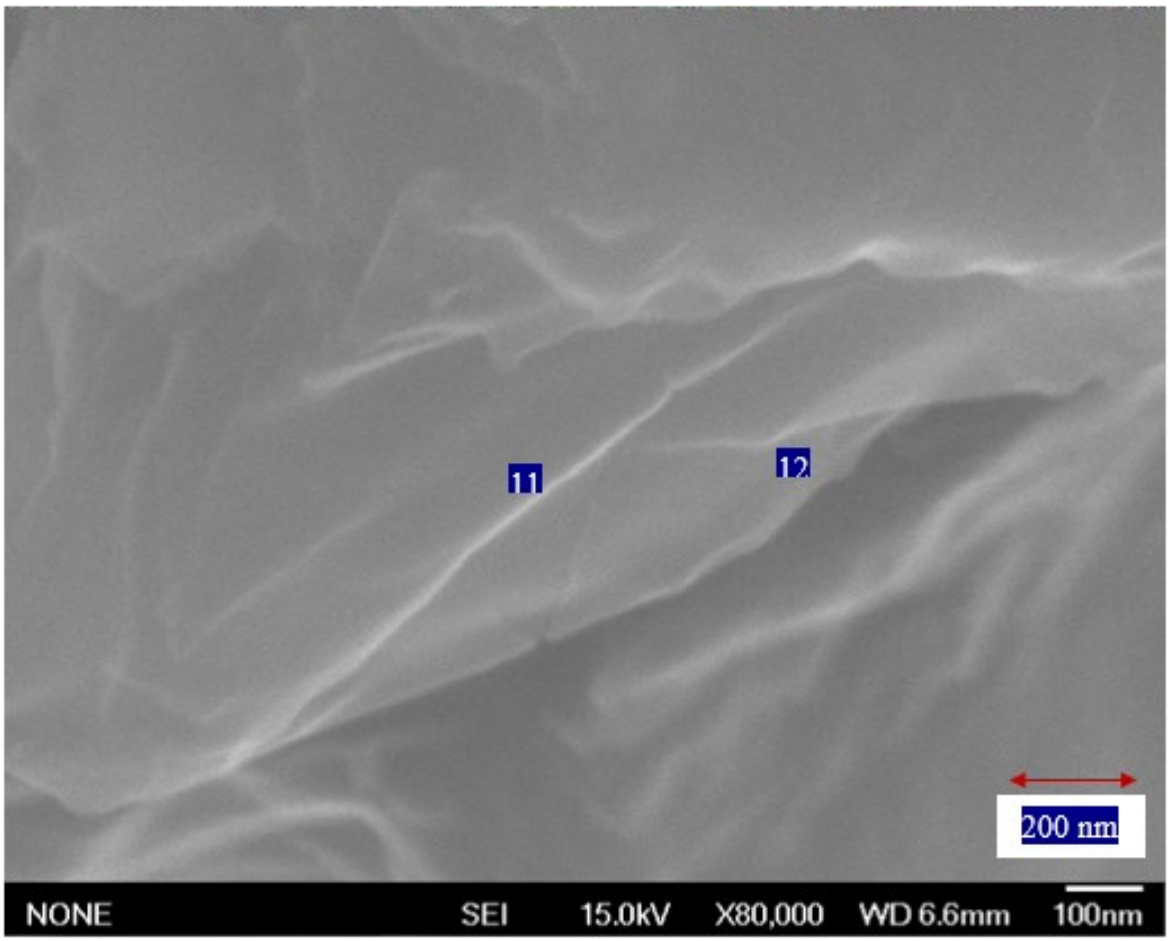

Figure B.3 Fig. 4.2.A._b (magnification of 80 kx)

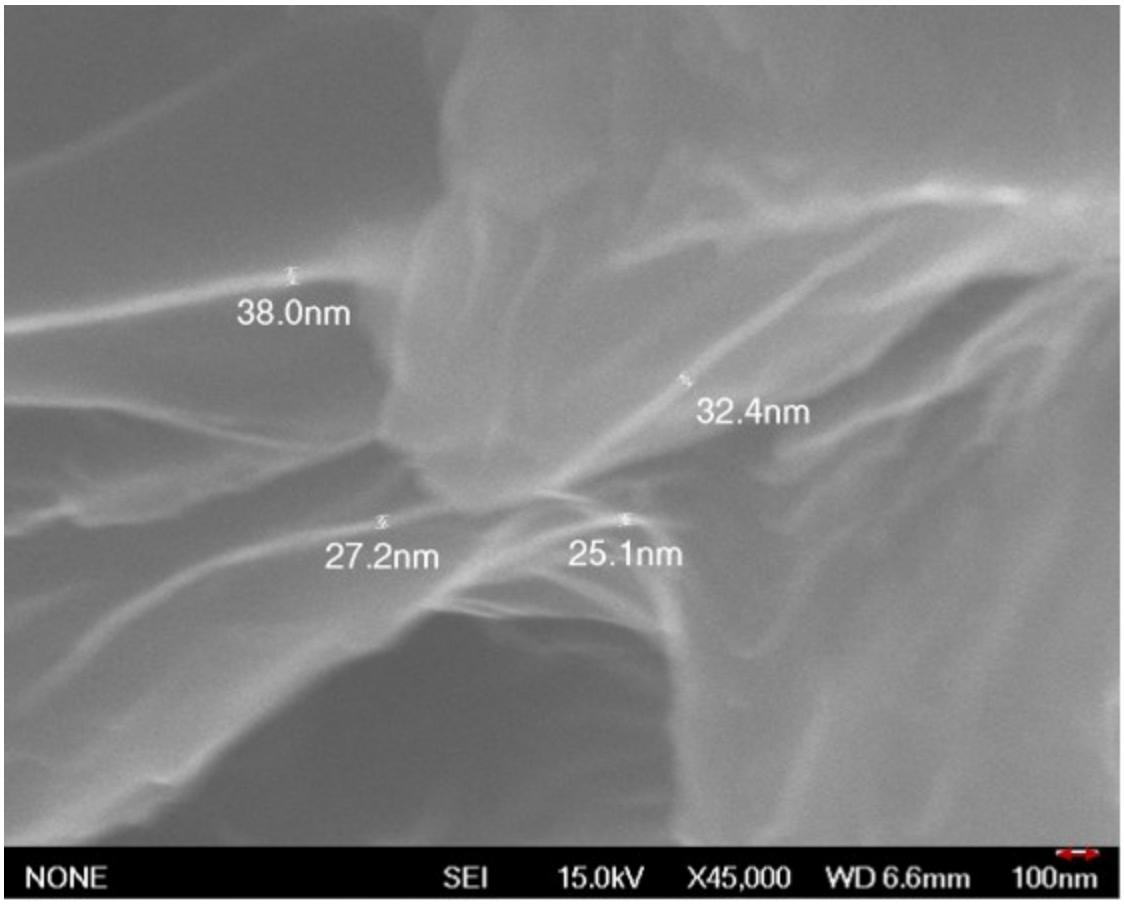

Figure B.4 Fig. 4.2.A._c (magnification of 45 kx).

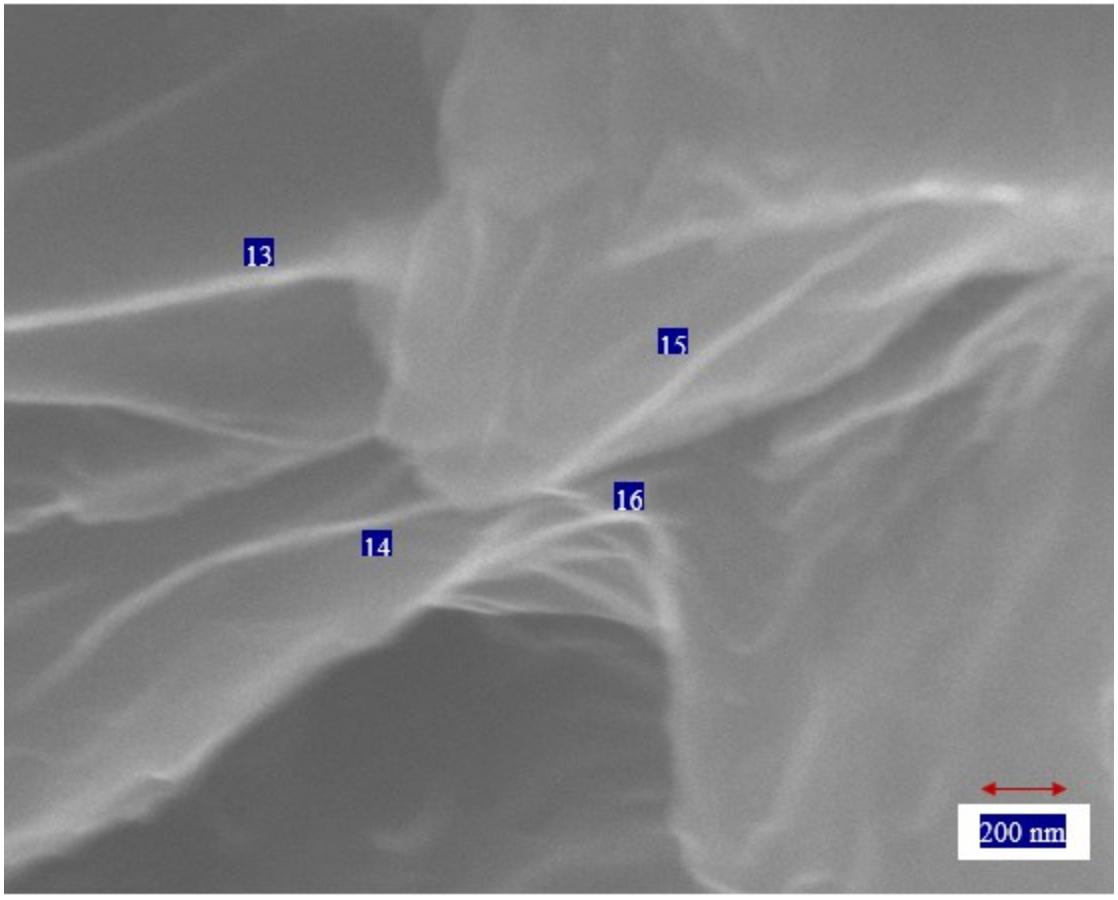

Figure B.5 Fig. 4.2.A_d (magnification of 45 kx).

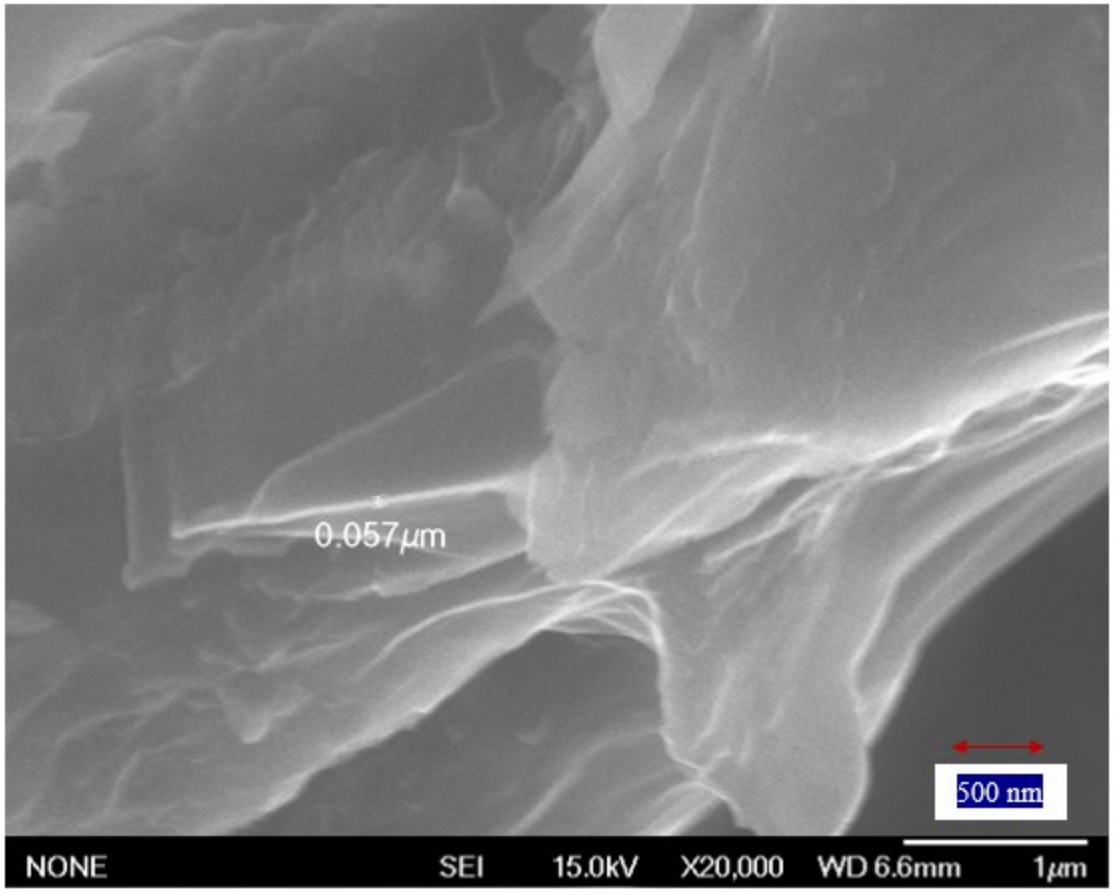

Figure B.6 Fig. 4.2.A_e (magnification of 20 kx).

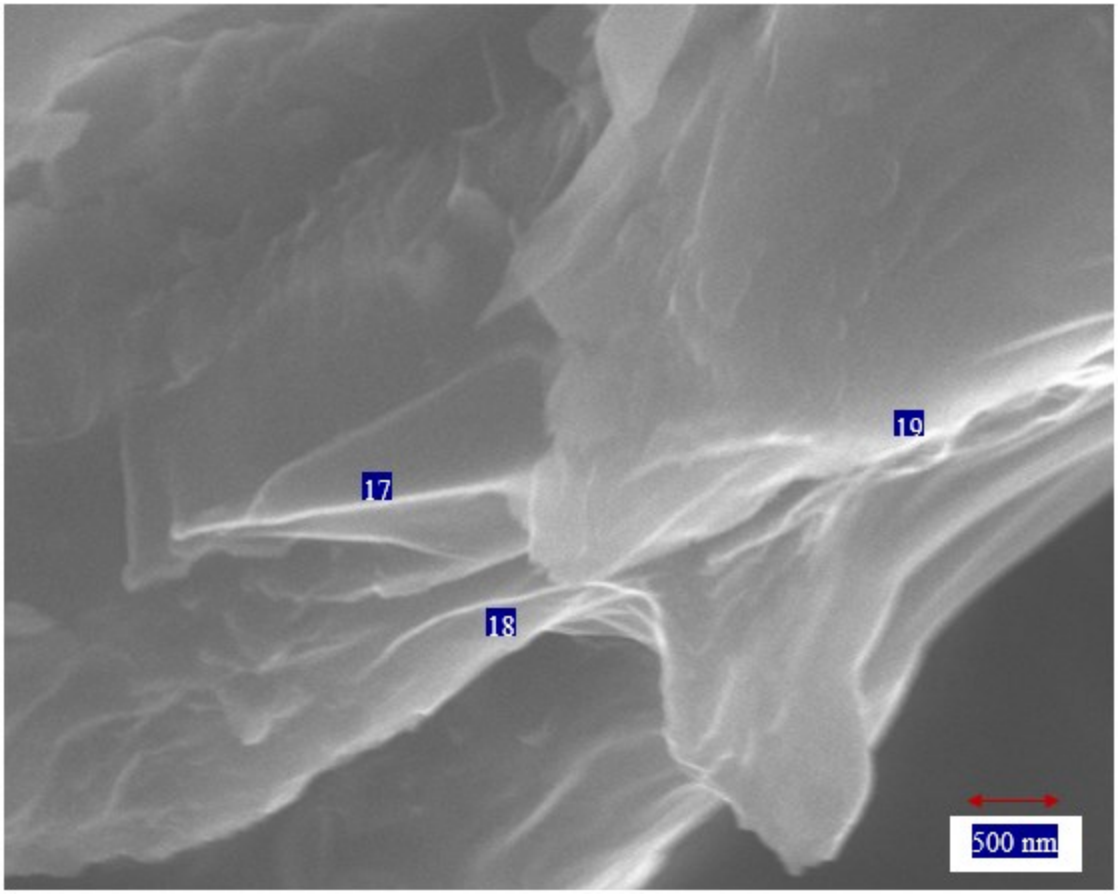

Figure B.7 Fig. 4.2.A_f (magnification of 20 kx).

Table B.5 Table 4.3.A. 19 NC platelet thicknesses measured from SEM.

Point No.	Size (nm)
1	25
2	20
3	18
4	30
5	15
6	37
7	12
8	35
9	40
10	15
11	7
12	8
13	27
14	19
15	29
16	21
17	38
18	20
19	26
Average	23.26
Standard deviation	9.89